Non-Wiener Characteristics of LMS Adaptive Equalizers: A Bit Error Rate Perspective

Tamoghna Roy

Dissertation submitted to the Faculty of the
Virginia Polytechnic Institute and State University
in partial fulfillment of the requirements for the degree of

Doctor of Philosophy
In
Electrical Engineering

A. A. (Louis) Beex, Chair
Jeffrey H. Reed
Harpreet S. Dhillon
William T. Baumann
Mazen Farhood

December 20, 2017

Blacksburg, VA

Keywords: (N)LMS Equalizer, Non-Wiener Effects, BER Modeling, Gaussian Sum Mixture

Non-Wiener Characteristics of LMS Adaptive Equalizers: A Bit Error Rate Perspective

Tamoghna Roy

ABSTRACT

Adaptive Least Mean Square (LMS) equalizers are widely used in digital communication systems primarily for their ease of implementation and lack of dependence on a priori knowledge of input signal statistics. LMS equalizers exhibit non-Wiener characteristics in the presence of a strong narrowband interference and can outperform the optimal Wiener equalizer in terms of both mean square error (MSE) and bit error rate (BER). There has been significant work in the past related to the analysis of the non-Wiener characteristics of the LMS equalizer, which includes the discovery of the shift in the mean of the LMS weights from the corresponding Wiener weights and the modeling of steady state MSE performance. BER performance is ultimately a more practically relevant metric than MSE for characterizing system performance. The present work focuses on modeling the steady state BER performance of the normalized LMS (NLMS) equalizer operating in the presence of a strong narrowband interference.

Initial observations showed that a 2 dB improvement in MSE may result in two orders of magnitude improvement in BER. However, some differences in the MSE and BER behavior of the NLMS equalizer were also seen, most notably the significant dependence (one order of magnitude variation) of the BER behavior on the interference frequency, a dependence not seen in MSE. Thus, MSE cannot be used as a predictor for the BER performance; the latter further motivates the pursuit of a separate BER model.

The primary contribution of this work is the derivation of the probability density of the output of the NLMS equalizer conditioned on a particular symbol having been transmitted, which can then be leveraged to predict its BER performance. The analysis of the NLMS equalizer, operating in a strong narrowband interference environment, resulted in a conditional probability density function in the form of a Gaussian Sum Mixture

(GSM). Simulation results verify the efficacy of the GSM expression for a wide range of system parameters, such as signal-to-noise ratio (SNR), interference-to-signal (ISR) ratio, interference frequency, and step-sizes over the range of mean-square stable operation of NLMS. Additionally, a low complexity approximate version of the GSM model is also derived and can be used to give a conservative lower bound on BER performance.

A thorough analysis of the MSE and BER behavior of the Bi-scale NLMS equalizer (BNLMS), a variant of the NLMS equalizer, constitutes another important contribution of this work. Prior results indicated a 2 dB MSE improvement of BNLMS over NLMS in the presence of a strong narrowband interference. A closed form MSE model is derived for the BLMS algorithm. Additionally, BNLMS BER behavior was studied and showed the potential of two orders of magnitude improvement over NLMS. Analysis led to a BER model in the form of a GSM similar to the NLMS case but with different parameters. Simulation results verified that both models for MSE and BER provided accurate prediction of system performance for different combinations of SNR, ISR, interference frequency, and step-size.

An enhanced GSM (EGSM) model to predict the BER performance for the NLMS equalizer is also introduced, specifically to address certain cases (low ISR cases) where the original GSM expression (derived for high ISR) was less accurate. Simulation results show that the EGSM model is more accurate in the low ISR region than the GSM expression. For the situations where the derived GSM expression was accurate, the BER estimates provided by the heuristic EGSM model coincided with those computed from the GSM expression.

Finally, the two-interferer problem is introduced, where NLMS equalizer performance is studied in the presence of two narrowband interferers. Initial results show the presence of non-Wiener characteristics for the two-interferer case. Additionally, experimental results indicate that the BER performance of the NLMS equalizer operating in the presence of a single narrowband interferer may be improved by purposeful injection of a second narrowband interferer.

Non-Wiener Characteristics of LMS Adaptive Equalizers: A Bit Error Rate Perspective

Tamoghna Roy

GENERAL AUDIENCE ABSTRACT

Every practical communication system requires effective interference mitigation schemes that are able to nullify unwanted signals without distorting the desired signal. Adaptive equalizers are among the prevalent systems used to cancel interfering signals. In particular, for narrowband interference (a particular class of interference) mitigation with (normalized) least mean square type (NLMS) equalizers has been found to be extremely effective. In fact, in the narrowband interference-dominated environment, NLMS equalizers have been found to work better than the solution with the same structure that is optimal according to linear filtering theory. This departure from the linear filtering theory is a result of the non-Wiener characteristics of NLMS type equalizers.

This work investigates the bit error rate (BER) behavior, a common metric used to characterize the performance of wireless communication systems, of the NLMS equalizer in the presence of a strong narrowband interference. The major contribution of this dissertation is the derivation of an accurate expression that links the BER performance of the NLMS equalizer with the system parameters and signal statistics. Another variant of the NLMS equalizer known as the Bi-scale LMS (BLMS) equalizer was also studied. Similar to the NLMS case, an accurate BER expression for the BLMS equalizer was also derived. Additionally, situations were investigated where the non-Wiener characteristics of the NLMS equalizers can be leveraged. Overall, this dissertation hopes to add to the existing body of work that pertains to the analysis of non-Wiener effects of NLMS equalizers and thus, in general, to the work related to analysis of adaptive equalizers.

DEDICATION

To my parents… Mr. Amitava Roy and Mrs. Sanchita Roy

ACKNOWLEDGEMENTS

This dissertation marks the end of a long and eventful journey and thus it is an appropriate time to thank everyone who helped along the way. I consider myself extremely fortunate to have Dr. A. A. (Louis) Beex as my advisor who was a constant source of support and inspiration during this arduous journey. Thank you, Dr. Beex for teaching me the systematic way of approaching a problem as well as presenting the results in an aesthetic way.

I would like to thank my committee members - Dr. Jeffrey H. Reed, Dr. Harpreet S. Dhillon, Dr. William T. Baumann and Dr. Mazen Farhood for their valuable feedback regarding this work.

Without the support and persistent encouragement from my family, this dissertation (and many other things) would not reach its fruition. So thanks again Maa, Baba, and Dr. Titas Roy - my sister - for your relentless support every time I needed reassurance.

Recently, I had the chance to collaborate with Dr. Timothy O'Shea. I want to thank him along with the team at Hume Center for presenting me with the opportunity

Dr. Sreyoshi Bhaduri - thank you for being there for me on this journey and sharing yours with me. From choosing the right career trajectory to a suitable attire for an interview - your suggestions have been invaluable.

I have been lucky to be in contact with great teachers during different phases of my life. Thank you, Dr. Debasis Barman for in nurturing my interest in Mathematics, Dr. Amitava Chatterjee, and Professor Sugata Munshi for their guidance during my under graduate studies at Jadavpur University, Dr. Sunanda Mitra for setting the foundation for my graduate research at Texas Tech University and Dr. Dhruv Batra for introducing me to the wonderful world of Machine Learning.

A special shout-out to all my friends scattered around the globe - Gourab, Poulomi, Debayan. Debsubhra, Debarshi, Shubham, Satyajit, Shuvodeep, Richa, Prateek and Nirmalya. Thank you for all the memorable discussion which were the most productive distractions anyone can ever hope for.

Finally, I would like to thank Dr. Santanu Das, for believing in my capabilities even before I myself was aware of them, and for his motivation and guidance throughout this entire journey.

“All models are wrong; some models are useful.”

- George Box

TABLE OF CONTENTS

LIST OF FIGURES

LIST OF TABLES

CHAPTER 1 INTRODUCTION

This chapter provides the necessary background for this work and motivates the research problem. A brief background regarding adaptive equalization and narrowband interference is presented first, followed by a literature review highlighting the relevant works that dealt with the non-Wiener characteristics of the adaptive LMS class of equalizers. The contribution of this work to the domain of the problem is summarized in Section 1.3. Lastly, Section 1.4 contains the mapping for the remainder of the document.

1.1 Background

Continuous Wave (CW) interferers and their mitigation techniques have been an active area of research for decades. One of the earliest works addressing the issue of CW interference dates back to 1941 [1]. For modern digital communication systems, unmodulated carrier signals caused by either malfunctioning devices or accidental and deliberate (tone jamming) transmissions are a common type of CW interference. For example, recent literature shows the vulnerability of GPS receivers to CW interferers [2-6]. The expected proliferation of Internet-of-things (IoT) devices will exacerbate the problem of CW interference due to unmodulated carrier signals.

Adaptive least mean square (LMS) equalizers have been widely used in various communications systems [7-11]. The popularity of LMS equalizers can be attributed to their ease of implementation and lack of dependence on the a priori knowledge of signal statistics. Prior work has already shown that in the presence of a strong CW interferer, LMS equalizers exhibit non-Wiener characteristics such as outperforming the corresponding Wiener equalizer – the optimal solution as per linear filtering theory – in terms of mean square error (MSE). However, there is very little work in the existing literature that deals with the analysis of the bit error rate (BER) – a more practical metric for characterizing the performance of a digital communication system than MSE – of LMS equalizers operating in the presence of a CW interferer.

The primary focus of this dissertation is to model the BER behavior of the LMS class of equalizers in the presence of a strong CW interferer – a situation where LMS equalizers exhibit non-Wiener characteristics.

1.2 Related Work

To our best knowledge, adaptive equalization for digital communication systems was first proposed by Lucky [12]. His work was based on minimizing the peak distortion criterion. Concurrently, Widrow et al. [13] devised the (LMS) algorithm which was computationally simple and converged to the optimal Wiener solution. Proakis and Miller [14] showed an adaptive receiver based on the LMS algorithm which was capable of adjusting to unknown slowly time-varying channel conditions. An excellent summary of adaptive equalization techniques is presented by Qureshi [15].

The primary objective of an equalization technique is to undo the unwanted effect of the channel characteristic – inter-symbol interference on the received communication signal. Although Qureshi [15] mentions that any technique employed to reduce inter-symbol interference can be considered an equalization technique, equalization can be viewed in general as a mitigation technique. In this work, our focal point will be modeling the performance of digital communication systems where narrowband interference has been suppressed by adaptive equalizers, more specifically by adaptive LMS or NLMS equalizers.

There has been a substantial amount of work regarding suppression of narrowband interference. Milstein [16] in his work gives a brief summary of methods for rejecting interference in spread spectrum communication systems, emphasizing primarily two schemes: 1. LMS based and 2. Transform domain processing structure based. Laster and Reed [17] provide a comprehensive survey of interference rejection methods for both spread spectrum and non-spread spectrum communication systems. Poor [18] gives a detailed account of various interference mitigation schemes based on different techniques, such as linear predictive methods, non-linear predictive methods, linear code aided methods, etc. Batra [19] examines the effect of severe narrowband interference on a

wireless communication system and proposes two novel methods: 1. Data-aided Initialization (DAI) and 2. Two stage filtering, which utilizes a prediction error filter (PEF) as a pre-filter to the equalizer, for faster convergence of the adaptive equalizer weights.

Adaptive LMS equalizers were seen to behave 'unconventionally' in the presence of a narrowband interference, as was first observed by North, Axford, and Zeidler [20]. The term 'unconventional' demands special attention.

Conventional adaptive filtering suggests the Wiener filter as the appropriate benchmark against which the performance of the adaptive filter is measured [21]. In this work, we are interested in LMS equalizers for which the Wiener equalizer is considered to provide the lower bound on performance (in terms of mean square error) for a LMS equalizer since the LMS algorithm is subject to misadjustment error due to weight adaptation. For this reason, traditionally LMS equalizers are implemented with small step-sizes. North, Axford, and Zeidler [20] observed that the performance of LMS equalizers was superior in terms of probability of error to the corresponding Wiener equalizer with the same structure in an environment dominated by narrowband interference. This effect will be referred to as a non-Wiener characteristic of adaptive LMS equalizers.

The topic of this dissertation is to analyze the bit error rate (BER) behavior of the (N)LMS equalizer in the presence of a strong narrowband interference, i.e. a scenario when the LMS equalizer is exhibiting non-Wiener behavior. Thus, it makes intuitive sense to review the literature that pertains to the analysis of the non-Wiener behavior. Reuter and Zeidler [22] demonstrated that the steady state Mean Square Error (MSE) of LMS equalizers can better the corresponding Wiener equalizer of the same structure. In this work [22] an attempt to model the non-linear nature of the LMS algorithm and to quantify the MSE performance of the LMS algorithm was made. However, the experimental results and the theoretical results did not coincide, pointing to limitations in the model. In subsequent works [23-25] was shown that LMS may outperform the corresponding Wiener filter and that the performance is dependent on system parameters

such as Signal to Noise Ratio (SNR), Signal to Interference Ratio (SIR), length of the equalizer, and the adaptation step-size.

Beex and Zeidler [26] modeled the interference canceller as a two channel Wiener filter with the interference signal as the input to the second channel. This work [26] showed that the adaptive NLMS filter is trying to track a time-varying target solution. Hence, the second characterization of non-Wiener effects is the time-varying nature of the filter weights. This two-channel model explanation was shown to apply to Recursive Least Squares (RLS) adaptation as well [27] and to adaptive noise cancellation [28].

Conventional adaptive filtering theory posits that the steady state weights for LMS equalizers converge to the corresponding Wiener weights. Ikuma, Beex, and Zeidler [29] derived a closed form expression for the mean of the LMS weight vectors in steady state. The expression was derived from the Butterweck expansion of the weight update equation [30]. Simulation results were in conformity with the analytical results for all step-sizes where the expansion converges. In a subsequent work [31] it was shown that the analytical solution holds true over a wide range of ISR.

Reuter and Zeidler [22] first proposed a transfer function based approach to quantify the MSE performance of LMS equalizers. The results were inaccurate since the model assumed that the mean of the LMS weights in steady state converged to the corresponding Wiener weights which, as shown in [29, 31], is not the case. Hence, the Reuter-Zeidler model for the MSE was not an accurate one. Ikuma and Beex [32] incorporate the shift in the mean of the steady state weights and proposed a new model for MSE. Simulation results illustrate the improvement of the new model over the previous Reuter-Zeidler model. The derivations for the mean LMS weights in steady state and the improved MSE model have been excellently documented [33].

Although there has been substantial past work on analyzing the dynamic weight behavior and the mean square error performance of the (N)LMS equalizer there is scant coverage in the literature that deals with BER modeling in a non-Gaussian environment. North, Axford, and Zeidler [20] compared the performances of different adaptive

equalizers in terms of probability of error. However, the error probability was computed via simulation and no model was proposed.

Prior to [20], Iltis and Milstein [34] provided a statistical analysis of the LMS algorithm where the adaptive filter was used to suppress a fading tone jammer. Their work provided a BER model while inherently assuming slow convergence (i.e. a near Wiener case) and a large equalizer length. In this thesis, we are primarily interested in large step-sizes where the non-Wiener characteristics are predominant. A Gaussian BER approach was also adopted [35]. However, no simulation results were provided to support the claims.

Coulson [36] investigates the effect of narrowband interference on OFDM systems. An analytical Gaussian model is provided to gauge the effect of the narrowband interference on receiver post detection BER performance. However, no analytical model is put forward to estimate the post interference suppression BER. Instead, a heuristic method to estimate the BER is provided where the latter is simply the ensemble median of the simulation results.

The BER for a fixed (time-invariant) Wiener filter equalizer under a strong narrowband interference was shown to be accurately predictable using the expression for the probability density function of the symbol-conditioned equalizer output, which took the form of a sum of Gaussians [37]. However, when the same model was extended for the adaptive NLMS case [38], the performance was reasonable for low step-sizes only. With the increase in step-size (which is the area of interest here, since it produces better BER performance), the BER obtained from the model deviated from the simulation result by an order of magnitude.

Scant coverage of modeling the BER behavior of (N)LMS equalizers in the existing literature, coupled with the fact that BER serves as a more practical metric for measuring the performance of a digital communication system than MSE, is the primary motivation for this dissertation. From a broader perspective this dissertation adds to the existing body of work related to analysis of adaptive equalizers such as, analysis for sinusoidal interference mitigation [39], arbitrary step-sizes [40], non-negative LMS [41], presence

of non-Gaussian noise [42-44], combination of LMS filters [45], and so on. There also has been a significant amount of work in analyzing other adaptive algorithms [46-49]. With a brief overview of related work in place, the next section highlights the contribution of this dissertation.

1.3 Contributions

The primary contribution of this work is to come up with a model for the BER behavior of the NLMS equalizer operating in the presence of a strong narrowband CW interference. Simulation results show that the model is accurate over a wide range of SNR, ISR, and interference frequency. The model also gives insight into the non-Wiener behavior of the equalizer and quantifies the superior BER performance at higher step-sizes in the presence of a strong narrowband interference.

The second contribution of this work is the in-depth analysis of the Bi-scale NLMS (BNLMS) equalizer, which also exhibits non-Wiener characteristics in the presence of a strong narrowband interference. In fact, in terms of MSE and BER performance, the Bi-scale NLMS equalizer outperforms NLMS. The performance gain, both in terms of MSE and in terms of BER, is analyzed and a closed form model for each is derived. Similar to the NLMS case, the models developed to assess the BNLMS equalizer performance provided accurate estimates for both MSE and BER for a wide range of system parameters.

1.4 Organization

This document has five chapters excluding Chapter 1. In Chapter 2 a description is provided of the system under consideration along with a description of the signals involved. In Chapter 3, the BER models for NLMS equalizers are derived and compared with simulation results. Chapter 4 contains an in-depth analysis of the Bi-scale LMS equalizer where both a steady state Mean Square Error (MSE) model and a BER model are derived and compared with simulation results. Situations where the proposed BER

models in Chapters 3 and Chapter 4 fail are analyzed in Chapter 5 along with the formulation of a corrected model. Chapter 6 introduces the two-interferer problem where the case studies show that similar to the single interferer case the non-Wiener characteristics of NLMS equalizers are present. Finally, concluding remarks – along with directions for future research – are presented in Chapter 7.

CHAPTER 2 NON WIENER EFFECTS IN NLMS EQUALIZATION

This chapter lays the foundation for the analysis by formally defining the problem and introducing the important notations, assumptions, and expressions, which will be used extensively throughout this work.

Section 2.1 introduces the adaptive equalization problem and gives an overview of the system with the input signals and assumptions, followed by Section 2.2 where the stochastic properties of the input signals are discussed. Section 2.3 contains the expressions for the optimal Wiener weights and the Wiener MSE. Sections 2.4 and 2.5 describe steady state weight and steady state MSE respectively for NLMS equalizers.

Finally, Section 2.6 motivates the importance of the problem at hand – developing a BER model when the NLMS equalizer is operating in a narrowband interference dominated environment. Simulation examples are provided specifically to distinguish between the MSE and the BER behavior of the NLMS equalizer.

2.1 Adaptive equalization problem

Figure 2.1 shows the system under consideration. The desired signal (d_n) is transmitted through the channel and corrupted by additive Gaussian white noise (v_n) and a narrowband interference (i_n), which is also additive in nature. Thus, at the *n*-th time instant the input to the adaptive equalizer (u_n) can be written as the sum of three independent random processes as shown in (2-1).

$$u_n = \tilde{d}_n + v_n + i_n \tag{2-1}$$

where $\tilde{d}_n$ is defined as:

$$\tilde{d}_n = h_n * d_n \tag{2-2}$$

with h_n being the channel impulse response.

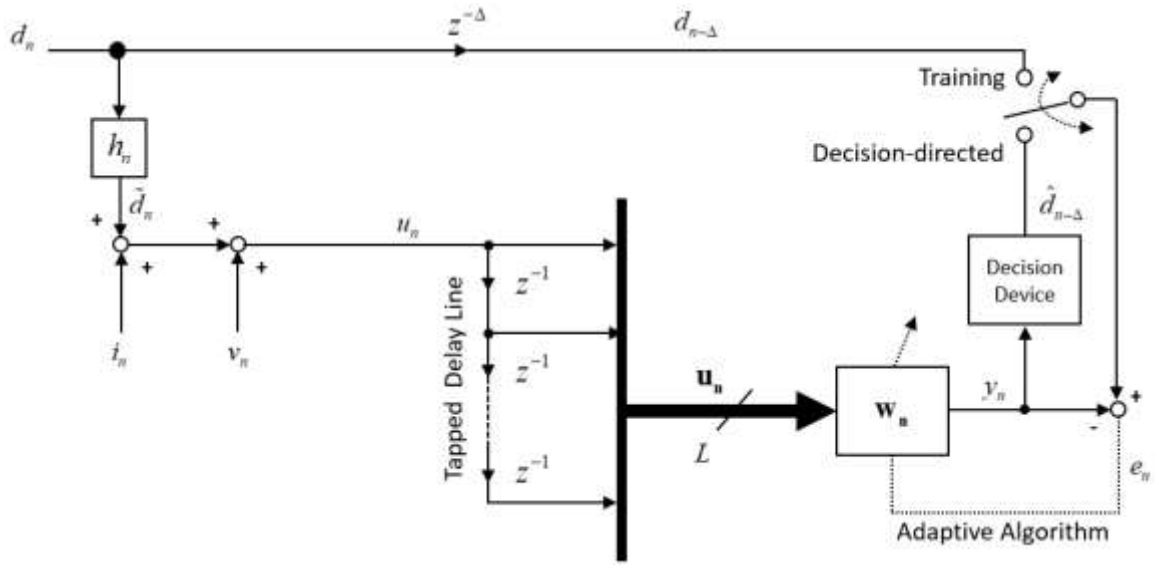

Figure 2-1: Block diagram of an adaptive equalizer.

The focus of this work is to study the system behavior in the presence of a narrowband interference. Since decision-direction equalization (DDE) assumes that the BER is "small enough" (e.g. <0.01), for our purposes of analysis the equalizer will operate in training mode. The channel h_n is considered ideal, i.e. $\tilde{d}_n = d_n$. This simplified system is similar to the one used in [20, 31-33, 37]. For non-ideal channel conditions, the assumption is that channel compensation has already been achieved (for example, based on the channel estimate derived from a/the previous packet transmission). Even when the channel is compensated, the problem of a narrowband interferer can arise which necessitates the need for an adaptive equalizer to realize interference mitigation. For example, if a narrowband IoT (NBIoT) device is malfunctioning (it is only transmitting the carrier) this may give rise to a narrowband interference at the receiver and – since the power and the frequency of the interference is unknown – an adaptive filter is required. With these assumptions in place, Figure 2-2 shows the corresponding simplified block diagram for the problem under consideration. Thus, the input to the adaptive equalizer given in (2-1) can be modified to:

$$u_n = d_n + v_n + i_n \tag{2-3}$$

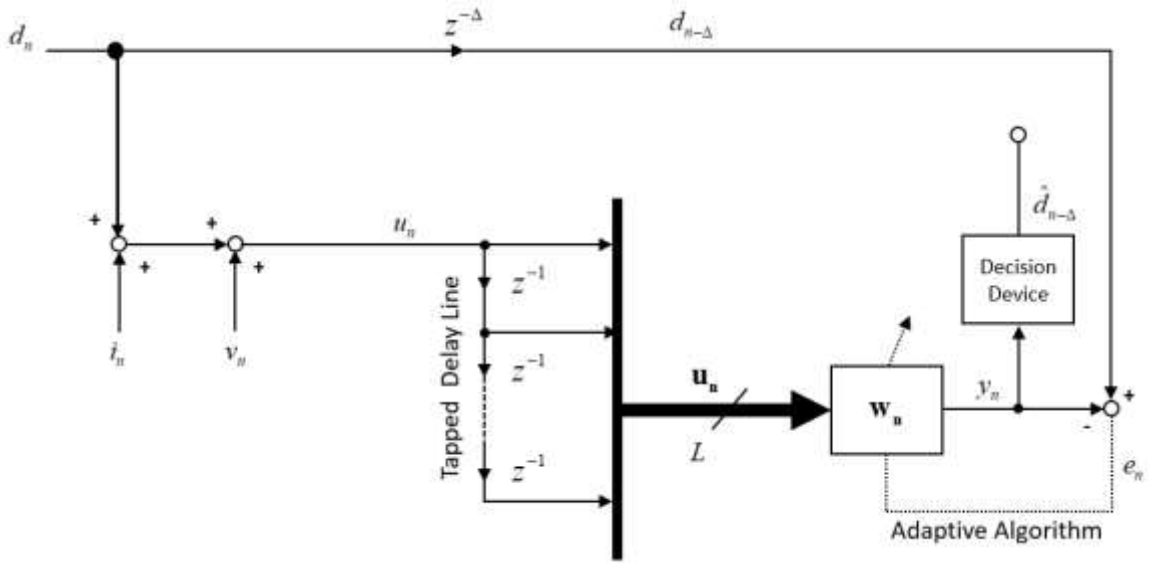

Figure 2-2: Simplified block diagram of an adaptive equalizer.

The tapped delay line adaptive equalizer is characterized by its weight vector $\mathbf{w_n} = \begin{bmatrix} w_{0,n} & w_{1,n} & \cdots & w_{L-1,n} \end{bmatrix}^T$, $(.)^T$ being the transpose operator, and has L tunable taps. The equalizer output y_n is given by (2-4),

$$y_n = \mathbf{w_n^H u_n} \tag{2-4}$$

where $(.)^H$ denotes the Hermitian transpose operator and $\mathbf{u_n} = \begin{bmatrix} u_n & u_{n-1} & \cdots & u_{n-L+1} \end{bmatrix}^T$ is the input vector containing the current input (u_n) along with the previous $L-1$ inputs.

For this work, the desired signal (d_n) is considered a complex baseband signal that assumes a value drawn from a finite set of constellation values. The finite set is completely defined by the modulation scheme used. Since the analysis is done at baseband, the Gaussian noise (v_n) is modeled by a complex Gaussian distribution.

$$v_n \sim CN\left(0, \sigma_v^2\right) \tag{2-5}$$

where $\chi \sim CN(m, 2s^2)$ indicates that χ is a complex normal random variable, or a real vector random variable with mean $m = \begin{bmatrix} \mathrm{Re}\{E(\chi)\} \\ \mathrm{Im}\{E(\chi)\} \end{bmatrix}$ and covariance $\begin{bmatrix} s^2 & 0 \\ 0 & s^2 \end{bmatrix}$.

Similar to the work done in [33] the narrowband interference is modeled by a complex sinusoid with a random phase as indicated in (2-6).

$$i_n = \sigma_i e^{j(2\pi f_i n + \theta)} \tag{2-6}$$

where $j = \sqrt{-1}$, f_i is the fractional frequency, and θ is a random phase drawn from a uniform distribution $[0, 2\pi)$. The stochastic properties of these inputs are discussed in detail in the next section.

As mentioned earlier, the adaptive equalizer has *L* tunable taps which are updated according to the NLMS update equation as given by (2-7).

$$\mathbf{w_{n+1}} = \mathbf{w_n} + \frac{\mu}{a + \|\mathbf{u_n}\|^2} \mathbf{u_n} e_n^* \tag{2-7}$$

where μ is the step-size, $\|.\|$ is the Euclidean norm, a is the regularization parameter, $(.)^*$ denotes the complex conjugate operator, and e_n is the instantaneous error described by (2-8).

$$e_n = d_{n-\Delta} - y_n \tag{2-8}$$

For stable operation of the equalizer the value of μ should be selected from $(0, 2)$. The regularization parameter is present to prevent division by zero (or a very small number) during practical implementation. For analysis purposes, the regularization parameter can be set to 0. Δ is the point of equalization and usually taken to be in the middle of the tapped delay line, i.e. $\Delta = \frac{L+1}{2}$, but any value in the range 0 to *L*-1 is permissible.

2.1.1 BER problem statement

With these definitions and notations in place, the problem of interest can now be defined. Let $\{\phi_m\}_{m=1}^{M}$ be the set of *M* distinct symbols of the modulation scheme chosen, then obtaining an expression for the conditional distribution of $y_n \mid d_{n-\Delta} = \phi_m$ and specifying the regions of interest that contribute bit error will be sufficient to compute the BER of the system. Note that the aforementioned "regions of interest" are determined by the decision device (Figure 2-2). For example, if the modulation scheme chosen is QPSK and ϕ_m is the first quadrant symbol then for this case the entire $\Re^2$ except for the first quadrant constitutes regions that will contribute to a single (second or fourth quadrant) or multiple (third quadrant) bit errors.

2.2 Stochastic properties of the input signals

One of the primary goals of this work is to find a conditional probability distribution. So it is essential to know the stochastic properties of the input signals. Since the analysis is done at baseband all the input signals are modeled as complex random processes that are zero-mean, wide sense stationary (WSS), mean ergodic, and proper [50].

The desired signal d_n is assumed to be a white process, i.e. there is no inter-symbol interference. The transmit power is denoted by σ_d^2. As stated earlier, d_n takes on one of the equally likely *M* symbols from the alphabet $\{\phi_m\}_{m=1}^{M}$ of the chosen modulation scheme. Thus, d_n follows a discrete uniform distribution with the auto-correlation function shown in (2-9).

$$r_{d,l} = \sigma_d^2 \delta_l \tag{2-9}$$

where *l* is the lag and δ_l is the Kronecker delta function, which equals 0 except for at $l = 0$, where it equals 1. The noise v_n is also white, with power σ_v^2 and the auto-correlation function given in (2-10).

$$r_{v,l} = \sigma_v^2 \delta_l \tag{2-10}$$

The narrowband interference as defined by (2-6) has a power of σ_i^2. The interference auto-correlation function is given in (2-11).

$$r_{i,l} = \sigma_i^2 e^{j\omega_i l} \tag{2-11}$$

where $\omega_i = 2\pi f_i$ is the angular interferer frequency. Combining (2-9), (2-10) and (2-11), the auto-correlation function of the input u_n to the equalizer is given in (2-12).

$$r_{u,l} = \left(\sigma_d^2 + \sigma_v^2\right)\delta_l + \sigma_i^2 e^{j\omega_i l} \tag{2-12}$$

This result directly follows from the fact that the input signals d_n, v_n, and i_n are independent and zero-mean.

2.3 Wiener Equalizer

The optimal weight vector $\mathbf{w_w}$ is obtained by solving the Wiener-Hopf equation given in (2-13):

$$\mathbf{E}\left[\mathbf{u_n}\mathbf{u_n^H}\right]\mathbf{w_w} = \mathbf{E}\left[\mathbf{u_n} d_{n-\Delta}^*\right] \tag{2-13}$$

The resulting Wiener filter is [33]:

$$\mathbf{w}_w = \eta\left(\mathbf{p}_\Delta - \tilde{\mathbf{w}}_w\right) \tag{2-14}$$

where

$$\eta \triangleq \frac{\sigma_d^2}{\sigma_d^2 + \sigma_v^2} \tag{2-15}$$

$$\mathbf{p}_{\Delta} = \left[\underbrace{0 \quad \cdots \quad 0}_{\Delta} \quad 1 \quad 0 \quad \cdots \quad 0 \right]^{T} \qquad \text{(2-16)}$$

$$\tilde{\mathbf{w}}_{w} = \frac{\sigma_i^2}{\lambda_{\max}} \mathbf{e} \qquad \text{(2-17)}$$

and

$$\mathbf{e} \triangleq e^{j\omega_i \Delta} \left[1 \quad e^{-j\omega_i} \quad \ldots \quad e^{-j\omega_i (L-1)} \right]^{T} \qquad \text{(2-18)}$$

$$\lambda_{\max} \triangleq L\sigma_i^2 + \sigma_v^2 + \sigma_d^2 \qquad \text{(2-19)}$$

The Wiener MSE is given by:

$$J_W = \eta \left(\sigma_v^2 + \sigma_d^2 \frac{\sigma_i^2}{\lambda_{\max}} \right) \qquad \text{(2-20)}$$

2.4 Steady state NLMS weights

For most applications, using small step-sizes, the LMS algorithm converges to approach the performance of the corresponding optimal Wiener filter [51]. However, in a narrowband interference dominated environment the LMS equalizer can outperform the optimal Wiener filter of the same FIR structure as the adaptive filter. It is non-intuitive that in a narrowband interference-dominated environment the weight vector will converge to something other than the Wiener weights given in (2-14). An expression for the steady state (N)LMS weights in a narrowband interference dominated environment has been derived [31, 33].

The steady state NLMS weight vector $\bar{\mathbf{w}}$ can be expressed [33] as:

$$\bar{\mathbf{w}} = \eta(\mathbf{p}_{\Delta} - \tilde{\mathbf{w}}) \qquad \text{(2-21)}$$

where $\tilde{\mathbf{w}}$ is given by (2-22):

$$\tilde{\mathbf{w}} = \left(\mathbf{I}_L - \frac{\mu}{L(\sigma_v^2 + \sigma_i^2 + \sigma_d^2)} \mathbf{R}_{\mathbf{u}}^{-1} \mathbf{Q} \right)^{-1} \tilde{\mathbf{w}}_w \tag{2-22}$$

where $\mathbf{I}_L$ denotes the $L \times L$ unit matrix, and $\mathbf{R}_{\mathbf{u}} \triangleq E\left\{ \mathbf{u_n} \mathbf{u_n^H} \right\}$ is the input auto-correlation matrix given in (2-23).

$$\mathbf{R}_{\mathbf{u}} = \left(\sigma_d^2 + \sigma_v^2 \right) \mathbf{I}_L + \sigma_i^2 \mathbf{e} \mathbf{e}^{\mathbf{H}} \tag{2-23}$$

The expression for $\mathbf{Q}$ in (2-22) is given by (2-24):

$$\mathbf{Q} \triangleq \sigma_v^2 \sigma_i^2 L \sum_{p=1}^{L-1} \mathbf{Z}^p e^{-j\omega_i p} \gamma^{p-1} \tag{2-24}$$

where

$$\gamma \triangleq 1 - \mu \lambda_{\max} \tag{2-25}$$

and $\mathbf{Z}$ is a unit lower triangular Toeplitz matrix:

$$\mathbf{Z} = \begin{bmatrix} \mathbf{0_{L-1}} & 0 \\ \mathbf{I_{L-1}} & \mathbf{0_{L-1}^T} \end{bmatrix} \tag{2-26}$$

with $\mathbf{0_{L-1}} = \begin{bmatrix} 0 & 0 & \ldots & 0 \end{bmatrix}$ a row vector containing $(L-1)$ zeros.

2.5 Steady state Mean Square Error

In previous work, such as [24, 32, 33], different expressions for the steady state Mean Square Error (MSE) estimate have been proposed. Although the focus of this work is on BER, it is important to refer to the MSE estimate for a couple of reasons. Firstly, the MSE analysis encompasses the previous endeavors regarding explaining the non-Wiener characteristics of the NLMS filter.

Secondly, the expressions for the MSE provide the necessary background for the analysis done in Section 2.6, which highlights the differences between the MSE and BER performances of the equalizer and factor(s) that affect these metrics. As shown [32], the Ikuma model MSE estimate is more accurate for a narrowband interference-dominated environment than the Reuter-Zeidler model MSE estimate [24]. The Ikuma model estimate for steady state MSE for a NLMS equalizer, J_N, is given by:

$$J_N = \frac{2\eta}{1+\alpha}\left[\sigma_v^2 + \sigma_d^2\left\{\left\|\tilde{\mathbf{w}}\right\|^2 - (1-\alpha)\left|\tilde{\mathbf{w}}\right|^T \mathbf{A}\left|\tilde{\mathbf{w}}\right|\right\}\right] \tag{2-27}$$

where

$$\alpha \triangleq 1 - \mu\frac{\sigma_i^2}{\sigma_i^2 + \sigma_v^2 + \sigma_d^2} \tag{2-28}$$

$\left\|.\right\|^2$ is the Euclidian Norm, $\left|.\right|$ denotes the absolute value, and $\mathbf{A}$ is given by (2-29).

$$\mathbf{A} \triangleq \begin{bmatrix} 0 & & \cdots & & 0 \\ 1 & 0 & & & \\ \alpha & 1 & \ddots & & \vdots \\ \vdots & & \ddots & 0 & \\ \alpha^{L-2} & \cdots & \alpha & 1 & 0 \end{bmatrix} \tag{2-29}$$

2.6 Comparison between MSE and BER behavior of NLMS equalizer

The non-Wiener characteristics exhibited by the NLMS equalizer operating in a narrowband interference dominated environment have been studied in depth. Prior work explains the phenomenon for different situations and, as described in Sections 2.4 and 2.5, there is a closed form expression for the steady state NLMS weights and steady state MSE. However, despite having all these efforts already in place, there has been no reported work on the performance of the equalizer in terms of BER. In this section, differences between the MSE and BER behavior of the equalizer are highlighted.

Figure 2-3 shows the MSE performance of a NLMS equalizer as a function of step-size μ. An equalizer length of $L = 5$ was chosen and the equalization point set as $\Delta = 0$. The signal to noise ratio (SNR) was set to 25 dB and the interference to signal ratio (ISR) was set to 20 dB, for an interference frequency $f_i = 1/e$. 100,000 independent QPSK symbols were chosen from $\phi = \left\{ e^{\pi/4},\ e^{3\pi/4},\ e^{5\pi/4},\ e^{7\pi/4} \right\}$ as the desired signal of interest d_n. 100 independent realizations were run for each of the step-sizes and the ensemble average of the MSE is shown in Figure 2-3. The performance for the corresponding Wiener Filter of the same structure is shown in red.

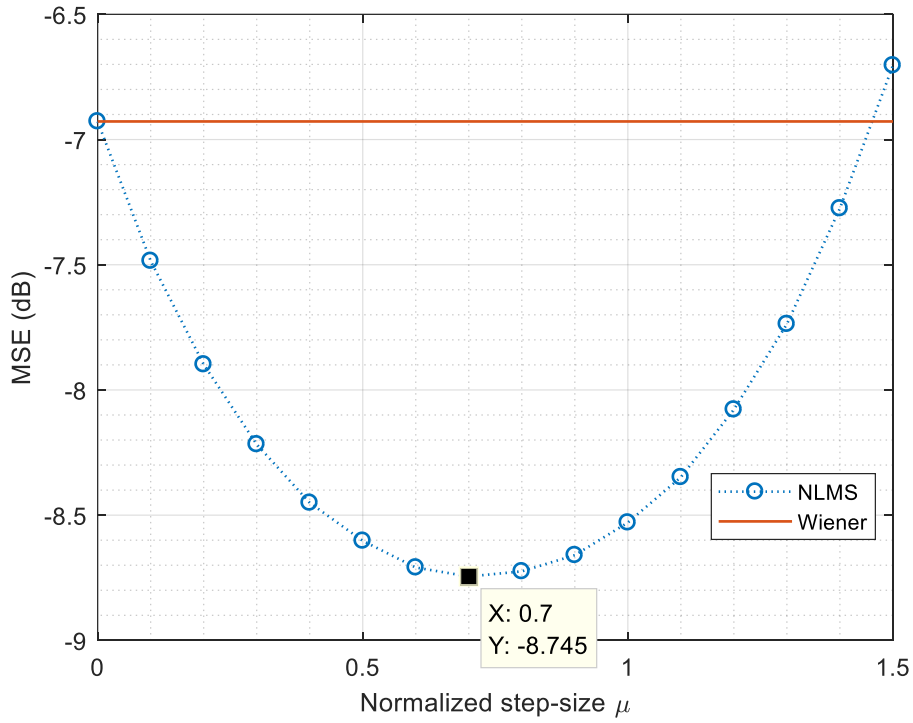

Figure 2-3: MSE performance for NLMS equalizer with *L* = 5, ISR = 20 dB, and SNR = 25 dB.

Figure 2-3 shows an improvement of ~1.75 dB for a step-size of $\mu = 0.7$. Note that the step-size μ was increased in increments of 0.1. It might be possible that the optimal MSE behavior occurs between $\mu = 0.7$ and $\mu = 0.8$. For this discussion the performance at $\mu = 0.7$ is taken to be the optimal MSE performance of the equalizer. Figure 2-4

shows the BER behavior of the same equalizer. All the parameters were kept the same as the ones used to generate Figure 2-3.

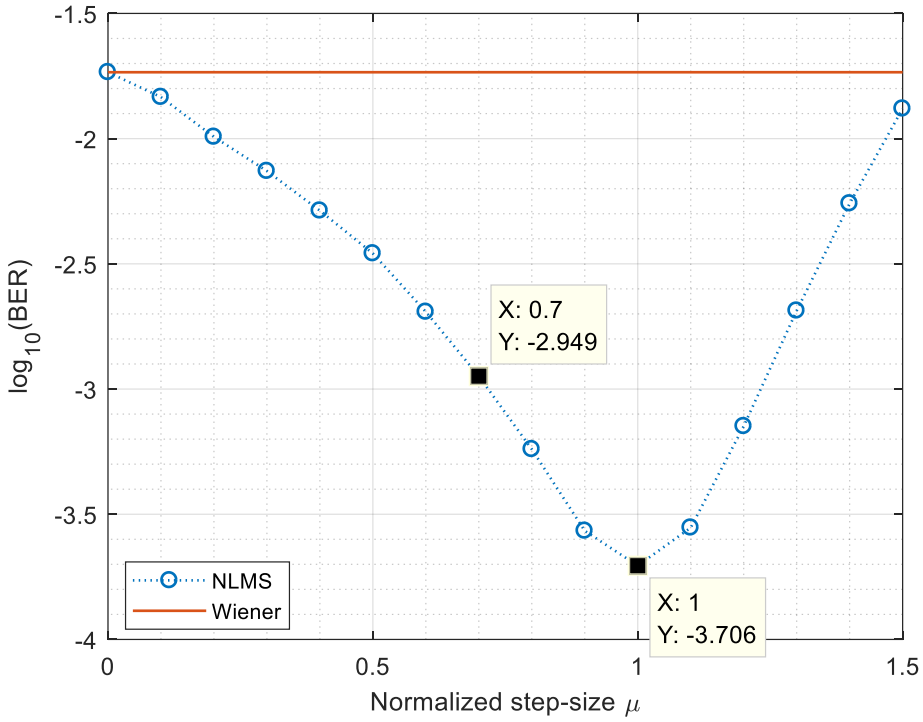

Figure 2-4: BER performance for NLMS equalizer with *L* = 5, ISR = 20 dB, and SNR = 25 dB.

Figure 2-4 shows that the non-Wiener effect is also reflected in the BER performance of the equalizer. An improvement of 2 orders of magnitude is seen for a step-size $\mu = 1$ compared to the fixed Wiener filter of the same structure. Note that the optimal BER performance takes place at a different step-size, $\mu = 1$, than the optimal MSE performance, which was for step-size $\mu = 0.7$. At $\mu = 0.7$ the BER is 11×10^{-4} $\left(= 10^{-2.949}\right)$, which translates to 11 errors out of 10,000 bits. At $\mu = 1$ the BER is 1.97×10^{-4} $\left(= 10^{-3.706}\right)$, which is the optimal performance of the equalizer in terms of BER. This implies 2 errors out of 10,000 bits or an approximately 5 times better performance than for the equalizer operating with $\mu = 0.7$.

The above example shows that although the non-Wiener effect can be observed both in MSE and BER performance of the equalizer, the optimal performance for each metric occurs at different step-sizes. Thus, there is a need for modeling the BER behavior explicitly instead of using the step-size for which MSE is minimized.

In Figure 2-5 the MSE performance of the NLMS equalizer is shown as a function of interference frequency f_i for six different step-sizes. The equalizer length is set to $L = 5$ and the equalization center to $\Delta = 0$. The SNR and ISR are set to 25 dB and 20 dB respectively. Similar to the simulation setup used to generate Figures 2-3 and 2-4, 100,000 independent QPSK symbols were chosen as the desired signal and the ensemble average of 100 realizations for each step-size and interference frequency combination is shown in Figure 2-5.

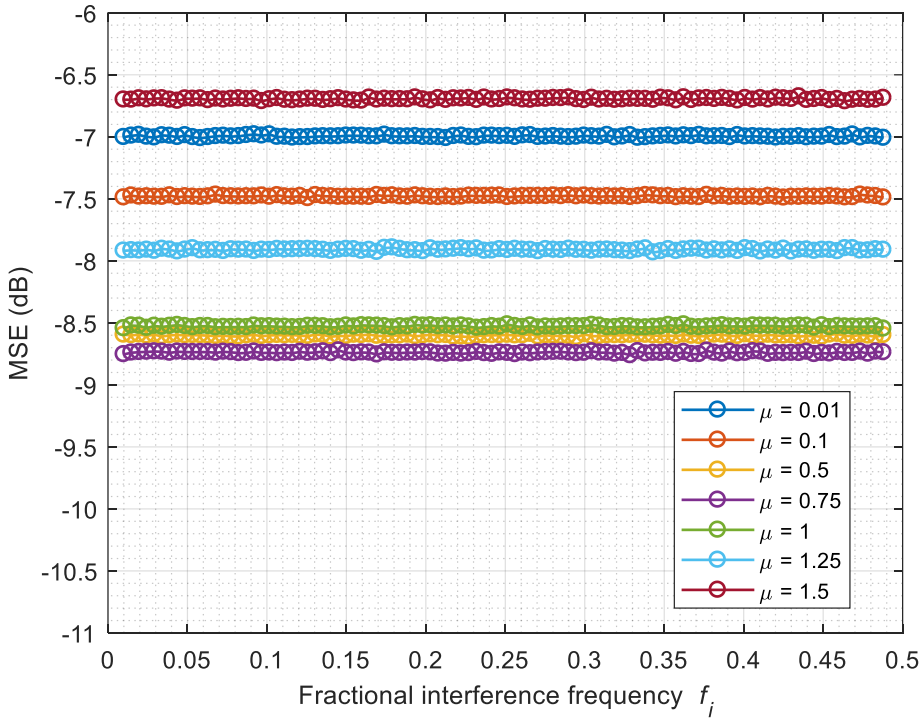

Figure 2-5: MSE vs fractional interference frequency for *L* = 5, ISR = 20 dB, and SNR = 25 dB.

From Figure 2-5, it is clear that MSE is not a function of interference frequency. This behavior is consistent with (2-27), where there is no frequency dependent term, and was

also observed in [33]. Figure 2-6 shows the BER as a function of interference frequency using the same simulation environment used to generate Figure 2-5.

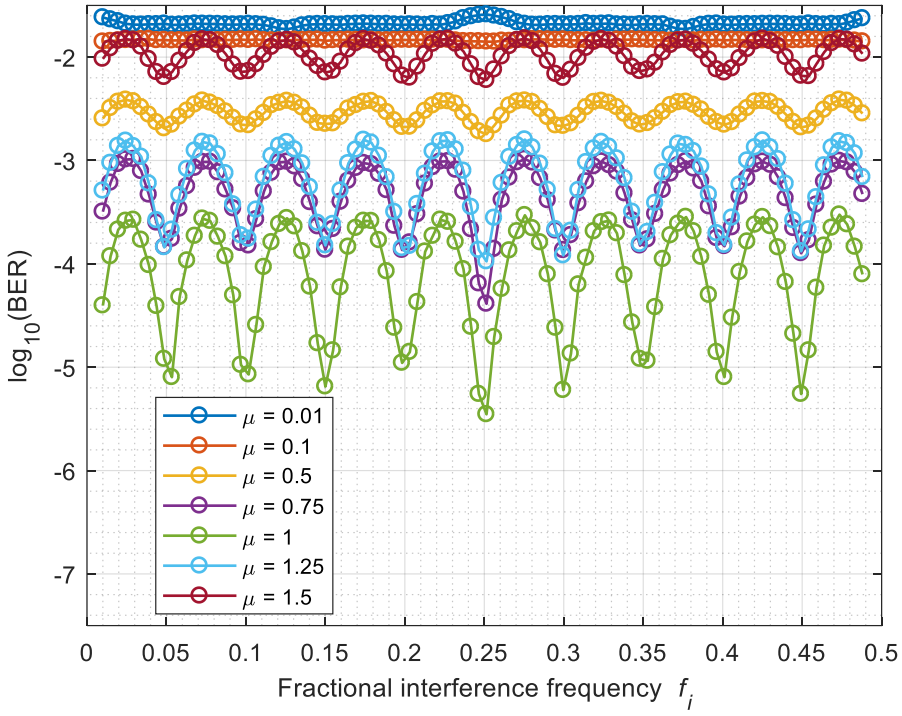

Figure 2-6: BER vs fractional interference frequency for *L* = 5, ISR = 20 dB, and SNR = 25 dB.

Figure 2-6 shows the dependence of BER performance of the NLMS equalizer on the interference frequency. For certain fractional frequencies (e.g. $f_i \approx 0.25$) changing the step-size from $\mu = 0.01$ to $\mu = 1$ can result in a BER improvement by 3 orders of magnitude. Moreover, Figure 2-5 shows that $\mu = 0.75$ is the MSE-optimal step-size for all frequencies, whereas Figure 2-6 shows that $\mu = 1$ is the optimal choice if BER is the metric. This result is also consistent with the previous example, shown in Figures 2-3 and 2-4. Thus, Figures 2-5 and 2-6 highlight a major difference between the MSE and BER behavior of the NLMS equalizer; while MSE is independent of the interference frequency, BER depends on interference frequency, which further necessitates the need for a BER model for NLMS equalizers.

2.7 Summary

In this chapter the adaptive equalization problem was formally introduced followed by the stochastic properties of the signals involved. Relevant previous work, such as that related to steady state NLMS weights and steady state MSE, is also reported. Section 2.5 provided examples to highlight the differences between the BER and MSE behaviors of the NLMS equalizer, thereby motivating the need for a separate BER model, which is the focus of the next chapter.

CHAPTER 3 BER MODELING FOR NLMS EQUALIZATION

With the problem statement defined, and the necessary information and assumptions regarding the system to be studied in place, a model is derived in this chapter for the description of the BER behavior of an NLMS equalizer operating in a narrowband interference dominated environment.

In Section 3.1 some simulation results are presented which distinguish between the output constellation $\left(y_n \mid d_{n-\Delta} = \phi_m\right)$ for a fixed filter $\left(\mu = 0\right)$, i.e. the Wiener case, and the adaptive case with a very high step-size $\left(\mu \approx 1\right)$. In Section 3.2 the BER model expression for the NLMS equalizer is derived. The derived model takes on the form of a Gaussian Sum Mixture (GSM). In Section 3.3 an approximate version of the GSM model is introduced, followed by Section 3.4 in which the performances of the proposed models are compared based on simulation results.

3.1 Behavior of the output constellation as a function of step-size

In the following case study the objective is to visualize the effect of the step-size μ on the output constellation y_n. For illustrative purposes, a communication system with QPSK modulation is chosen and the QPSK symbols are the signal of interest corrupted by AWGN with a SNR of 40 dB and a narrowband interference, with ISR 20 dB and interference frequency $f_i = 1/e$. The narrowband interference is modeled by a complex sinusoid, as in (2-6).

The equalizer length and the equalization point were set to $L = 5$ and $\Delta = 0$ respectively. Figures 3-1 a-f show the conditional output constellation $\left(y_n \middle| d_{n-\Delta} = e^{j\pi/4}\right)$ for different step-sizes along with the symbol conditioned on $\phi_m = e^{j\pi/4}$, i.e. the first

quadrant symbol for the QPSK modulation scheme, and the centroid (mean) of the conditioned constellation.

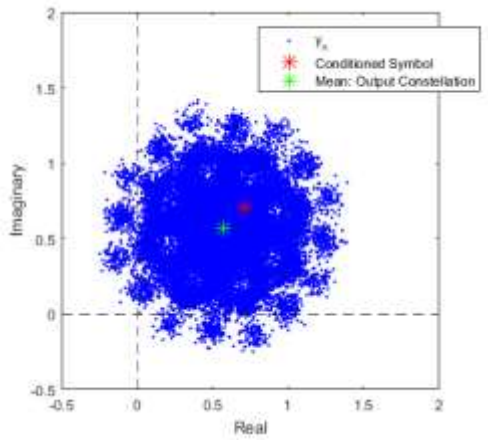

(a) μ = 0.01

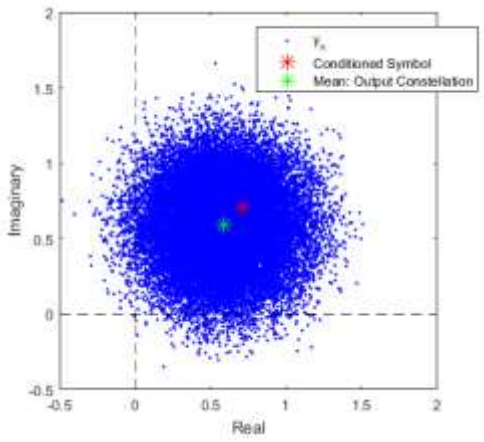

(b) μ = 0.1

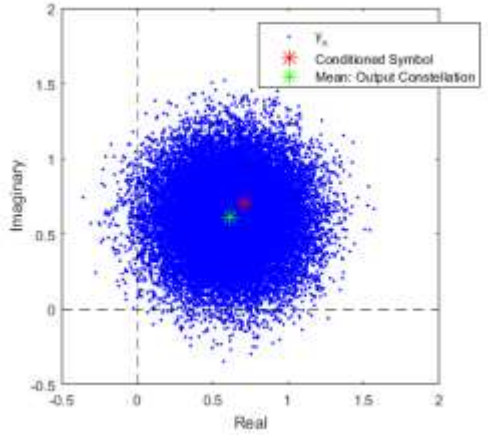

(c) μ = 0.25

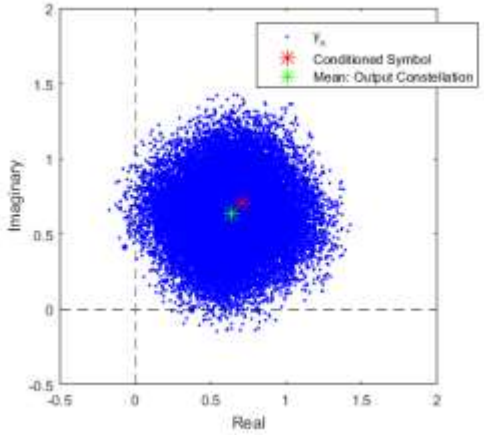

(d) μ = 0.5

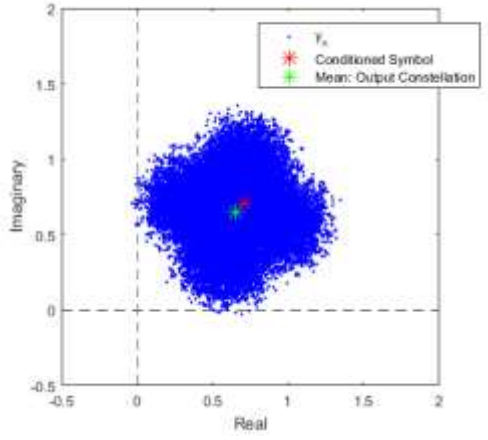

(e) μ = 0.75

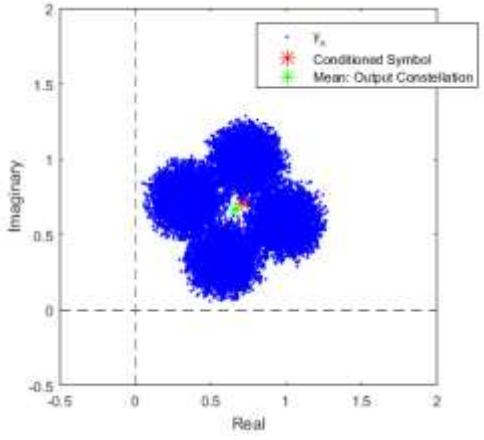

(f) μ = 1

Figure 3-1: Conditioned output constellation for different step-sizes with L = 5.

Figure 3-1a shows the output constellation for a step-size $\mu = 0.01$. The behavior of the output constellation is very similar to that in the non-adaptive FIR case [37]. This constellation was modeled accurately by a Gaussian Sum Mixture and for computational efficiency well approximated by a single Gaussian model.

Observe that with an increase in step-size the output constellation attains a circular shape in Figures 3-1b and 3-1c, i.e. for $\mu = 0.1$ to $\mu = 0.25$. This observation suggests that at these step-sizes modeling with a Gaussian distribution might be an appropriate choice as well, provided again that the mean and the covariance matrix are accurately estimated from known parameters. Further increases in step-size show another interesting phenomenon. Figures 3-1d through 3-1f show that the single Gaussian perceived in Figures 3-1b and 3-1c is morphing into four nearly circular overlapping blobs.

Figure 3-1 highlights several interesting points. Firstly, the dashed lines represent the decision boundaries. The points of the output constellation that fall in the top right quadrant will be correctly classified, whereas the other output constellation points will contribute towards bit errors.

Thus, with an increase in step-size the constellation is observed to be contracting, which results in better BER performance. This behavior suggests moving away from conventional practice where low step-sizes are used for (N)LMS equalizers. In fact, in the presence of a narrowband interference the equalizer shows the best BER performance for $\mu = 1$, in Figure 3-1f. In actuality, the optimal BER performance is achieved for $\mu = 0.9$; however, to facilitate a compact representation of behavior in the composite figure, that particular step-size is not shown in Figure 3-1.

Secondly, observe that the output constellation is not centered on the conditioned symbol. The centroid is shifted. Moreover, at higher step-sizes such as exemplified by Figure 3-1e-f, the constellation not only has a shifted mean but almost none of the mass is actually at that shifted mean. Instead, it appears that the mass is divided into four sub-clusters. This observation indicates that modeling the BER phenomenon at higher step-sizes with a single Gaussian [38] is not appropriate.

As observed earlier, in Figure 3-1f four nearly distinct blobs are seen. In order to investigate this behavior further, a BPSK system $(M = 2)$ is simulated under the same simulation environment used to generate Figure 3-1, with $\phi_m = \{e^{j\pi/4}, e^{j3\pi/4}\}$ and $\mu = 1$. Figure 3-2 shows the output constellation conditioned on $\phi_m = e^{j\pi/4}$.

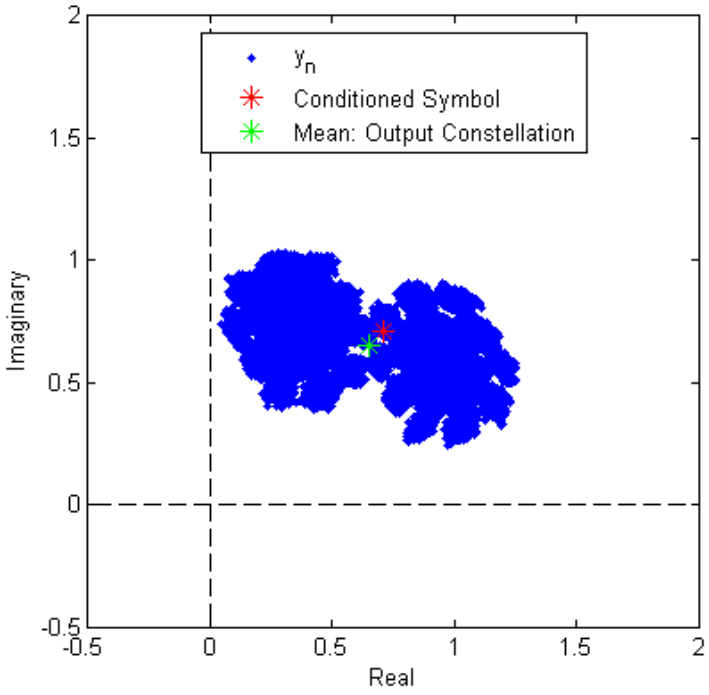

Figure 3-2: Conditional output constellation of BPSK system for μ = 1.

Figure 3-2 shows two distinct blobs, a number that corresponds to the alphabet size of $M = 2$. Figure 3-1f also follows the same trend with four distinct blobs for an alphabet size of $M = 4$. For higher step-sizes, where the output constellation morphs into separate blobs, the number of these blobs appears to be equal to the alphabet size of the modulation scheme of the communication system.

This behavior of the conditioned output constellation morphing into M blobs is the key difference between low step-sizes (e.g. $\mu = 0.01$) and high step-sizes (e.g. $\mu = 1$). Figure 3-3 compares the conditional output constellation for a QPSK modulation conditioned on $\left(y_n \middle| d_{n-\Delta} = e^{j\pi/4}\right)$ for the two step-sizes $\mu = 0.01$ (Figure 3-3a) and $\mu = 1$

(Figure 3-3b). All the simulation parameters, that were used to generate Figure 3-1, are kept the same (SNR = 40 dB, ISR = 20 dB, $f_i = 1/e$, $\Delta = 0$) except for the equalizer length L which is set to L = 3 instead of L = 5.

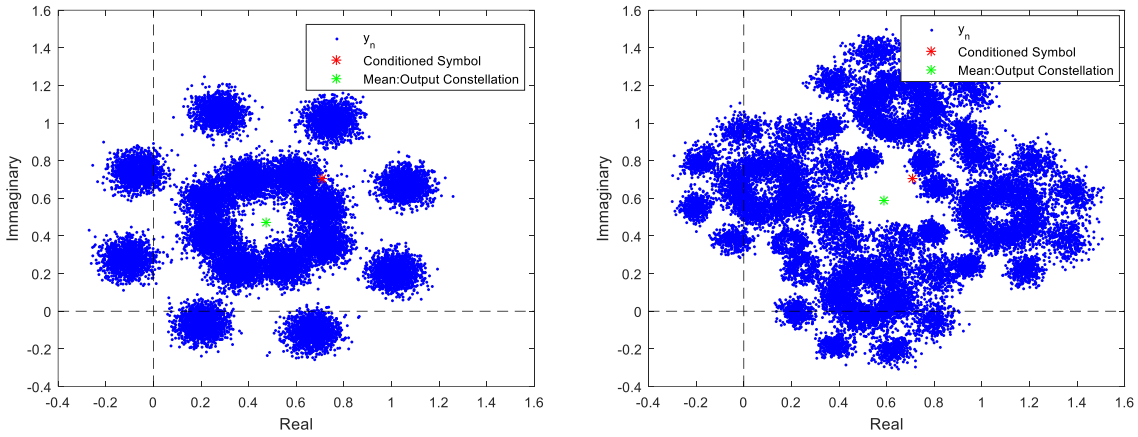

(a) μ = 0.01 **(b) μ = 1**

Figure 3-3: Conditioned output constellation for different step-sizes with L = 3.

Figure 3-3a has $M^{L-1} = 16$ blobs, with $M = 4$ and $L = 3$. This result is consistent with the fact that for small step-sizes the conditional output constellation can be modeled by a Gaussian Sum Mixture [38]. This phenomenon is also present in Figure 3-1a, but because of the larger equalizer length $L = 5$ is not as readily observable.

For a large step-size $\mu = 1$ as shown in Figure 3-3b, it is observed that the conditioned output constellation is comprised of M blobs, similar to the phenomenon observed in Figures 3-1f and 3-2. What is interesting to note is that each of these M blobs appear to be rotated and shifted versions of the constellation for low step-size, as observed in Figure 3-3a. Thus, if an expression for the factors that cause this shift and rotation is obtained in terms of the system parameters then the conditioned output constellation for higher step-sizes can be modeled by a sum of M Gaussian Sum Mixtures, i.e. still a Gaussian Sum Mixture model. To summarize, the following are the key observations obtained from the simulations discussed in this section:

i. With an increase in step-size, the output constellation shows contraction, thereby resulting in better BER performance.

ii. For high step-sizes (e.g. $\mu = 1$), the constellation appears to be composed of M blobs, where M is the alphabet size of the modulation scheme used.

iii. Moreover, each of the M blobs appears to be a rotated and shifted version of the constellation obtained for low step-sizes.

3.2 BER model for NLMS equalizers

After the previous observations, we now derive the conditional PDF of interest by analysis. Using the update equation for NLMS weights in (2-7), the output of the NLMS equalizer in (2-4) can be re-written as:

$$\begin{aligned} y_n &= \left(\mathbf{w}_{n-1} + \frac{\mu}{\left\| \mathbf{u}_{n-1} \right\|^2} \mathbf{u}_{n-1} e_{n-1}^* \right)^H \mathbf{u}_n \\ &= \mathbf{w}_{n-1}^{\mathbf{H}} \mathbf{u}_n + \frac{\mu}{\mathbf{u}_{n-1}^{\mathbf{H}} \mathbf{u}_{n-1}} \left(\mathbf{u}_{n-1}^{\mathbf{H}} \mathbf{u}_n \right) e_{n-1} \end{aligned} \tag{3-1}$$

The regularization parameter a plays an important role in the practical implementation of NLMS equalizers; a small, non-zero regularization parameter prevents division by zero when the energy $\left(\left\| \mathbf{u}_n \right\|^2 \right)$ of the signal in the input delay line is insignificant. Since this analysis is focused towards the analytical aspects of the NLMS equalizer, the regularization parameter is set to 0.

As discussed in Section 2.2, all the input processes involved are ergodic. Under this assumption, Clarkson and White [52] asserted that the auto-correlation function in (2-12) serves as a good time-invariant approximation for the dot-product of the form $\mathbf{u}_{n-k}^{\mathbf{H}} \mathbf{u}_n$ for $k > 0$.

$$\mathbf{u}_{n-k}^{\mathbf{H}} \mathbf{u}_n \approx L r_{uu,k} = L \left[\left(\sigma_d^2 + \sigma_v^2 \right) \delta_k + \sigma_i^2 e^{j \omega_i k} \right] \tag{3-2}$$

Substituting for the dot-products in (3-1), using (3-2), the former can be further simplified as:

$$\begin{aligned} y_n &\approx \mathbf{w}_{n-1}^{\mathbf{H}}\mathbf{u}_n + \frac{\mu}{\sigma_d^2+\sigma_v^2+\sigma_i^2}\left(\sigma_i^2 e^{j\omega_i}\right)e_{n-1} \\ &= \mathbf{w}_{n-1}^{\mathbf{H}}\mathbf{u}_n + \mu\beta e^{j\omega_i}e_{n-1} \end{aligned} \tag{3-3}$$

where

$$\beta \triangleq \frac{\sigma_i^2}{\sigma_d^2+\sigma_v^2+\sigma_i^2} \tag{3-4}$$

Substituting for e_{n-1} in (3-3), using (2-8), and re-arranging terms yields:

$$\begin{aligned} y_n &= \mathbf{w}_{n-1}^{\mathbf{H}}\mathbf{u}_n + \mu\beta e^{j\omega_i}\left(d_{n-1-\Delta} - y_{n-1}\right) \\ &= \mathbf{w}_{n-1}^{\mathbf{H}}\mathbf{u}_n + \mu\beta e^{j\omega_i}\left(d_{n-1-\Delta} - \mathbf{w}_{n-1}^{\mathbf{H}}\mathbf{u}_{n-1}\right) \\ &= \mathbf{w}_{n-1}^{\mathbf{H}}\left(\mathbf{u}_n - \mu\beta e^{j\omega_i}\mathbf{u}_{n-1}\right) + \mu\beta e^{j\omega_i}d_{n-1-\Delta} \end{aligned} \tag{3-5}$$

Since the goal of this work is to obtain a steady state BER model, the time varying weights in (3-5) will be replaced by the steady state NLMS weights given in (2-21). We note that the time-varying aspects of the weight vector are very small when the interference power is high (high ISR). Thus, (3-5) is re-written as:

$$\tilde{y}_n = \bar{\mathbf{w}}^{\mathbf{H}}\left(\mathbf{u}_n - \mu\beta e^{j\omega_i}\mathbf{u}_{n-1}\right) + \mu\beta e^{j\omega_i}d_{n-1-\Delta} \tag{3-6}$$

The only time-varying component in (3-6) is the input vector $\mathbf{u}_n$, which can be further split into three constituent signals, the desired symbols, the Gaussian noise, and the narrowband interference, as given in (2-3). Writing (3-6) in a more compact form:

$$\tilde{y}_n = \tilde{y}_{d,n} + \tilde{y}_{i,n} + \tilde{y}_{v,n} \tag{3-7}$$

where $\tilde{y}_{d,n}$, $\tilde{y}_{i,n}$, and $\tilde{y}_{v,n}$ are contributions from the desired symbols, the Gaussian noise, and the narrowband interference respectively. The expressions for $\tilde{y}_{d,n}$, $\tilde{y}_{i,n}$, and $\tilde{y}_{v,n}$ are given by the following equations.

$$\tilde{y}_{d,n} = \bar{\mathbf{w}}^{\mathbf{H}}\left(\mathbf{d}_n - \mu\beta e^{j\omega_i}\mathbf{d}_{n-1}\right) + \mu\beta e^{j\omega_i} d_{n-1-\Delta} \tag{3-8}$$

$$\tilde{y}_{i,n} = \bar{\mathbf{w}}^{\mathbf{H}}\left(\mathbf{i}_n - \mu\beta e^{j\omega_i}\mathbf{i}_{n-1}\right) \tag{3-9}$$

$$\tilde{y}_{v,n} = \bar{\mathbf{w}}^{\mathbf{H}}\left(\mathbf{v_n} - \mu\beta e^{j\omega_i}\mathbf{v_{n-1}}\right) \tag{3-10}$$

Note that the three terms in (3-7) are mutually independent since d_n, v_n and i_n are independent (Section 2.2). Thus, the conditional PDF $\left(\tilde{y}_n \mid d_{n-\Delta} = \phi_m\right)$ can be computed by convolving the individual conditional PDFs of the three components $\tilde{y}_{d,n}$, $\tilde{y}_{i,n}$, and $\tilde{y}_{v,n}$.

3.2.1 Conditional PDF of the noise component $\tilde{y}_{v,n}$

As discussed in Section 2.2, the additive Gaussian Noise is independent of the symbols transmitted, which implies that the conditional PDF $\left(\tilde{y}_{v,n} \mid d_{n-\Delta} = \phi_m\right)$ is equivalent to the unconditional PDF. Writing (3-10) in summation form, where $\bar{\mathbf{w}} = \begin{bmatrix}\bar{w}_0 & \bar{w}_1 & \dots & \bar{w}_{L-1}\end{bmatrix}^T$, yields:

$$\begin{aligned}\tilde{y}_{v,n} &= \sum_{k=0}^{L-1} \bar{w}_k^*\left(v_{n-k} - \mu\beta e^{j\omega_i} v_{n-1-k}\right) \\ &= \bar{w}_0^* v_n + \sum_{k=1}^{L-1}\left(\bar{w}_k^* - \bar{w}_{k-1}^*\mu\beta e^{j\omega_i}\right)v_{n-k} - \bar{w}_{L-1}^*\mu\beta e^{j\omega_i} v_{n-L}\end{aligned} \tag{3-11}$$

Note that $\tilde{y}_{v,n}$ is expressed as a linear combination of $(L+1)$ independent Gaussian random variables. Thus $\tilde{y}_{v,n}$ also follows a Gaussian distribution [53]. Using the fact that the input AWGN is zero mean, the mean of $\tilde{y}_{v,n}$ can be expressed as:

$$\begin{aligned} E\left[\tilde{y}_{v,n}\right] &= E\left[\bar{w}_0^* v_n + \sum_{k=1}^{L-1}\left(\bar{w}_k^* - \bar{w}_{k-1}^* \mu\beta e^{j\omega_i}\right) v_{n-k} - \bar{w}_{L-1}^* \mu\beta e^{j\omega_i} v_{n-L}\right] \\ &= E\left[\bar{w}_0^* v_n\right] + E\left[\sum_{k=1}^{L-1}\left(\bar{w}_k^* - \bar{w}_{k-1}^* \mu\beta e^{j\omega_i}\right) v_{n-k}\right] - E\left[\bar{w}_{L-1}^* \mu\beta e^{j\omega_i} v_{n-L}\right] \\ &= \bar{w}_0^* E\left[v_n\right] + \sum_{k=1}^{L-1}\left(\bar{w}_k^* - \bar{w}_{k-1}^* \mu\beta e^{j\omega_i}\right) E\left[v_{n-k}\right] - \bar{w}_{L-1}^* \mu\beta e^{j\omega_i} E\left[v_{n-L}\right] \\ &= 0 \end{aligned} \tag{3-12}$$

Similarly, using the auto-correlation function of v_n in (2-10), the variance of $\tilde{y}_{v,n}$ can be derived as:

$$\begin{aligned} Var\left[\tilde{y}_{v,n}\right] &= Var\left[\bar{w}_0^* v_n\right] + Var\left[\sum_{k=1}^{L-1}\left(\bar{w}_k^* - \bar{w}_{k-1}^* \mu\beta e^{j\omega_i}\right) v_{n-k}\right] + Var\left[\bar{w}_{L-1}^* \mu\beta e^{j\omega_i} v_{n-L}\right] \\ &= \left|\bar{w}_0\right|^2 Var\left[v_n\right] + \sum_{k=1}^{L-1}\left|\bar{w}_k^* - \bar{w}_{k-1}^* \mu\beta e^{j\omega_i}\right|^2 Var\left[v_{n-k}\right] + \mu^2\beta^2 \left|\bar{w}_{L-1}\right|^2 Var\left[v_{n-L}\right] \\ &= \xi_v \sigma_v^2 \end{aligned} \tag{3-13}$$

where $\xi_v \triangleq \left|\bar{w}_0\right|^2 + \sum_{k=1}^{L-1}\left|\bar{w}_k^* - \bar{w}_{k-1}^* \mu\beta e^{j\omega_i}\right|^2 + \mu^2\beta^2 \left|\bar{w}_{L-1}\right|^2$. Thus, in the equalizer output the input noise power is scaled by the factor ξ_v. The second term of the scaling factor ξ_v can be further simplified as:

$$\begin{aligned} \left|\bar{w}_k^* - \bar{w}_{k-1}^* \mu\beta e^{j\omega_i}\right|^2 &= \left(\bar{w}_k^* - \bar{w}_{k-1}^* \mu\beta e^{j\omega_i}\right)^* \left(\bar{w}_k^* - \bar{w}_{k-1}^* \mu\beta e^{j\omega_i}\right) \\ &= \left(\bar{w}_k - \bar{w}_{k-1} \mu\beta e^{-j\omega_i}\right)\left(\bar{w}_k^* - \bar{w}_{k-1}^* \mu\beta e^{j\omega_i}\right) \\ &= \left|\bar{w}_k\right|^2 - \mu\beta\left(\bar{w}_{k-1} e^{-j\omega_i} \bar{w}_k^* + \bar{w}_k \bar{w}_{k-1}^* e^{j\omega_i}\right) + \mu^2\beta^2 \left|\bar{w}_{k-1}\right|^2 \\ &= \left|\bar{w}_k\right|^2 - 2\mu\beta\,\mathrm{Re}\left[\bar{w}_k \bar{w}_{k-1}^* e^{j\omega_i}\right] + \mu^2\beta^2 \left|\bar{w}_{k-1}\right|^2 \end{aligned} \tag{3-14}$$

where $\mathrm{Re}[C] \triangleq X$ if C is a complex number of the form $X + jY$, where X and Y are real numbers. Using the expression obtained in (3-14), ξ_v can be written as:

$$\begin{aligned}\xi_v &= |\bar{w}_0|^2 + \sum_{k=1}^{L-1}\left(|\bar{w}_k|^2 - 2\mu\beta\,\mathrm{Re}\left[\bar{w}_k \bar{w}_{k-1}^* e^{j\omega_i}\right] + \mu^2\beta^2 |\bar{w}_{k-1}|^2\right) + \mu^2\beta^2 |\bar{w}_{L-1}|^2 \\ &= \left(1+\mu^2\beta^2\right)\sum_{k=0}^{L-1}|\bar{w}_k|^2 - 2\mu\beta\sum_{k=1}^{L-1}\mathrm{Re}\left[\bar{w}_k \bar{w}_{k-1}^* e^{j\omega_i}\right] \\ &= \|\bar{\mathbf{w}}\|^2\left(1+\mu^2\beta^2\right) - 2\mu\beta\sum_{k=1}^{L-1}\mathrm{Re}\left[\bar{w}_k \bar{w}_{k-1}^* e^{j\omega_i}\right]\end{aligned} \tag{3-15}$$

Note that for $\mu = 0$, $\xi_v = \|\bar{\mathbf{w}}\|^2$, which coincides with the result obtained previously for the (time-invariant) Wiener case [37]. Combining the results obtained in (3-12) and (3-13) along with the fact that $\tilde{y}_{v,n}$ is the sum of $L+1$ independent Gaussian random variables (3-11), it follows that $\tilde{y}_{v,n}$ follows a complex normal distribution as described in (3-16).

$$\tilde{y}_{v,n} \sim CN\left(0, \xi_v \sigma_v^2\right) \tag{3-16}$$

3.2.2 Conditional PDF of the interference component $\tilde{y}_{i,n}$

The narrowband interference modeled by the complex exponential in (2-6) is also independent of the transmitted signal. So, similar to the noise component, the conditional PDF of $\left(\tilde{y}_{i,n} \mid d_{n-\Delta} = \phi_m\right)$ is equivalent to the unconditional PDF. Re-arranging the complex exponential in (2-6) yields a recursive expression for i_n:

$$\begin{aligned} i_n &= \sigma_i e^{j(\omega_i n + \theta)} \\ &= \sigma_i e^{j\omega_i} e^{j(\omega_i (n-1) + \theta)} \\ &= e^{j\omega_i} i_{n-1} \end{aligned} \tag{3-17}$$

With the recursive relation obtained in (3-17), $\tilde{y}_{i,n}$ can be written as:

$$\begin{aligned}\tilde{y}_{i,n} &= \bar{\mathbf{w}}^{\mathbf{H}}\left(\mathbf{i_n} - \mu\beta e^{j\omega_i}\mathbf{i_{n-1}}\right) \\ &= \bar{\mathbf{w}}^{\mathbf{H}}\left(\mathbf{i_n} - \mu\beta\mathbf{i_n}\right) \\ &= \left(1-\mu\beta\right)\bar{\mathbf{w}}^{\mathbf{H}}\mathbf{i_n}\end{aligned} \tag{3-18}$$

The expression obtained in (3-18) highlights a couple of interesting facts. Firstly, at high ISR conditions $\beta = \dfrac{\sigma_i^2}{\sigma_d^2 + \sigma_v^2 + \sigma_i^2} \approx 1$. Thus, setting a high step-size (e.g. $\mu = 1$) can virtually nullify the interference component in the equalizer output. This is consistent with the simulations shown in Section 2.6, where step-sizes close to $\mu = 1$ were shown to lead to the optimal BER performance.

Secondly, the expression for $\tilde{y}_n^i$ is identical to the interference component at the output of the fixed (time-invariant) Wiener filter except for the scalar multiplier $\left(1-\mu\beta\right)$. The Wiener case has been discussed in detail in [38] where the interference component at the output, i.e. $\tilde{y}_n^i$, was modeled by a Gaussian distribution. Identical to the analysis done in [38], the mean and the variance of the distribution are given in (3-19) and (3-20) respectively.

$$\begin{aligned}E\left[\tilde{y}_n^i\right] &= E\left[\left(1-\mu\beta\right)\bar{\mathbf{w}}^{\mathbf{H}}\mathbf{i_n}\right] \\ &= \left(1-\mu\beta\right)E\left[\bar{\mathbf{w}}^{\mathbf{H}}\mathbf{i_n}\right] \\ &= \left(1-\mu\beta\right)E\left[\sum_{k=0}^{L-1}\bar{w}_k^* i_{n-k}\right] \\ &= \left(1-\mu\beta\right)\sum_{k=1}^{L}\bar{w}_k^* E\left[i_{n-k}\right] \\ &= 0\end{aligned} \tag{3-19}$$

$$
\begin{aligned}
Var\left[\tilde{y}_n^i\right] &= Var\left[\left(1-\mu\beta\right)\bar{\mathbf{w}}^{\mathbf{H}}\mathbf{i_n}\right] \\
&= \left(1-\mu\beta\right)^2 E\left[\left(\bar{\mathbf{w}}^{\mathbf{H}}\mathbf{i_n}\right)\left(\bar{\mathbf{w}}^{\mathbf{H}}\mathbf{i_n}\right)^H\right] \\
&= \left(1-\mu\beta\right)^2 E\left[\bar{\mathbf{w}}^{\mathbf{H}}\mathbf{i_n}\mathbf{i_n}^{\mathbf{H}}\bar{\mathbf{w}}\right] \\
&= \left(1-\mu\beta\right)^2 \bar{\mathbf{w}}^{\mathbf{H}} E\left[\mathbf{i_n}\mathbf{i_n}^{\mathbf{H}}\right]\bar{\mathbf{w}} \\
&= \left(1-\mu\beta\right)^2 \bar{\mathbf{w}}^{\mathbf{H}}\mathbf{R_i}\bar{\mathbf{w}}
\end{aligned}
\tag{3-20}
$$

where $\mathbf{R_i} \triangleq \sigma_i^2\mathbf{e}\mathbf{e}^{\mathbf{H}}$ is the auto-correlation function for the narrowband interference signal. The variance of the variable $\tilde{y}_n^i$ decreases as $1-\mu\beta \to 0$ which, as discussed earlier, takes place under high ISR conditions with a large step-size. Combining the results obtained in (3-19) and (3-20), the PDF for $\tilde{y}_n^i$ is given by:

$$
\tilde{y}_n^i \sim CN\left(0, \xi_i\sigma_i^2\right) \tag{3-21}
$$

where

$$
\xi_i \triangleq \left(1-\mu\beta\right)^2 \bar{\mathbf{w}}^{\mathbf{H}}\mathbf{e}\mathbf{e}^{\mathbf{H}}\bar{\mathbf{w}} \tag{3-22}
$$

Note that modeling the interference component with a Gaussian distribution is an approximation and its effects will be discussed in Section 3.4.

3.2.3 Conditional PDF of the desired symbol component $\tilde{y}_{d,n}$

From (3-8), it is clear that the conditional PDF of $\left(\tilde{y}_{d,n} \mid d_{n-\Delta} = \phi_m\right)$ is dependent on the transmitted symbols, unlike the noise and the interference component. Similar to (3-11), $\tilde{y}_{d,n}$ can also be written in summation form:

$$
\begin{aligned}
\tilde{y}_{d,n} &= \bar{\mathbf{w}}^{\mathbf{H}}\left(\mathbf{d}_n - \mu\beta e^{j\omega_i}\mathbf{d}_{n-1}\right) + \mu\beta e^{j\omega_i} d_{n-1-\Delta} \\
&= \bar{w}_0^* d_n + \sum_{k=1}^{L-1}\left(\bar{w}_k^* - \bar{w}_{k-1}^*\mu\beta e^{j\omega_i}\right) d_{n-k} - \bar{w}_{L-1}^*\mu\beta e^{j\omega_i} d_{n-L} + \mu\beta e^{j\omega_i} d_{n-1-\Delta}
\end{aligned}
\tag{3-23}
$$

From (3-23), observe that there is a total of $L+2$ terms. Depending on the value of Δ, the coefficients contributing to $d_{n-1-\Delta}$ can be combined and thus, effectively, $\tilde{y}_{d,n}$ can be expressed as a sum of $L+1$ terms. Figure 3-4 provides a visualization of the vectors $\mathbf{d}_{n-1}$ and $\mathbf{d}_n$ for all the possible values of Δ. Note that Δ is assumed to only take integer values between 0 and $L-1$, including the boundary values of 0 and $L-1$.

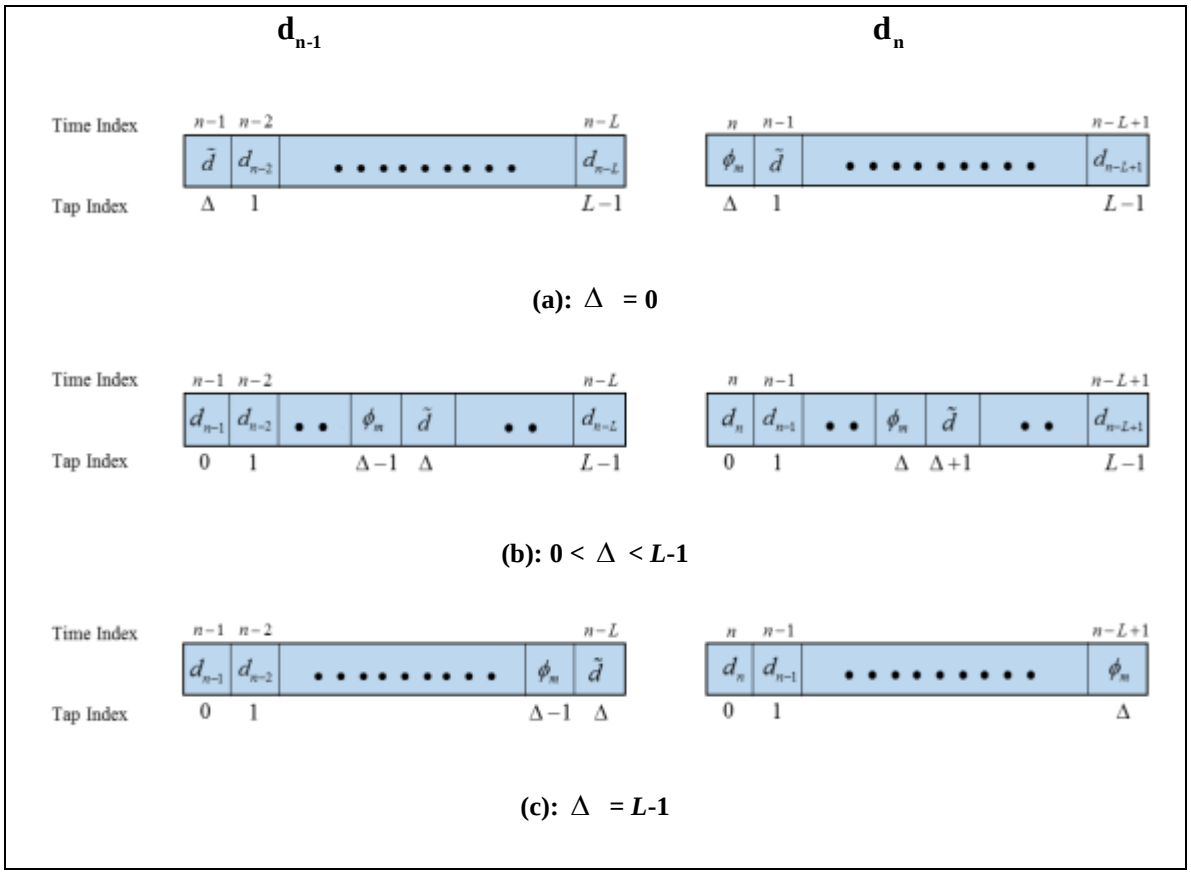

Figure 3-4: Comparison of $\mathbf{d}_{n-1}$ and $\mathbf{d}_n$ for different values of Δ.

From Figure 3-4a, for $\Delta = 0$, $d_n = \phi_m$. Substituting them in (3-23) yields:

$$\begin{aligned}\tilde{y}_{d,n}\Big|_{\substack{\Delta=0\\ d_n=\phi_m}} &= \bar{w}_\Delta^*\phi_m + \sum_{k=1}^{L-1}\left(\bar{w}_k^* - \bar{w}_{k-1}^*\mu\beta e^{j\omega_i}\right)d_{n-k} - \bar{w}_{L-1}^*\mu\beta e^{j\omega_i}d_{n-L} + \mu\beta e^{j\omega_i}d_{n-1-\Delta} \\ &= \kappa\Big|_{\substack{\Delta=0\\ d_n=\phi_m}} + \Upsilon\Big|_{\substack{\Delta=0\\ d_n=\phi_m}}\end{aligned} \tag{3-24}$$

where $\kappa\Big|_{\substack{\Delta=0\\ d_n=\phi_m}}$ and $\Upsilon\Big|_{\substack{\Delta=0\\ d_n=\phi_m}}$ are given by:

$$\kappa\Big|_{\substack{\Delta=0\\ d_n=\phi_m}} = \bar{w}_{\Delta}^{*}\phi_m \tag{3-25}$$

$$\Upsilon\Big|_{\substack{\Delta=0\\ d_n=\phi_m}} = \sum_{\substack{k=1\\ k\neq\Delta+1}}^{L-1}\left(\bar{w}_k^{*} - \bar{w}_{k-1}^{*}\mu\beta e^{j\omega_i}\right)d_{n-k} + w_{\tilde{d}}\,d_{n-1-\Delta} - \bar{w}_{L-1}^{*}\mu\beta e^{j\omega_i}d_{n-L} \tag{3-26}$$

where $w_{\tilde{d}}\Big|_{\substack{\Delta=0\\ d_n=\phi_m}} = \bar{w}_{\Delta+1}^{*} - \bar{w}_{\Delta}^{*}\mu\beta e^{j\omega_i} + \mu\beta e^{j\omega_i}$ is the coefficient for $d_{n-1-\Delta}$.

From Figure 3-4b, for $0<\Delta<L-1$, substituting the value of $d_{n-\Delta}=\phi_m$ in (3-23), yields:

$$\begin{aligned}\tilde{y}_{d,n}\Big|_{\substack{0<\Delta<L-1\\ d_{n-\Delta}=\phi_m}} &= \bar{w}_0^{*}d_n + \sum_{k=1}^{L-1}\left(\bar{w}_k^{*} - \bar{w}_{k-1}^{*}\mu\beta e^{j\omega_i}\right)d_{n-k} - \bar{w}_{L-1}^{*}\mu\beta e^{j\omega_i}d_{n-L} + \mu\beta e^{j\omega_i}d_{n-1-\Delta}\\ &= \kappa\Big|_{\substack{0<\Delta<L-1\\ d_{n-\Delta}=\phi_m}} + \Upsilon\Big|_{\substack{0<\Delta<L-1\\ d_{n-\Delta}=\phi_m}}\end{aligned} \tag{3-27}$$

where $\kappa\Big|_{\substack{0<\Delta<L-1\\ d_{n-\Delta}=\phi_m}}$ and $\Upsilon\Big|_{\substack{0<\Delta<L-1\\ d_{n-\Delta}=\phi_m}}$ are given by:

$$\kappa\Big|_{\substack{0<\Delta<L-1\\ d_{n-\Delta}=\phi_m}} = \left(\bar{w}_{\Delta}^{*} - \bar{w}_{\Delta-1}^{*}\mu\beta e^{j\omega_i}\right)\phi_m \tag{3-28}$$

$$\Upsilon\Big|_{\substack{0<\Delta<L-1\\ d_{n-\Delta}=\phi_m}} = \bar{w}_0^{*}d_n + \sum_{\substack{k=1\\ k\neq\Delta,\Delta+1}}^{L-1}\left(\bar{w}_k^{*} - \bar{w}_{k-1}^{*}\mu\beta e^{j\omega_i}\right)d_{n-k} + w_{\tilde{d}}\,d_{n-1-\Delta} - \bar{w}_{L-1}^{*}\mu\beta e^{j\omega_i}d_{n-L} \tag{3-29}$$

where $w_{\tilde{d}}\Big|_{\substack{0<\Delta<L-1\\ d_{n-\Delta}=\phi_m}} = \bar{w}_{\Delta+1}^{*} - \bar{w}_{\Delta}^{*}\mu\beta e^{j\omega_i} + \mu\beta e^{j\omega_i}$ is the coefficient for $d_{n-1-\Delta}$.

Finally, from Figure 3-4c, for $\Delta = L-1$, substituting the values of $d_{n-L+1}=\phi_m$ in (3-23):

$$\begin{aligned}\tilde{y}_{d,n}\Big|_{\substack{\Delta=L-1\\ d_{L-1}=\phi_m}} &= \bar{w}_0^{*}d_n + \sum_{k=1}^{L-1}\left(\bar{w}_k^{*} - \bar{w}_{k-1}^{*}\mu\beta e^{j\omega_i}\right)d_{n-k} - \bar{w}_{\Delta}^{*}\mu\beta e^{j\omega_i}d_{n-1-\Delta} + \mu\beta e^{j\omega_i}d_{n-1-\Delta}\\ &= \kappa\Big|_{\substack{\Delta=L-1\\ d_{L-1}=\phi_m}} + \Upsilon\Big|_{\substack{\Delta=L-1\\ d_{L-1}=\phi_m}}\end{aligned} \tag{3-30}$$

where $\kappa\big|_{\substack{\Delta=L-1\\ d_{L-1}=\phi_m}}$ and $\Upsilon\big|_{\substack{\Delta=L-1\\ d_{L-1}=\phi_m}}$ are given by:

$$\kappa\big|_{\substack{\Delta=L-1\\ d_{L-1}=\phi_m}} = \left(\bar{w}_{\Delta}^{*} - \bar{w}_{\Delta-1}^{*}\mu\beta e^{j\omega_i}\right)\phi_m \tag{3-31}$$

$$\Upsilon\big|_{\substack{\Delta=L-1\\ d_{L-1}=\phi_m}} = \bar{w}_0^{*} d_n + \sum_{\substack{k=1\\ k\neq\Delta}}^{L-1}\left(\bar{w}_k^{*} - \bar{w}_{k-1}^{*}\mu\beta e^{j\omega_i}\right)d_{n-k} + w_{\tilde{d}}\, d_{n-1-\Delta} \tag{3-32}$$

where $w_{\tilde{d}}\big|_{\substack{\Delta=L-1\\ d_{n-L+1}=\phi_m}} = -\bar{w}_{\Delta}^{*}\mu\beta e^{j\omega_i} + \mu\beta e^{j\omega_i}$ is the coefficient for $d_{n-1-\Delta}$. Note that Υ is a sum of L random variables for all the values of $0 \le \Delta \le L-1$.

$$\Upsilon = \sum_{\substack{k=0\\ k\neq\Delta}}^{L} c_k d_{n-k} \tag{3-33}$$

Table 3-1 summarizes the results obtained in (3-24) through (3-33).

Table 3-1: Deterministic and Stochastic Components of $\tilde{y}_{d,n}$ for NLMS equalizer.

Δ	κ	c_k
0	$\bar{w}_{\Delta}^{*}\phi_m$	$c_k = \begin{cases} \bar{w}_{k+1}^{*} - \bar{w}_k^{*}\mu\beta e^{j\omega_i} + \mu\beta e^{j\omega_i} & k=1 \\ \bar{w}_{k+1}^{*} - \bar{w}_k^{*}\mu\beta e^{j\omega_i} & k=\{2,3,\ldots,L-1\} \\ -\bar{w}_{k-1}^{*}\mu\beta e^{j\omega_i} & k=L \end{cases}$
$0<\Delta<L-1$	$\left(\bar{w}_{\Delta}^{*} - \bar{w}_{\Delta-1}^{*}\mu\beta e^{j\omega_i}\right)\phi_m$	$c_k = \begin{cases} \bar{w}_k^{*} & k=0 \\ \bar{w}_{k+1}^{*} - \bar{w}_k^{*}\mu\beta e^{j\omega_i} + \mu\beta e^{j\omega_i} & k=\Delta+1 \\ \bar{w}_{k+1}^{*} - \bar{w}_k^{*}\mu\beta e^{j\omega_i} & k=\{0,1,\ldots,L-1\}-\{\Delta,\Delta+1\} \\ -\bar{w}_{k-1}^{*}\mu\beta e^{j\omega_i} & k=L \end{cases}$
$L-1$	$\left(\bar{w}_{\Delta}^{*} - \bar{w}_{\Delta-1}^{*}\mu\beta e^{j\omega_i}\right)\phi_m$	$c_k = \begin{cases} \bar{w}_k^{*} & k=0 \\ \bar{w}_{k+1}^{*} - \bar{w}_k^{*}\mu\beta e^{j\omega_i} & k=\{1,2,\ldots,L-2\} \\ -\bar{w}_{k-1}^{*}\mu\beta e^{j\omega_i} + \mu\beta e^{j\omega_i} & k=L \end{cases}$

Each of the terms in the summation in (3-33) represents a scaled and rotated version of the input constellation $\{\phi_m\}_{m=1}^{M}$ with the complex constant scaling factor c_k. The scaling factors are a function of the steady state NLMS weight vector $\bar{\mathbf{w}}, \mu, \beta$, and ω_i as shown in Table 3-1. Each term in (3-33) can be represented by a probability mass function (PMF) that takes *M* equally likely values, since the symbols are equally likely.

$$c_k d_{n-k} \sim \frac{1}{M}\sum_{l=1}^{M}\delta\left(x - c_k\phi_l\right) \tag{3-34}$$

$\tilde{y}_{d,n}$ comprises of *L* random variables which are of the form of (3-34). The weighted linear combination of these *L* random variables can be represented by a probability mass function (PMF) which can take on M^L values. Since the symbols of the input constellation are equally likely then the PMF at each of the M^L values will have a probability of $1/M^L$. Thus, the conditional PMF $\tilde{y}_{d,n}$ is of the form:

$$f\left(\tilde{y}_{d,n}\big|_{d_{n-\Delta}=\phi_m}\right) = \frac{1}{M^L}\sum_{k_0=1}^{M}\sum_{\substack{k_1=1 \\ k_l\neq\Delta}}^{M}\cdots\sum_{k_L=1}^{M}\left(\delta - \kappa - \tilde{\phi}\right) \tag{3-35}$$

where $\tilde{\phi}$ is defined as:

$$\tilde{\phi} \triangleq \sum_{\substack{l=0 \\ l\neq\Delta}}^{L} c_l\phi_{k_l} \tag{3-36}$$

3.2.4 Conditional PDF of output $\tilde{y}_n$

The approximate conditional output $\left(\tilde{y}_n \middle| d_{n-\Delta} = \phi_m\right)$ was expressed as a sum of three mutually independent terms in (3-7). Thus, the overall PDF will be a convolution of the densities shown in (3-16), (3-21), and (3-35). Note that the first two are Gaussian distributions while the last one is a discrete uniform distributions. Summation of two independent Gaussian variable leads to another Gaussian variable. Convolving the

resultant Gaussian with the discrete uniform distribution (which is represented by a dirac-delta function (3-35)) will cause a shift in the mean of the Gaussian to the location where there the dirac-delta function is non-zero i.e., where the PMF has a non-zero probability. From (3-35), observe that there are a total of M^L points where the PMF is non-zero. So the overall PDF can be expressed as a Gaussian Sum Mixture containing M^L terms :

$$f\left(\tilde{y}_n \middle| d_{n-\Delta} = \phi_m\right) = \frac{1}{M^L} \sum_{k_0=1}^{M} \sum_{\substack{k_1=1 \\ k_l \neq \Delta}}^{M} \cdots \sum_{k_L=1}^{M} CN\left(\kappa + \tilde{\phi}, \xi_i \sigma_i^2 + \xi_v \sigma_v^2\right) \tag{3-37}$$

Figure 3-5 shows an example of the conditional PDF of $\tilde{y}_n \middle| d_{n-\Delta} = e^{j\pi/4}$ computed using (3-37). The simulation parameters are identical to the ones used to generate Figure 3-3b (SNR = 40 dB, ISR = 20 dB, $f_i = 1/e$, $L = 3$, and $\Delta = 0$).

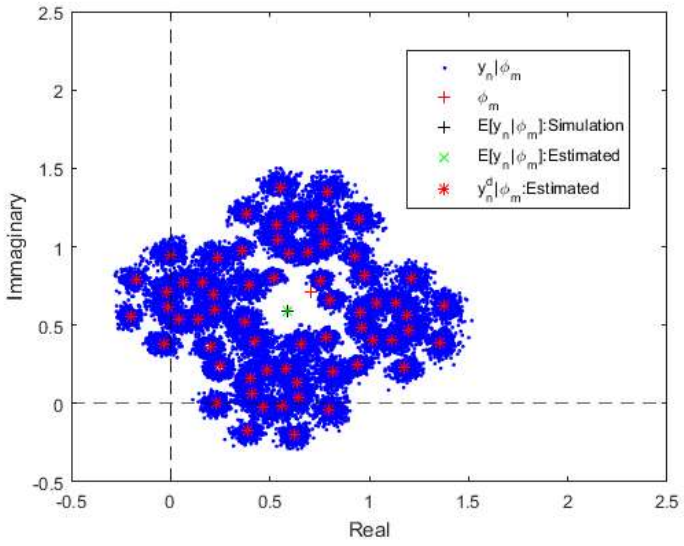

(a) $\Delta = 0$

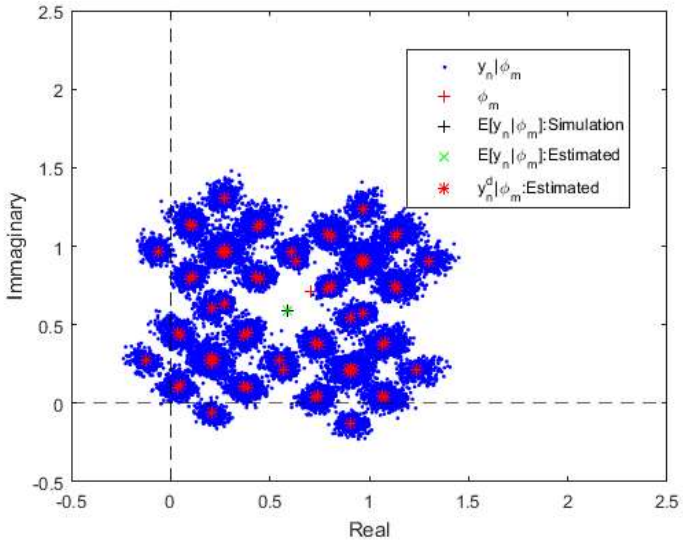

(b) $\Delta = 1$

Figure 3-5: $\tilde{y}_n$ with the estimated $\tilde{y}_{d,n}$ centers for different values of Δ for $L = 3$.

The only differentiating factor between Figure 3-5a and Figure 3-5b is the value of Δ. The conditional output is shown highlighting the centers of the Gaussians along with the conditional means - both estimated and simulated - and the conditioned symbol $\phi_m = e^{j\pi/4}$. Note that the estimated and the conditional means coincide. In Fig. 3-5b the

effect of changing the equalization point can be observed; there is less probability mass outside the first quadrant and therefore a smaller contribution to bit error when the equalization point is towards the center of the tapped delay line.

The modeled probability of error $\hat{P}_e$ is computed using the Gaussian Sum Mixture in (3-37) and given by:

$$\hat{P}_e = \iint_A f\left(\tilde{y}_n \middle| d_{n-\Delta} = \phi_m\right) dA \tag{3-38}$$

where A is the region which corresponds to a Bit Error. For example, if a QPSK modulation scheme is used (as shown in Figure 3-5) and ϕ_m is chosen as the first quadrant symbol, then A will be the entire $\Re^2$ excluding the first quadrant, with the third quadrant contributing two bit errors while the second and fourth quadrant each contribute single bit errors. Thus, (3-38) for this particular case can be written as:

$$\begin{aligned}\hat{P}_e = &\frac{1}{2}\int_{y_I=-\infty}^{0}\int_{y_Q=0}^{\infty} f\left(\tilde{y}_n \middle| d_{n-\Delta} = \phi_m\right) dy_I dy_Q \\ &+\frac{2}{2}\int_{y_I=-\infty}^{0}\int_{y_Q=-\infty}^{0} f\left(\tilde{y}_n \middle| d_{n-\Delta} = \phi_m\right) dy_I dy_Q \\ &+\frac{1}{2}\int_{y_I=0}^{\infty}\int_{y_Q=-\infty}^{0} f\left(\tilde{y}_n \middle| d_{n-\Delta} = \phi_m\right) dy_I dy_Q\end{aligned} \tag{3-39}$$

where y_I and y_Q represent the in-phase and quadrature components of y_n respectively.

3.3 Approximate BER model for NLMS equalization

The examples shown in Figures 3-1 and 3-3, where the equalizer length is $L = 5$ and $L = 3$ respectively, serve more as an illustrative example. In practice, it is more likely that equalizers of larger lengths are used. Keeping the modulation scheme the same, the number of components in the Gaussian Sum Mixture in (3-37) increases exponentially with an increase in equalizer length. For example, if QPSK modulation is used then an

equalizer length of $L=10$ results in more than a million components in (3-37). It is obvious that if a more sophisticated modulation scheme is used, with a higher value of *M*, computing the BER using (3-38) can become cumbersome. To address this issue, in this section an approximate version of the Gaussian Sum Mixture in (3-37) is introduced.

Figure 3-1 shows that with an increase in step-size the shape of the conditional output constellation changes. Figure 3-3 further shows that at higher step-sizes the output constellation is composed of *M* constellations, each of which is a rotated and scaled version of the corresponding constellation at low step-size. From (3-23), we observe that the coefficient of d_{n-L} is dependent on μ. For $\mu=0$ that coefficient becomes zero irrespective of other parameters. An approximate version of the Gaussian Sum Mixture is thus proposed where each of the *M* constellations is modeled by a Single Gaussian. Thus, instead of a total of M^L components, the approximating Gaussian Sum Mixture model contains M terms.

Taking the last term, i.e. the coefficient of d_{n-L}, outside the summation in (3-35):

$$\begin{aligned}\tilde{y}_{d,n}\big|_{d_{n-\Delta}=\phi_m} &= \kappa+\sum_{\substack{k=0\\k\neq\Delta}}^{L} c_k d_{n-k}\\ &= \kappa+c_L d_{n-L}+\sum_{\substack{k=0\\k\neq\Delta}}^{L-1} c_k d_{n-k}\\ &= \kappa+c_L\sum_{l=1}^{M}\phi_m+\sum_{\substack{k=0\\k\neq\Delta}}^{L-1} c_k d_{n-k}\end{aligned} \tag{3-40}$$

The term $\kappa+c_L\sum_{l=1}^{M}\phi_m$ represents the center of the *M* Gaussians. The variability in $\sum_{\substack{k=0\\k\neq\Delta}}^{L-1} c_k d_{n-k}$ is modeled by the variance of the summation. Note that the d_{n-k} are independent symbols.

$$Var\left[\sum_{\substack{k=0\\k\neq\Delta}}^{L-1} c_k d_{n-k}\right] = \sum_{\substack{k=0\\k\neq\Delta}}^{L-1} Var\left[c_k d_{n-k}\right]$$
$$= \sum_{\substack{k=0\\k\neq\Delta}}^{L-1} |c_k|^2 Var\left[d_{n-k}\right] \quad (3\text{-}41)$$
$$= \xi_d \sigma_d^2$$

where

$$\xi_d \triangleq \sum_{\substack{k=0\\k\neq\Delta}}^{L-1} |c_k|^2 \quad (3\text{-}42)$$

The overall variance of each of the M Gaussians is a summation of the variances derived for the noise in (3-13), the interference in (3-20), and finally the 'variance' from the desired symbol component derived in (3-41). The Approximate Gaussian Sum Mixture (AGSM) model is given by:

$$g\left(\tilde{y}_n \middle| d_{n-\Delta} = \phi_m\right) = \frac{1}{M}\sum_{l=1}^{M} CN\left(\kappa + c_L \phi_{k_l}, \xi_v \sigma_v^2 + \xi_d \sigma_d^2 + \xi_i \sigma_i^2\right) \quad (3\text{-}43)$$

Similar to (3-38), the probability of error computed using (3-43) is given by:

$$\hat{P}_e = \iint_A g\left(\tilde{y}_n \middle| d_{n-\Delta} = \phi_m\right) dA \quad (3\text{-}44)$$

Figure 3-6 shows an example of the conditional PDF of $\tilde{y}_n \middle| d_{n-\Delta} = e^{j\pi/4}$ computed using (3-43). The simulation parameters are identical to the ones used to generate Figure 3-5, i.e. SNR = 40 dB, ISR = 20 dB, $f_i = 1/e$, $L = 3$, and $\Delta = 0$.

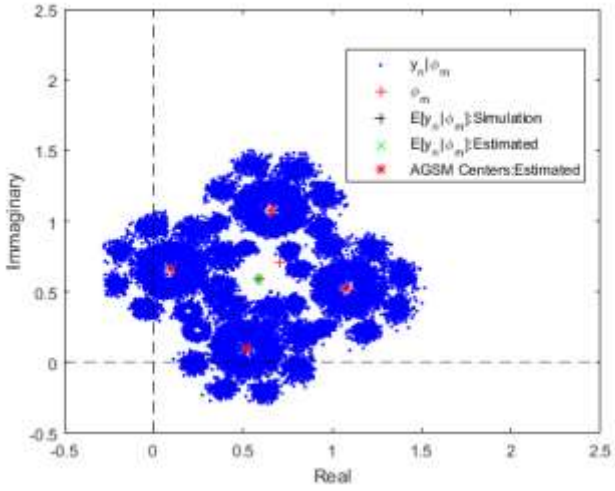

(a) $\Delta = 0$

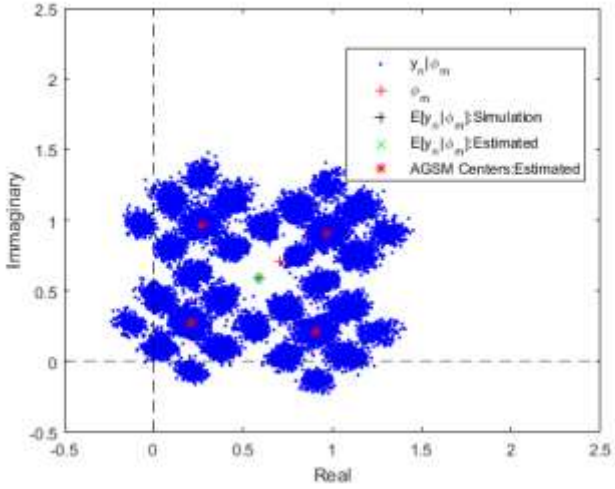

(b) $\Delta = 1$

Figure 3-6: y_n **with the estimated AGSM centers for different values of** Δ **and** $L = 3$**.**

From visual inspection it appears that the estimated centers obtained using the AGSM model for each of the M constellations are accurate. A quantitative comparison between the two models and the simulation results is presented in the next section.

3.4 Results

For simulation purposes, the desired signal is represented by two digital modulation schemes:

i. QPSK symbols, which makes the alphabet size $M = 4$;

ii. 16-QAM symbols, which makes the alphabet size $M = 16$.

The observed value of BER is calculated using a Monte Carlo simulation technique by ensemble averaging of independent runs. Unless specified otherwise, the ensemble size is 100 for all of the subsequent simulations. A single run consists of 100,000 independent symbols generated randomly, which are then corrupted by AWGN and the narrowband interference. Note that with an ensemble size of 100 and 100,000 independent symbols per run, BER up to a magnitude of 10^{-6} can be estimated relatively accurately. If the BER is less than 10^{-6} either the ensemble size or the number of independent symbols per run, or both, should be increased appropriately.

When the desired signal is represented by QPSK symbols (Figures 3-7 through 3-10), the BER estimate using the GSM and AGSM model is computed using (3-39).

Figure 3-7 shows the comparison between the BER ($\hat{P}_e$) calculated using the GSM expression in (3-38) and the AGSM model in (3-43), together with the observed BER, as a function of step-size for an equalizer of length $L = 7$ and $\Delta = 0$ for a QPSK system. ISR was set to 20 dB with the fractional interference frequency $f_i = 0.368$ and SNR was set to 20 dB.

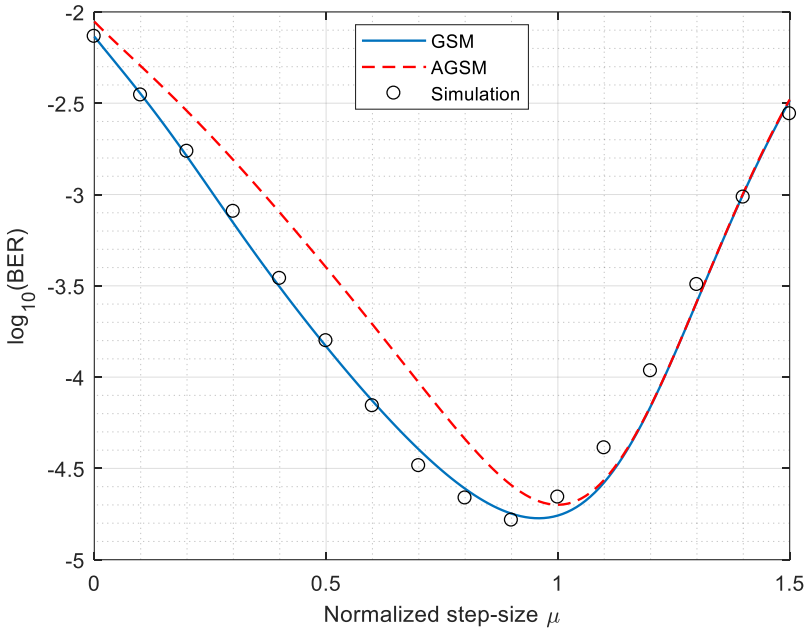

Figure 3-7: BER calculated by GSM (-), AGSM (--) and observed BER (o) for a QPSK system as a function of step-size μ for L = 7, SNR = 20 dB and ISR = 20 dB.

Figure 3-7 shows that the BER predicted by the GSM expression is accurate for the entire range of step-sizes from $[0,1.5]$. The maximum deviation between the observed value and the BER predicted by the GSM expression is observed at $\mu = 1.1$ where the derived GSM expression prediction over-estimates the equalizer BER performance by a factor of $1/5^{th}$ of an order of magnitude. The AGSM model underestimates the equalizer performance for $0 \le \mu < 1$. The amount of deviation between the observed BER and the predicted BER by AGSM increases as μ increases from 0 to 0.6. For $\mu > 0.6$ the difference between the predicted BER and the observed BER decreases and finally, for $\mu \ge 1$, both of the predictions coincide.

Figure 3-8 shows the comparison between the $\hat{P}_e$ calculated using the GSM expression in (3-38) and the AGSM model (3-43) as well as the observed BER as a function of SNR for a QPSK system. For Figure 3-8, the simulation parameters used are $L = 7$, $\Delta = 0$, $\mu = 1$, ISR = 20 dB, and $f_i = 0.368$.

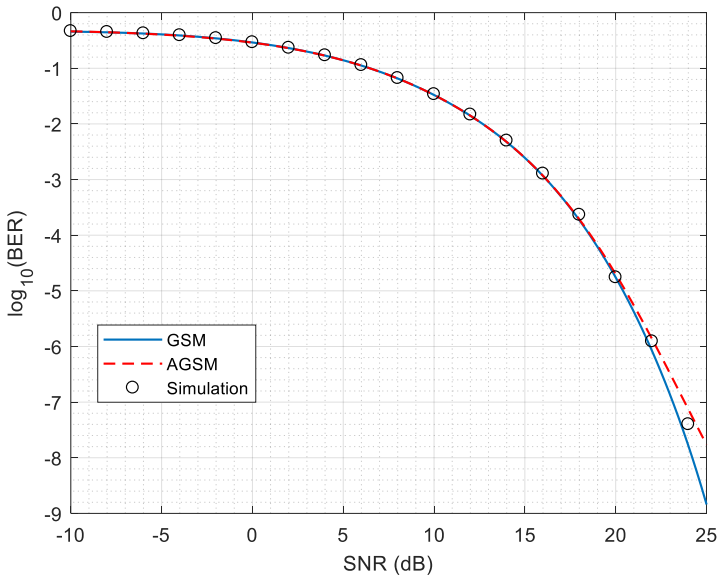

Figure 3-8: BER calculated by GSM (-), AGSM (--) and observed BER (o) for a QPSK system as a function of SNR for L = 7, μ = 1 and ISR = 20 dB.

Note that for SNR > 20 dB, in order to obtain the observed values, the ensemble size was increased from 100 to 1000. Figure 3-8 shows that both predictions are identical for SNR $\leq$ 20 dB. For larger SNR there is a slight deviation. The predicted BER performance of the NLMS equalizer by both models is consistent with the simulation results.

In Figure 3-9 both predictions are compared with the observed BER as a function of ISR. Similar to the previous cases, an equalizer of length $L = 7$ and $\Delta = 0$ was chosen. Although the interference power varied, its frequency was kept the same, at $f_i = 0.368$. SNR was set to 20 dB.

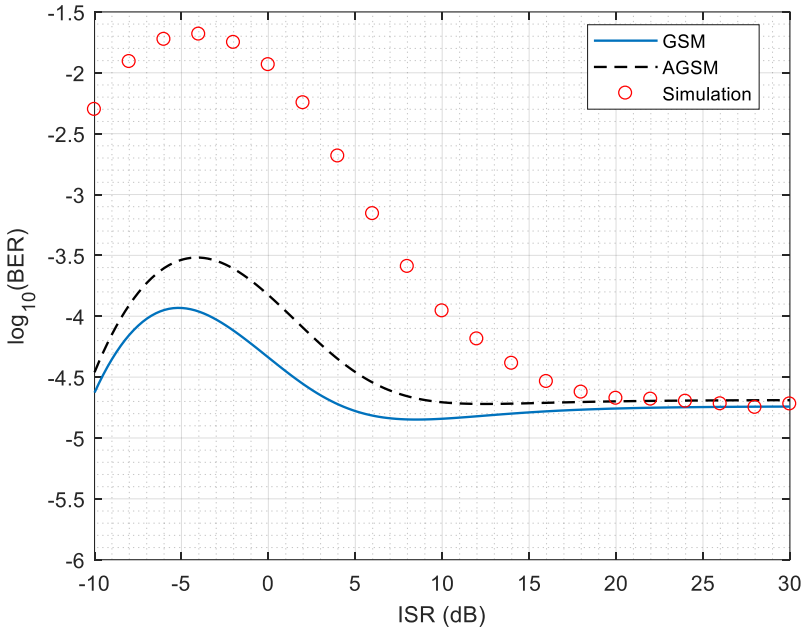

Figure 3-9: BER calculated by GSM (-), AGSM (--) and observed BER (o) for a QPSK system as a function of ISR for L = 7, μ = 1, SNR = 20 dB and ISR = 20 dB.

In Figure 3-9, for ISR values less than 15 dB, the deviation of the observed BER from the predicted values is significant. For example, at ISR = 0 dB, i.e. when the interference power σ_i^2 is equal to the signal power σ_d^2, both models over-estimate equalizer performance by almost 2 orders of magnitude. The deviation reduces to 1 order of magnitude for ISR = 10 dB with both models still over-estimating. Finally, for ISR > 15 dB, the model predictions are consistent with the observed values. Note that similar behavior was observed in [33] where the Ikuma model for steady state MSE, given as J_N in (2-27), was accurate for ISR > 10 dB.

Finally, in Figure 3-10 the comparison is shown between the GSM and AGSM predicted BER performance and the observed BER performance as a function of the fractional interference frequency f_i. The SNR and ISR are both set to 20 dB. Similar to the previous cases, the equalizer length $L = 7$ and $\Delta = 0$.

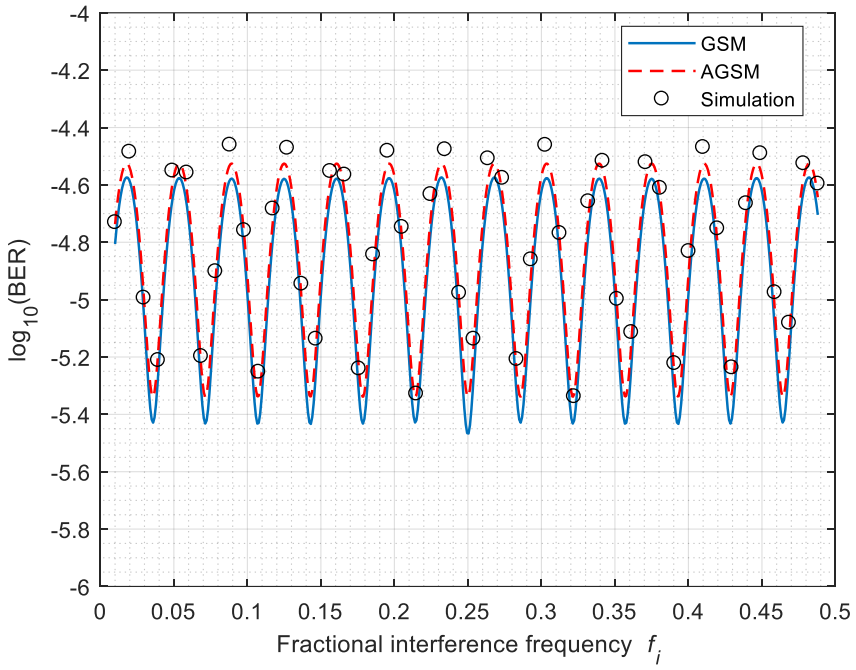

Figure 3-10: BER predictions by GSM (-), AGSM (--) and BER observed (o) for a QPSK system as a function of f_i for L = 7, μ = 1, SNR = 20 dB, ISR = 20 dB.

Note that Figure 3-10 once again shows the frequency dependence of the BER performance of the NLMS equalizer similar to what was observed in Figure 2-6. Both the GSM and AGSM expressions are able to capture the frequency dependence of the BER performance and the difference between the observed and predicted values never exceeds $10^{-0.2}$ for the entire range of fractional frequency $[0, 0.5)$.

Figures 3-6 through 3-10 show that the derived GSM expression as well as its more readily computable approximate version (AGSM) are able to predict the BER performance of the equalizer accurately for a wide range of system parameters for a communication system using the QPSK modulation scheme. In fact, the derived GSM expression provides an accurate estimate for the BER performance of the NLMS equalizer for all the cases other than ISR < 15 dB. The AGSM model on the other hand under-estimates the performance for $0 \le \mu < 1$ (as seen in Figure 3-7) and thus can be utilized to ascertain a conservative upper bound for the BER performance.

Higher order modulation schemes are gaining popularity in modern communication systems due to their better throughput. Figure 3-11 shows a grey coded 16-QAM constellation, which is a popular choice of digital modulation for modern communication systems such as LTE.

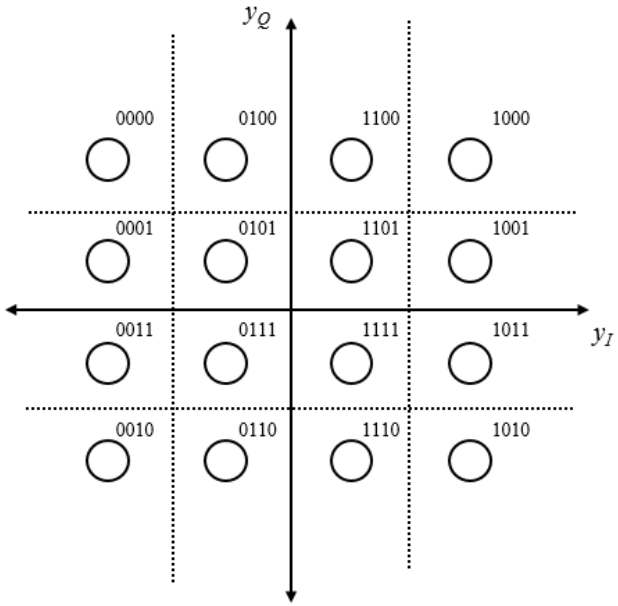

Figure 3-11: 16-QAM constellation (grey coded).

With higher order modulations, the computation of a BER estimate using the GSM and AGSM expressions is slightly different from what is shown in (3-39). We first compute the symbol error rate (S_E) by integrating our PDF expressions over the appropriate regions of interest – denoted by dotted lines in Figure 3-11.

$$S_E = \int\int f\left(y_n \middle| d_{n-\Delta} = \phi_m\right) dy_I dy_Q \tag{3-45}$$

Since the input constellation is grey-coded, $\hat{P}_e$ can be approximated using the following relation:

$$\hat{P}_e = \frac{S_E}{\log_2 M} \tag{3-46}$$

Figure 3-12 shows the comparison between the BER ($\hat{P}_e$) calculated using the AGSM model in (3-43) and the observed BER as a function of step-size for an equalizer of length $L = 7$ and $\Delta = 0$ for a 16-QAM system. ISR was set to 20 dB with the fractional interference frequency $f_i = 0.368$ and SNR was set to 20 dB.

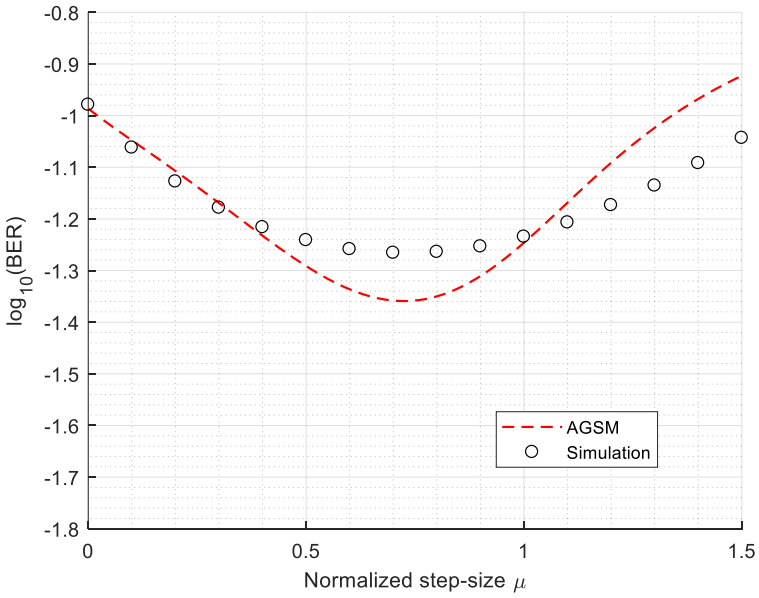

Figure 3-12: BER calculated by AGSM (--) and observed BER (o) for a 16-QAM system as a function of step-size μ for L = 7, SNR = 20 dB, ISR = 20 dB.

With $M = 16$, computing the BER estimate using the GSM expression becomes cumbersome as there are $16^7 \left(\approx 10^9\right)$ Gaussian components for each ϕ_m. Thus, for the 16-QAM case, only BER estimates using the AGSM model are shown in Figure 3-12 (and in the subsequent Figures 3-13 through 3-16). Note that for the 16-QAM case with $L = 7$ the BER performance improvement is less than one order of magnitude as the step-size is increased, with the maximum improvement observed at $\mu = 0.7$.

Figure 3-13 shows the BER performance (both observed and predicted by the AGSM model) of a NLMS equalizer for the 16-QAM case with $L = 21$ and $\Delta = 0$ as a function of step-size. ISR was set to 20 dB with the fractional interference frequency $f_i = 0.368$ and SNR was set to 22 dB.

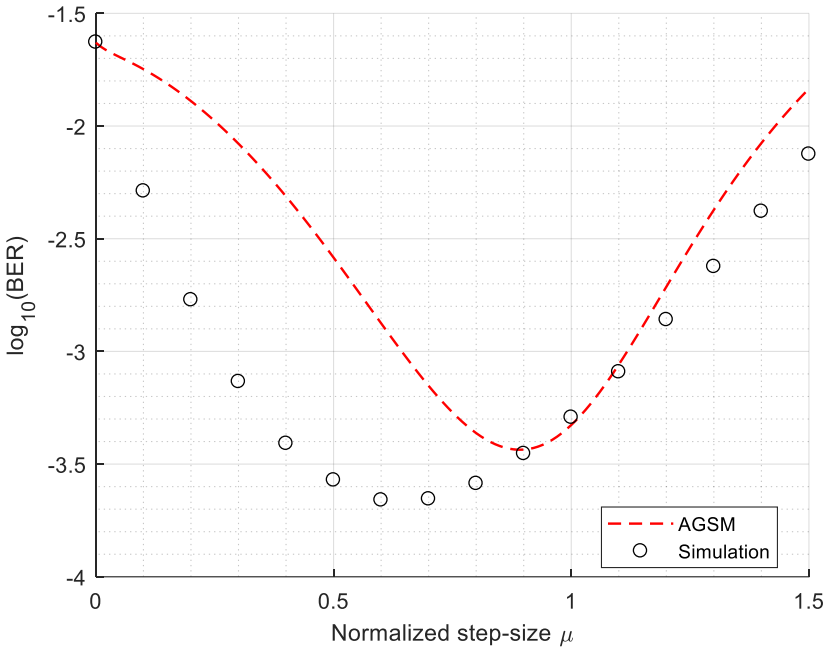

Figure 3-13: BER predicted from AGSM (--) and observed BER (o) for a 16-QAM system as a function of step-size μ for L = 21, SNR = 22 dB and ISR = 20 dB.

In Figure 3-13, observe that the BER performance improves by 2 orders of magnitude when step-size is changed from $\mu = 0$ to $\mu = 0.6$, thus showing that the non-Wiener characteristic of NLMS equalizers is present for higher order modulations. The AGSM model under-estimates the BER performance for $0 < \mu < 0.8$. However, the AGSM model suggests the BER-optimal step-size to be $\mu = 0.9$ and the corresponding BER performance is very close (~1/5th order of magnitude) to the observed BER-optimal step-size of $\mu = 0.6$. Thus, in terms of BER performance, the optimal step-size predicted by AGSM model is close to the actual optimal step-size.

Figure 3-14 shows the comparison between the $\hat{P}_e$ calculated using the AGSM model (3-43) and the observed BER as a function of SNR for a 16-QAM system. For Figure 3-14, the simulation parameters used are $L = 21$, $\Delta = 0$, $\mu = 1$, ISR = 20 dB, and $f_i = 0.368$.

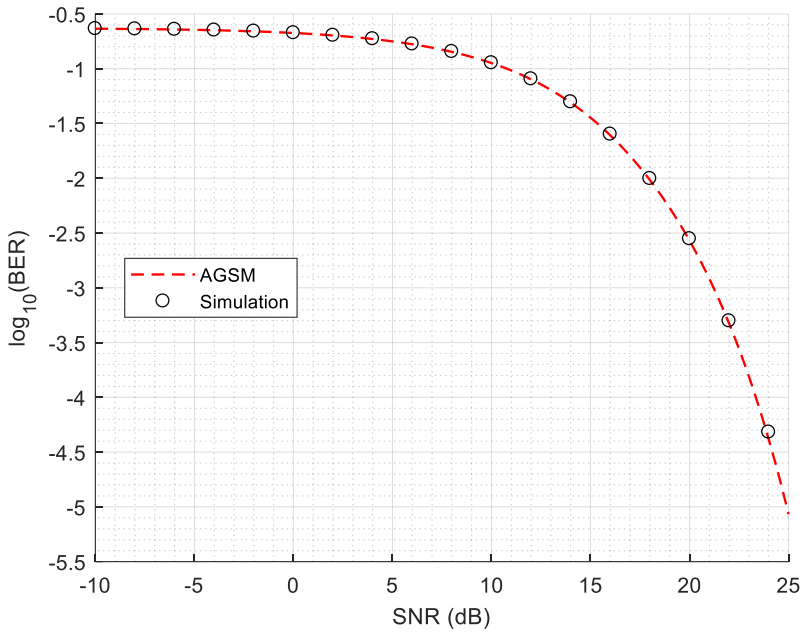

Figure 3-14: BER calculated by AGSM (--) and observed BER (o) for a 16-QAM system as a function of SNR for L = 21, μ = 1 and ISR = 20 dB.

For the given scenario, the AGSM model accurately predicts the BER performance for the entire range of SNR shown.

Figure 3-15 shows the comparison between the $\hat{P}_e$ calculated using the AGSM model (3-43) and the observed BER as a function of SNR for a 16-QAM system. For Figure 3-14, the simulation parameters used are $L = 21$, $\Delta = 0$, $\mu = 1$, SNR = 22 dB, and $f_i = 0.368$.

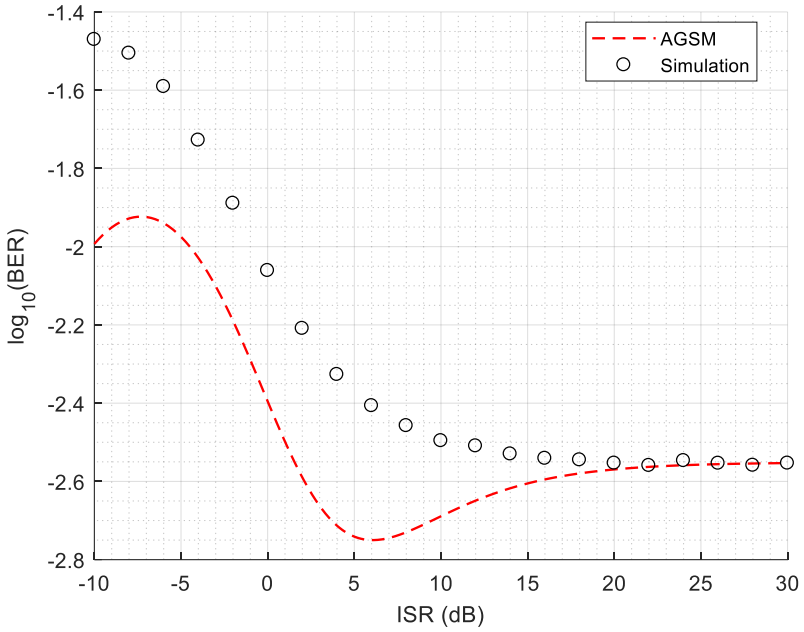

Figure 3-15: BER calculated by AGSM (--) and observed BER (o) for a 16-QAM system as a function of ISR for L = 21, μ = 1 and SNR = 22 dB.

Similar to Figure 3-9, the AGSM model over-estimates the system performance for ISR < 15 dB. Note that the over-estimation in this case is less than an order of magnitude and thus is not as severe as seen in Figure 3-9, where it was as high as 2 orders of magnitude.

Finally, in Figure 3-16 the comparison is shown between the AGSM model predicted BER performance and the observed BER performance as a function of the fractional interference frequency f_i. The SNR and ISR are set to 22 dB and 20 dB respectively. The equalizer parameters were set to $L = 21$, $\Delta = 0$, and $\mu = 1$.

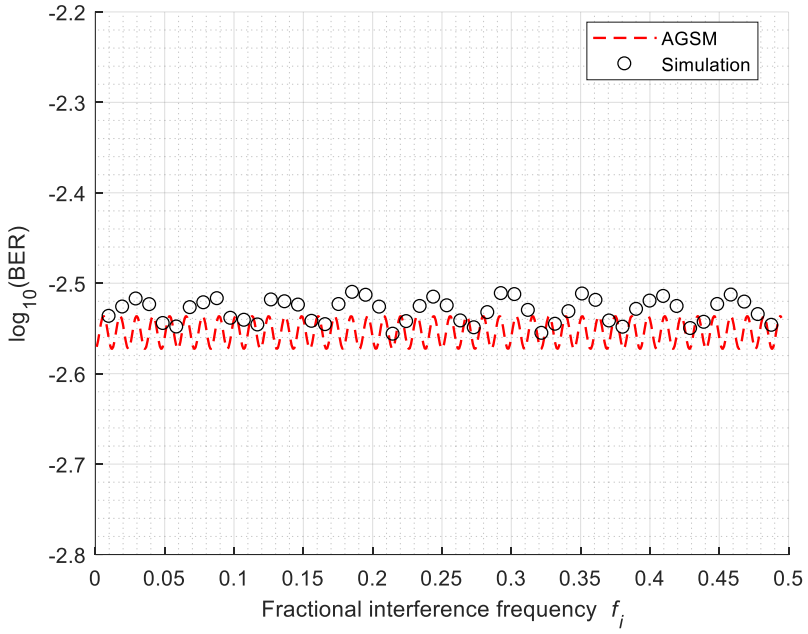

Figure 3-16: BER calculated by AGSM (--) and observed BER (o) for a 16-QAM system as a function of fractional interference frequency for L = 21, μ = 1, SNR = 22 dB and ISR = 20 dB.

In Figure 3-16, observe that the frequency dependence of the BER performance is considerably less pronounced for a 16-QAM system compared to for a QPSK system (Figure 3-10). The predictions made by the AGSM model are consistent with the simulation results.

Figures 3-13 through 3-16 highlight that the non-Wiener characteristic of NLMS equalization is not limited to constant amplitude modulation schemes, like QPSK, and that the derived GSM expression – as approximated by the AGSM model – is equally applicable for higher order modulation schemes, such as 16-QAM. Thus, for high ISR cases, the BER performance gain at high step-sizes can be leveraged by communication systems that use higher order modulations. The usefulness of the AGSM model is illustrated through the examples shown for a 16-QAM system, a case where the derived GSM expression is computationally infeasible for large equalizers.

3.5 Summary

In this chapter, a detailed analytical derivation was presented of the BER expression for the NLMS equalizer operating in a narrowband interference dominated environment. Several experiments highlighted the change in the equalizer behavior when the step-size is increased from $\mu = 0.01$ to $\mu = 1$. Analysis of the symbol-conditioned PDF of the equalizer output led to an expression in the form of a Gaussian Sum Mixture, from which probability of error (BER or SER) can then be predicted via appropriate integrations. Simulation results corroborated the efficacy of the derived Gaussian Sum Mixture (GSM). A more computationally efficient, approximate version of the Gaussian Sum Mixture was also derived and evaluated. The analytical framework that was followed and resulted in a Gaussian Sum Mixture expression for the equalizer output PDF can be extended to other flavors of the LMS algorithm, such as Bi-scale LMS.

CHAPTER 4 BI-SCALE NLMS EQUALIZATION

In this chapter an in-depth analysis is presented of the Bi-scale NLMS (BNLMS) equalizer introduced in [54]. The motivation for our interest in the Bi-scale NLMS equalizer is presented in Section 4.1 while in Section 4.2 a detailed description of the BLMS equalizer is presented. The MSE and BER behaviors of the BLMS equalizer are modeled in Sections 4.3 and 4.4 respectively. Finally, in Section 4.5, the model-predicted values of MSE and BER are compared with simulation results.

4.1 Motivation

Figure 4-1 shows the instantaneous MSE performance of a NLMS equalizer as a function of the number of iterations for four different initializations of the NLMS weight vector. These initializations are listed below:

i. Mean Steady State NLMS weights $\bar{\mathbf{w}}$, as given in (2-21)

ii. Wiener Weights $\mathbf{w}_W$, as given in (2-14)

iii. All Zeros

iv. Random initialization where the random numbers are drawn from a uniform distribution over $[0,1]$.

Apart from the initializations, all other system parameters, i.e. $L = 7$, $\Delta = 0$, SNR = 25 dB, ISR = 20 dB, and $f_i = 1/e$, were kept constant. The steady state NLMS MSE, as given in (2-27), is also shown.

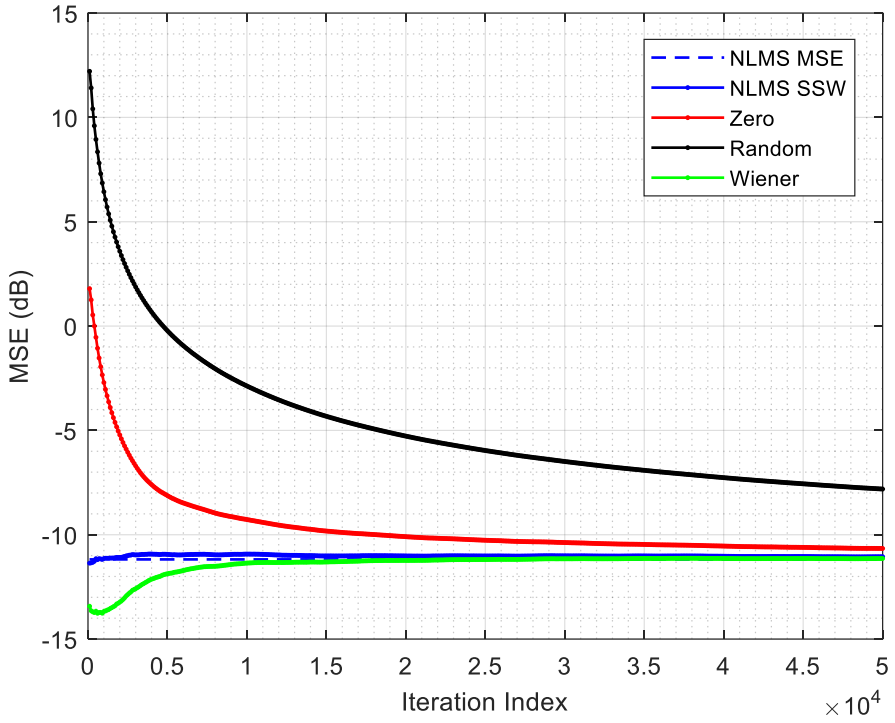

Figure 4-1: Instantaneous MSE performance of NLMS equalizer for different weight vector initializations.

Note that, except for case ii, the MSE curve approaches the steady state MSE from above. However, when the NLMS weights are initialized as the Wiener weights the instantaneous MSE initially is actually lower than the steady state MSE. This implies that – if by some means the NLMS weights are kept close to the Wiener weights – the MSE performance of the equalizer can be improved further. However, in Chapter 3 has been shown that in the presence of a narrowband interference high step-sizes yield superior performance. High step-sizes force the equalizer weights to converge to the steady state NLMS weights $\bar{\mathbf{w}}$, as given in (2-21) and these are away from the Wiener weights.

The Bi-scale LMS Equalizer introduced in [54] aims to solve the problem of keeping the adaptive filter weights close to the Wiener weights while simultaneously operating at high step-sizes. In Section 4.2 the BLMS equalizer is formally introduced, making its weight vector update rules explicit.

4.2 Bi-scale NLMS equalizer

The Bi-scale NLMS equalizer has two sets of weights: $\{\mathbf{w}_n \quad \mathbf{w}_{B,n}\}$, each of which consist of L tunable taps. Thus, the weight vectors can be written as:

$$\begin{aligned}\mathbf{w}_n &= \begin{bmatrix} w_n^{(0)} & w_n^{(1)} & \cdots & w_n^{(L-1)} \end{bmatrix}^T \\ \mathbf{w}_{B,\mathrm{n}} &= \begin{bmatrix} w_{B,n}^{(0)} & w_{B,n}^{(1)} & \cdots & w_{B,n}^{(L-1)} \end{bmatrix}^T \end{aligned} \tag{4-1}$$

The system block diagram is identical to the one shown in Figure 2-1, which renders the simplified block diagram the same as that in Figure 2-2. Thus, the input-output relationship of the BNLMS equalizer is given by:

$$y_{B,n} = \mathbf{w}_{B,n}^H \mathbf{u}_n \tag{4-2}$$

Similar to the NLMS case, the analysis for the BNLMS equalizer is also done at baseband. The signal statistics are the same as described in Section 2.2. The only difference with the NLMS equalizer is in the adaptive algorithm steps used to update the weight vectors shown in (4-1). Figure 4-2 shows the block diagram of a BNLMS equalizer.

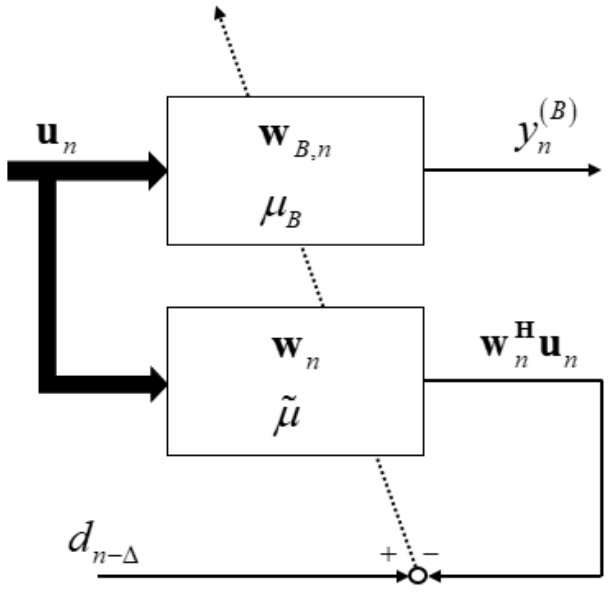

Figure 4-2: Block diagram of a BNLMS equalizer.

The update equation for the BNLMS weight vector is given by:

$$\mathbf{w}_{n+1} = \mathbf{w}_n + \tilde{\mu}\frac{\mathbf{u}_n}{\|\mathbf{u}_n\|^2 + a}e_n^* \tag{4-3}$$

$$\mathbf{w}_{B,n+1} = \mathbf{w}_n + \mu_B\frac{\mathbf{u}_n}{\|\mathbf{u}_n\|^2 + a}e_n^* \tag{4-4}$$

The error follows the expression $e_n = d_{n-\Delta} - \mathbf{w}_n^H\mathbf{u}_n$, i.e. e_n is the slow time-scale error. Along with two sets of weights, the BNLMS equalizer also has two step-sizes, $\tilde{\mu}$ and μ_B. The value of μ_B is large, roughly in the range of 0.5 to 1, to achieve the performance improvement of the NLMS equalizer at high step-sizes, while $\tilde{\mu}$ is chosen to be a small fraction (≈ 0.001) of μ_B. For analysis purposes the regularization parameter *a* is set to 0. Typically both $\mathbf{w}_{B,n}$ and $\mathbf{w}_n$ are initialized as the Wiener weights $\mathbf{w}_W$, as given in (2-14).

Observe from update equation (4-3) that $\mathbf{w}_n$ represents a conventional NLMS equalizer operating at a low step-size. Since $\mathbf{w}_n$ is initialized with the Wiener weights, low values of $\tilde{\mu}$ ensure that $\mathbf{w}_n$ does not deviate significantly from $\mathbf{w}_W$. Since the step-size μ_B is high, the instantaneous updates in (4-4) leverage the superior performance of the equalizer for high step-sizes. Thus, using the update equations in (4-3) and (4-4) both objectives – of keeping the weights close to the Wiener weights and operating the equalizer at a high step-size – are achieved simultaneously when using the BLMS weight vector to compute the equalizer output.

4.3 BNLMS MSE analysis

In this section, the MSE behavior of the BLMS equalizer is analyzed. As mentioned earlier, $\tilde{\mu}$ is typically chosen to be very small. Consequently, the steady-state assumption that $\mathbf{w_n} \simeq \mathbf{w}_W$ is reasonable. The error signal for the B(N)LMS equalizer is given by:

$$\varepsilon_n = d_{n-\Delta} - y_{B,n} \tag{4-5}$$

The next goal is to establish a relationship between e_n, which is the error signal for the slow step-size NLMS filter, and ε_n, which is the error signal for the BLMS filter as defined in (4-5), i.e. after the fast time-scale adaptation step. Substituting (4-4) in (4-5):

$$\begin{aligned}
\varepsilon_n &= d_{n-\Delta} - \mathbf{w}_{B,n}^H \mathbf{u}_n \\
&= d_{n-\Delta} - \left(\mathbf{w}_{n-1} + \mu_B \frac{\mathbf{u}_{n-1}}{\left\| \mathbf{u}_{n-1} \right\|^2} e_{n-1}^* \right)^H \mathbf{u}_n \\
&= d_{n-\Delta} - \mathbf{w}_{n-1}^H \mathbf{u}_n - \mu_B \frac{\mathbf{u}_{n-1}^H \mathbf{u}_n}{\left\| \mathbf{u}_{n-1} \right\|^2} e_{n-1}
\end{aligned} \tag{4-6}$$

Note that since $\tilde{\mu}$ in (4-3) is very small, $\mathbf{w}_{n-1} \simeq \mathbf{w}_n$. Furthermore, using the Clarkson and White approximation in (3-2) and substituting the values of $r_{uu,1}$ and $r_{uu,0}$ in (4-6):

$$\begin{aligned}
\varepsilon_n &= d_{n-\Delta} - \mathbf{w}_{n-1}^H \mathbf{u}_n - \mu_B \frac{\mathbf{u}_{n-1}^H \mathbf{u}_n}{\left\| \mathbf{u}_{n-1} \right\|^2} e_{n-1} \\
&\approx d_{n-\Delta} - \mathbf{w}_n^H \mathbf{u}_n - \mu_B \frac{L\sigma_i^2 e^{j\omega_i}}{L\left(\sigma_d^2 + \sigma_v^2 + \sigma_i^2\right)} e_{n-1}
\end{aligned} \tag{4-7}$$

From (2-8) and (4-7):

$$\varepsilon_n \approx e_n - \mu_B \frac{\sigma_i^2 e^{j\omega_i}}{\left(\sigma_d^2 + \sigma_v^2 + \sigma_i^2\right)} e_{n-1} \tag{4-8}$$

Equation (4-8) reveals that ε_n, the BNLMS error signal, is approximately a FIR filtered version of e_n, the slow time-scale NLMS error signal. The frequency response of this FIR filter is given by:

$$\begin{aligned} H_B(\omega) &\triangleq \frac{DTFT(\varepsilon_n)}{DTFT(e_n)} \\ &= 1-\mu_B \frac{\sigma_i^2}{\left(\sigma_d^2+\sigma_v^2+\sigma_i^2\right)} e^{-j(\omega-\omega_i)} \end{aligned} \tag{4-9}$$

By Parseval's Theorem, the MSE of the B(N)LMS equalizer can be deduced by evaluating:

$$J_B \triangleq E\left[\left|\varepsilon_n\right|^2\right] = \frac{1}{2\pi}\int_{-\pi}^{\pi}\left|H_B(\omega)\right|^2 S_E(\omega)\,d\omega \tag{4-10}$$

Out of the two terms inside the integral in (4-10), using (4-9), the magnitude response $\left|H_B(\omega)\right|^2$ can be written as:

$$\left|H_B(\omega)\right|^2 = 1+\xi^2-2\xi\cos(\omega-\omega_i) \tag{4-11}$$

where $\omega_i = 2\pi f_i$ is the angular frequency of the sinusoidal interference and ξ is defined as:

$$\xi \triangleq \mu_B \frac{\sigma_i^2}{\left(\sigma_d^2+\sigma_v^2+\sigma_i^2\right)} \tag{4-12}$$

The second term in (4-10), $S_{E_w}(\omega)$, due to $e_n \approx e_{n,W}$ is well approximated by the spectrum of the Wiener error process, which is given by [21]:

$$S_{E_w}(\omega) = \sigma_d^2\left|e^{-j\omega\Delta} - W_w(\omega)\right|^2 + \sigma_v^2\left|W_w(\omega)\right|^2 \tag{4-13}$$

where $W_w(\omega)$ is the frequency response of the Wiener filter in (2-14) and given by:

$$
\begin{aligned}
W_w(\omega) &= \sum_{m=0}^{L-1} w_m^* e^{-j\omega m} \\
&= \eta e^{-j\omega\Delta} - \eta\zeta \sum_{\substack{m=0 \\ m\neq\Delta}}^{L-1} e^{-j(\omega-\omega_i)m}
\end{aligned}
\tag{4-14}
$$

where

$$
\zeta \triangleq \frac{\sigma_i^2}{\lambda_{\max}} \tag{4-15}
$$

Using $\breve{\omega} = \omega - \omega_i$, the two magnitude squared terms in (4-13) can be simplified to:

$$
\begin{aligned}
\left|e^{-j\omega\Delta} - W_w(\omega)\right|^2 &= (1-\eta)^2 + 2\,\mathrm{Re}\left\{(1-\eta)\eta\zeta \sum_{m=0}^{L-1} e^{j(\breve{\omega}m-\omega\Delta)}\right\} \\
&\quad + \eta^2\zeta^2 \sum_{m=0}^{L-1}\sum_{n=0}^{L-1} e^{-j\breve{\omega}m} e^{j\breve{\omega}n} \\
&= (1-\eta)^2 + 2(1-\eta)\eta\zeta\cos(\breve{\omega}m - \omega\Delta) + \eta^2\zeta^2 L \\
&\quad + 2\eta^2\zeta^2 \sum_{m=1}^{L-1}\sum_{n=0}^{m-1} \cos\breve{\omega}(m-n)
\end{aligned}
\tag{4-16}
$$

$$
\begin{aligned}
\left|W_w(\omega)\right|^2 &= \eta^2 - 2\,\mathrm{Re}\left\{\eta^2\zeta \sum_{m=0}^{L-1} e^{j(\breve{\omega}m-\omega\Delta)}\right\} + \eta^2\zeta^2 \sum_{m=0}^{L-1}\sum_{n=0}^{L-1} e^{-j\breve{\omega}m} e^{j\breve{\omega}n} \\
&= \eta^2 - 2\eta^2\zeta\cos(\breve{\omega}m - \omega\Delta) + \eta^2\zeta^2 L + 2\eta^2\zeta^2 \sum_{m=1}^{L-1}\sum_{n=0}^{m-1} \cos\breve{\omega}(m-n)
\end{aligned}
\tag{4-17}
$$

Substituting (4-16) and (4-17) into (4-13) yields:

$$
\begin{aligned}
S_{E_w}(\omega) &= \sigma_d^2(1-\eta)^2 + \sigma_v^2\eta^2 + \left[\sigma_d^2(1-\eta) - \sigma_v^2\eta\right] 2\eta\zeta\cos(\breve{\omega}m - \omega\Delta) \\
&\quad + \left(\sigma_d^2 + \sigma_v^2\right)\eta^2\kappa^2 \left[L + 2\sum_{m=1}^{L-1}\sum_{n=0}^{m-1} \cos\breve{\omega}(m-n)\right] \\
&= \eta\left(\sigma_v^2 + \sigma_d^2\zeta^2 L\right) + 2\sigma_d^2\eta\zeta^2 \sum_{m=1}^{L-1}\sum_{n=0}^{m-1} \cos\breve{\omega}(m-n)
\end{aligned}
\tag{4-18}
$$

Finally, substituting (4-18) into (4-10) yields

$$J_B \approx \eta\left(\sigma_v^2 + \sigma_d^2\zeta^2 L\right)T_1 + 2\sigma_d^2\eta\zeta^2\sum_{m=1}^{L-1}\sum_{n=0}^{m-1}T_2 \tag{4-19}$$

where

$$\begin{aligned} T_1 &= \frac{1}{2\pi}\int_{-\pi}^{\pi}\left|H_B\left(e^{j\omega}\right)\right|^2 d\omega \\ &= \frac{1}{2\pi}\int_{-\pi}^{\pi}\left[1+\xi^2-2\xi\cos\left(\omega-\omega_i\right)\right]d\omega \\ &= 1+\xi^2 \end{aligned} \tag{4-20}$$

$$\begin{aligned} T_2 &= \frac{1}{2\pi}\int_{-\pi}^{\pi}\left|H_B\left(e^{j\omega}\right)\right|^2\cos\breve{\omega}\left(m-n\right)d\omega \\ &= \left(1+\xi^2\right)\frac{1}{2\pi}\int_{-\pi}^{\pi}\cos\left\{\breve{\omega}(m-n)\right\}d\omega - \frac{\xi}{\pi}\int_{-\pi}^{\pi}\cos\breve{\omega}\cos\left\{\breve{\omega}(m-n)\right\}d\omega \end{aligned} \tag{4-21}$$

Using the identity

$$\frac{1}{\pi}\int_{-\pi}^{\pi}\cos\omega\cos n\omega d\omega = \begin{cases} 1, & \text{if } n=1 \\ 0, & \text{o.w.} \end{cases} \tag{4-22}$$

T_2 in (4-21) simplifies to

$$T_2 = \begin{cases} -\xi, & m-n=1 \\ 0, & \text{otherwise} \end{cases} \tag{4-23}$$

Substituting (4-20) and (4-23) into (4-19) results in:

$$\begin{aligned} J_B &\approx \eta\left(\sigma_v^2+\sigma_d^2\zeta^2 L\right)\left(1+\xi^2\right)+2\sigma_d^2\eta\zeta^2\left[-\xi\left(L-1\right)\right] \\ &= \eta\left[\sigma_v^2\left(1+\xi^2\right)+\sigma_d^2\zeta^2\left\{L\left(1-\xi\right)^2+2\xi\right\}\right] \end{aligned} \tag{4-24}$$

Thus, (4-24) provides a closed form expression for the steady state MSE performance of the BNLMS equalizer in the presence of a narrowband interference. Note that the NLMS counterpart for the steady state MSE under the same conditions is expressed in

(2-27). In Section 4.6.1 the performance of the MSE model for the BNLMS algorithm, given in (4-24), is analyzed for a wide range of system parameters.

4.4 BLMS BER modeling

In this section, the BER behavior of the B(N)LMS equalizer is modeled. Using the update equation in (4-4), (4-2) can be re-written as:

$$\begin{aligned} y_{B,n} &= \left(\mathbf{w}_{n-1} + \frac{\mu_B}{\left\| \mathbf{u}_{n-1} \right\|^2} \mathbf{u}_{n-1} e_{n-1}^* \right)^H \mathbf{u}_n \\ &= \mathbf{w}_{n-1}^{\mathbf{H}} \mathbf{u}_n + \frac{\mu_B}{\mathbf{u}_{n-1}^{\mathbf{H}} \mathbf{u}_{n-1}} \left(\mathbf{u}_{n-1}^{\mathbf{H}} \mathbf{u}_n \right) e_{n-1} \end{aligned} \tag{4-25}$$

Applying the Clarkson and White approximation from (3-2) yields:

$$\begin{aligned} y_{B,n} &\approx \mathbf{w}_{n-1}^{\mathbf{H}} \mathbf{u}_n + \frac{\mu_B}{L\left(\sigma_d^2 + \sigma_v^2 + \sigma_i^2 \right)} \left(L\sigma_i^2 e^{j\omega_i} \right) e_{n-1} \\ &= \mathbf{w}_{n-1}^{\mathbf{H}} \mathbf{u}_n + \mu_B \beta e^{j\omega_i} e_{n-1} \end{aligned} \tag{4-26}$$

Note that β is defined in (3-4). Substituting for e_{n-1}:

$$\begin{aligned} y_{B,n} &= \mathbf{w}_{n-1}^{\mathbf{H}} \mathbf{u}_n + \mu_B \beta e^{j\omega_i} \left(d_{n-1-\Delta} - y_{n-1} \right) \\ &= \mathbf{w}_{n-1}^{\mathbf{H}} \left(\mathbf{u}_n - \mu_B \beta e^{j\omega_i} \mathbf{u}_{n-1} \right) + \mu_B \beta e^{j\omega_i} d_{n-1-\Delta} \end{aligned} \tag{4-27}$$

Since $\tilde{\mu}$ is chosen to be very small, the approximation used in Section 4.3 that $\mathbf{w}_{n-1} \approx \mathbf{w}_W$ is again used. Thus (4-27) can be re-written as:

$$\tilde{y}_{B,n} \approx \mathbf{w}_W^{\mathbf{H}} \left(\mathbf{u}_n - \mu_B \beta e^{j\omega_i} \mathbf{u}_{n-1} \right) + \mu_B \beta e^{j\omega_i} d_{n-1-\Delta} \tag{4-28}$$

Observe that (4-28) is similar to (3-6) with the only difference being that the weight vectors are the Wiener weights $\mathbf{w}_W$ instead of the steady state NLMS weights $\bar{\mathbf{w}}$. Since the closed form expression for $\mathbf{w}_W$ is available, and given in (2-14), the derivation for the

BER model for the B(N)LMS equalizer will follow the same steps as used to derive the BER model for the NLMS equalizer in Section 3.2. Recall that the closed form expression for the mean of the steady state NLMS weights is also available, and given in (2-21).

Splitting the input vector $\mathbf{u}_n$ into its three constituent components, as given in (2-3), (4-28) can be written as:

$$\tilde{y}_{B,n} = \tilde{y}_{d,n} + \tilde{y}_{i,n} + \tilde{y}_{v,n} \tag{4-29}$$

where $\tilde{y}_{d,n}$, $\tilde{y}_{i,n}$, and $\tilde{y}_{v,n}$ are the contributions associated with the desired symbols, the Gaussian noise, and the narrowband interference respectively. The expressions for $\tilde{y}_{d,n}$, $\tilde{y}_{i,n}$, and $\tilde{y}_{v,n}$ are given by the following equations.

$$\tilde{y}_{d,n} = \mathbf{w}_W^{\mathbf{H}} \left(\mathbf{d}_n - \mu_B \beta e^{j\omega_i} \mathbf{d}_{n-1} \right) + \mu_B \beta e^{j\omega_i} d_{n-1-\Delta} \tag{4-30}$$

$$\tilde{y}_{i,n} = \mathbf{w}_W^{\mathbf{H}} \left(\mathbf{i}_n - \mu_B \beta e^{j\omega_i} \mathbf{i}_{n-1} \right) \tag{4-31}$$

$$\tilde{y}_{v,n} = \mathbf{w}_W^{\mathbf{H}} \left(\mathbf{v}_n - \mu_B \beta e^{j\omega_i} \mathbf{v}_{n-1} \right) \tag{4-32}$$

Similar to the NLMS case, the three terms in (4-29) are mutually independent. Thus, the conditional PDF $f\left(y_n \mid d_{n-\Delta} = \phi_m\right)$ can be computed by convolving the individual conditional PDFs of the three components $\tilde{y}_{d,n}$, $\tilde{y}_{i,n}$, and $\tilde{y}_{v,n}$.

4.4.1 Conditional PDF of the noise component $\tilde{y}_{v,n}$

The additive Gaussian noise is independent of the symbols that were transmitted, which implies that the conditional PDF of $\left(\tilde{y}_{v,n} \mid d_{n-\Delta} = \phi_m\right)$ is equivalent to the

unconditional PDF. The derivation of the PDF is identical to the one shown in Section 3.2.1. $\tilde{y}_n^v$ thus follows a complex normal distribution and can be written as:

$$\tilde{y}_{v,n} \sim CN\left(0, \xi_v^{(B)} \sigma_v^2\right) \tag{4-33}$$

where

$$\xi_v^{(B)} = \left\|\mathbf{w}_W\right\|^2 \left(1 + \mu_B^2 \beta^2\right) - 2\mu_B \beta \,\mathrm{Re}\left[w_{W,k} w_{W,k-1}^* e^{j\omega_i} \right] \tag{4-34}$$

Note that $\mathbf{w}_W = \left[w_{W,0} \quad w_{W,1} \quad \ldots \quad w_{W,L-1} \right]^T$.

4.4.2 Conditional PDF of the interference component $\tilde{y}_{i,n}$

The narrowband interference modeled by the complex exponential given in (2-6) is also independent of the transmitted signal. Therefore, similar to the case of the noise component, the conditional PDF of $\tilde{y}_{i,n} \,|\, d_{n-\Delta} = \phi_m$ is equivalent to the unconditional PDF. Again, the derivation of the PDF is identical to the one described in Section 3.2.2.

Similar to (3-21), $\tilde{y}_{i,n}$ also follows a complex normal distribution.

$$\tilde{y}_{i,n} \sim CN\left(0, \xi_i^{(B)} \sigma_i^2\right) \tag{4-35}$$

where

$$\xi_i^{(B)} = \left(1 - \mu_B \beta\right)^2 \mathbf{w}_W^{\mathbf{H}} \mathbf{e}\mathbf{e}^{\mathbf{H}} \mathbf{w}_W \tag{4-36}$$

4.4.3 Conditional PDF of the symbol component $\tilde{y}_{d,n}$

$\tilde{y}_{d,n}$ can be expressed as the sum of a deterministic component κ and a stochastic component which is a sum of L random variables and each of the components depends

on Δ as was shown in Figure 3-4. Table 4-1 shows the individual components for different values of Δ. Note that the derivation is identical to the one shown in Section 3.2.3. The only difference between c_k (Table 3-1) and $\tilde{c}_k$ (Table 4-1) is that the former is a function of the steady state NLMS weights as given in (2-21) while the latter is a function of the Wiener weights given in (2-14).

Table 4-1: Deterministic and Stochastic Components of $\tilde{y}_{d,n}$ for BNLMS equalizer.

Δ	κ	$\tilde{c}_k$
0	$w^*_{W,\Delta}\phi_m$	$\tilde{c}_k = \begin{cases} w^*_{W,k+1} - w^*_{W,k}\mu\beta e^{j\omega_i} + \mu\beta e^{j\omega_i} & k=1 \\ w^*_{W,k+1} - w^*_{W,k}\mu\beta e^{j\omega_i} & k=\{2,3,\ldots,L-1\} \\ -w^*_{W,k-1}\mu\beta e^{j\omega_i} & k=L \end{cases}$
$\Delta>0$ $\Delta<L-1$	$\left(w^*_{W,\Delta} - w^*_{W,\Delta-1}\mu\beta e^{j\omega_i}\right)\phi_m$	$\tilde{c}_k = \begin{cases} w^*_{W,k} & k=0 \\ w^*_{W,k+1} - w^*_{W,k}\mu\beta e^{j\omega_i} + \mu\beta e^{j\omega_i} & k=\Delta+1 \\ w^*_{W,k+1} - w^*_{W,k}\mu\beta e^{j\omega_i} & k=\{0,\ldots,L-1\}-\{\Delta,\Delta+1\} \\ -w^*_{W,k-1}\mu\beta e^{j\omega_i} & k=L \end{cases}$
$L-1$	$\left(w^*_{W,\Delta} - w^*_{W,\Delta-1}\mu\beta e^{j\omega_i}\right)\phi_m$	$\tilde{c}_k = \begin{cases} w^*_{W,k} & k=0 \\ w^*_{W,k+1} - w^*_{W,k}\mu\beta e^{j\omega_i} & k=\{1,2,\ldots,L-2\} \\ -w^*_{W,k-1}\mu\beta e^{j\omega_i} + \mu\beta e^{j\omega_i} & k=L \end{cases}$

With the desired symbols coming from a discrete constellation with an alphabet size of *M* similar to the NLMS case, the weighted linear combination of L random variables can be represented by a probability mass function (PMF) which can take on M^L values. Thus, the conditional PMF for $\tilde{y}_{d,n}$ is of the form:

$$f\left(\tilde{y}_{d,n}\Big|_{d_{n-\Delta}=\phi_m}\right) = \frac{1}{M^L}\sum_{k_0=1}^{M}\sum_{\substack{k_1=1 \\ k_l\neq\Delta}}^{M}\cdots\sum_{k_L=1}^{M}\left(\delta-\kappa-\breve{\phi}\right) \tag{4-37}$$

where the values of $\tilde{c}_k$ and κ depend on Δ as shown in Table 4-1 and $\breve{\phi}_{\mathbf{k}}$ is defined as:

$$\breve{\phi} \triangleq \sum_{\substack{l=0 \\ l\neq\Delta}}^{L} \tilde{c}_l \phi_{k_l} \tag{4-38}$$

4.4.4 Conditional PDF of the output $\tilde{y}_{B,n}$

The conditional output $\tilde{y}_{B,n}\left|d_{n-\Delta}=\phi_m\right.$ was expressed as a sum of three mutually independent terms in (4-29). Thus, the overall PDF will be a convolution of the PDFs derived in (4-33), (4-35) and (4-37). Note that the first two are Gaussian distributions while the last one is a discrete uniform distribution. So the overall conditional PDF turns out to have the form of a Gaussian Sum Mixture (GSM) containing M^L terms and provides the approximation to the conditional PDF of interest:

$$f\left(\tilde{y}_{B,n}\left|d_{n-\Delta}=\phi_m\right.\right)=\frac{1}{M^L}\sum_{k_0=1}^{M}\sum_{\substack{k_1=1 \\ k_l\neq\Delta}}^{M}\cdots\sum_{k_L=1}^{M} CN\left(\kappa+\breve{\phi},\xi_i^{(B)}\sigma_i^2+\xi_v^{(B)}\sigma_v^2\right) \tag{4-39}$$

Analogous to the NLMS case, the BER estimate $\hat{P}_e$ is computed by integrating the PDF in (4-39) over regions in the I/Q plane contributing to bit errors. The accuracy of the model is compared with simulation results in Section 4.6.2.

4.5 Approximate BER model for BNLMS equalizer

In this section, an approximate BER model for the BNLMS equalizer is presented with M Gaussians, similar to the one presented in Section 3.3. Tables 4-1 shows that $\tilde{c}_k$ depends on the Wiener weights $\mathbf{w}_W$. Following a similar approach which led to (3-41):

$$Var\left[\sum_{\substack{k=0 \\ k\neq\Delta}}^{L-1}\tilde{c}_k d_{n-k}\right]=\xi_d^{(B)}\sigma_d^2 \tag{4-40}$$

where

$$\xi_d^{(B)} \triangleq \sum_{\substack{k=0 \\ k\neq\Delta}}^{L-1} \left|\tilde{c}_k\right|^2 \tag{4-41}$$

The approximate version of the conditional PDF (4-39) for the BNLMS equalizer is given by:

$$g\left(\tilde{y}_{B,n}\middle| d_{n-\Delta}=\phi_m\right)=\frac{1}{M}\sum_{l=1}^{M} CN\left(\kappa+c_L\phi_{k_l}, \xi_v^{(B)}\sigma_v^2+\xi_d^{(B)}\sigma_d^2+\xi_i^{(B)}\sigma_i^2\right) \tag{4-42}$$

The performance of the BER predictions using (4-42) is compared to the simulation results in Section 4.6.2.

4.6 Results

In this section, the predicted MSE given in (4-24) and the BER predicted from both the full model in (4-39) and its approximation in (4-42) for the BNLMS equalizer are compared to simulation results.

4.6.1 MSE Performance of BNLMS equalizer

For simulation purposes, the desired signal is represented by QPSK symbols, which makes the alphabet size $M=4$. The observed value of MSE is calculated using a Monte Carlo simulation technique by ensemble averaging of independent runs. Unless specified otherwise, the ensemble size is 100 runs for all of the subsequent simulations. A single run consists of 100,000 independent symbols generated randomly, which are then corrupted by AWGN and the narrowband interference.

Figure 4-3 shows a comparison between NLMS and BNLMS equalizers in terms of MSE performance as a function of normalized step-size, i.e. μ and μ_B for NLMS and B(N)LMS respectively. For the NLMS equalizer the weights were initialized as steady state NLMS weights, as given in (2-21). For the BNLMS equalizer both sets of weights, i.e. $\mathbf{w}_{B,\mathrm{n}}$ and $\mathbf{w}_{\mathrm{n}}$, were initialized as Wiener weights (2-14), and $\tilde{\mu}=0.001\mu_B$.

An equalizer of length $L = 7$ and equalization center $\Delta = 0$ was used. ISR was set to 20 dB with a fractional frequency of $f_i = 0.368$ and SNR was set to 18 dB. The observed values are compared with the values predicted according to (2-27) and (4-24).

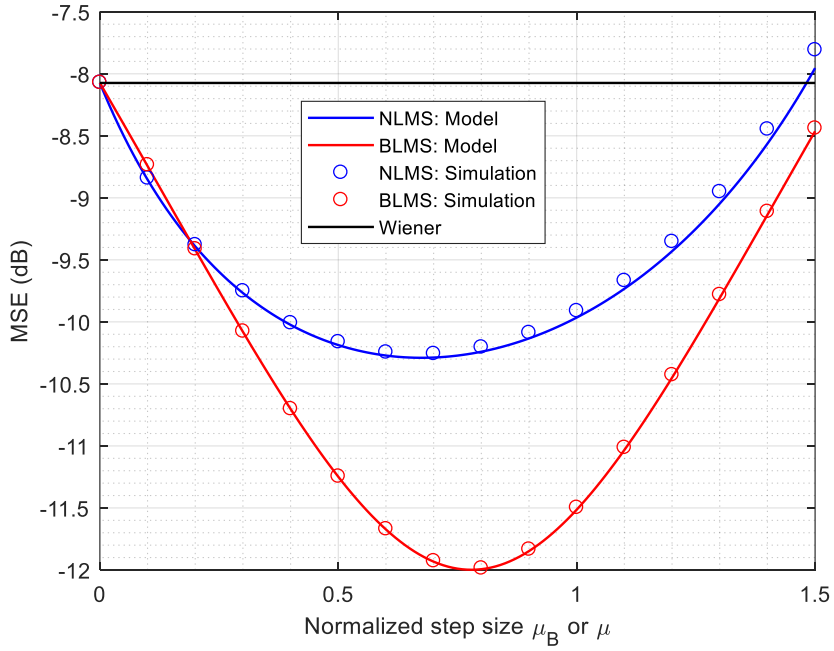

Figure 4-3: Predicted MSE (-) and observed MSE (o) for NLMS and BNLMS for different step-sizes.

Note that NLMS provides a 2 dB improvement in MSE over Wiener performance (seen for $\mu = 0$), consistent with [32], and BNLMS provides a further improvement in MSE by 2 dB over NLMS. The MSE estimate for BNLMS given in (4-24), as derived in this work, is accurate for the entire range of step-sizes of interest. With the relative performance gain of the BNLMS equalizer over its NLMS counterpart shown in Figure 4-3, the performance of the MSE prediction for BNLMS given in (4-24) is now investigated in more detail.

Figure 4-4 shows the comparison between J_B and the observed MSE for an equalizer of length $L = 7$ and equalization center $\Delta = 0$ as a function SNR. ISR was set to 20 dB with a fractional frequency $f = 0.368$ for the interference. Similar to the settings used to generate Figure 4-2, both sets of weights for the BNLMS equalizer, i.e. $\mathbf{w}_{B,\mathrm{n}}$ and $\mathbf{w}_{\mathrm{n}}$,

were initialized as Wiener weights, as given by (2-14). The step-sizes were set to $\mu_B = 1$ and $\tilde{\mu} = 0.001$.

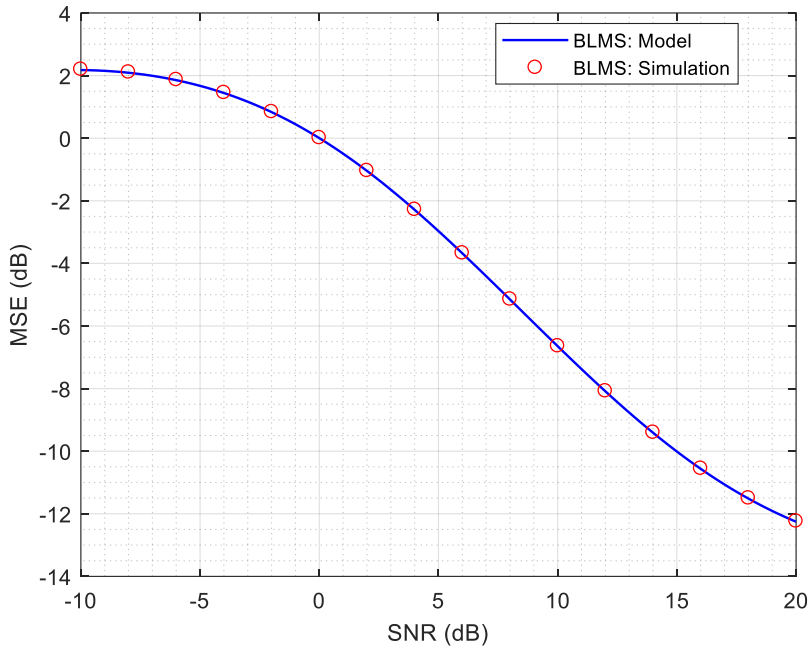

Figure 4-4: Predicted MSE (-) and observed MSE (o) for BNLMS as a function of SNR for μ_B = 1.

Figure 4-4 shows that the proposed model predicts the MSE accurately for the entire range of SNR.

Figure 4-5 shows the comparison between predicted and observed MSE as a function of ISR. SNR was set to 18 dB with the interference fractional frequency set to $f = 0.368$. An equalizer of length $L = 7$ with equalization center $\Delta = 0$ was used with the step-sizes set to $\mu_B = 1$ and $\tilde{\mu} = 0.001$.

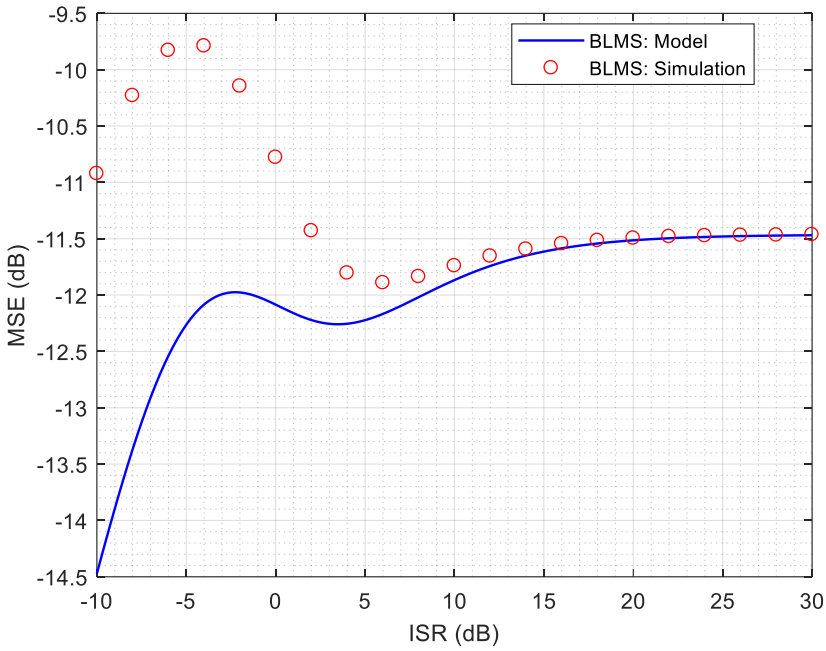

Figure 4-5: Predicted MSE (-) and observed MSE (o) for BNLMS as a function of ISR for μ_B = 1.

From Figure 4-5, it is seen that the predicted MSE over-estimates equalizer performance by ~3.5 dB for ISR = -10 dB. The difference between the predicted and the observed values reduces to ~1 dB for ISR = 2 dB. For ISR > 10 dB the predicted MSE is consistent with the observed values. In other words, the model is accurate when the narrowband interference is strong. Note that the Ikuma estimate for the steady state MSE for a NLMS equalizer also exhibits the same characteristic of accuracy improving with the increase in interference power [33].

Finally, Figure 4-6 shows the comparison between the predicted and observed MSE as a function of fractional interference frequency f_i . SNR and ISR were set to 18 dB and 20 dB respectively. Similar to Figures 4-2 through 4-4 an equalizer of length $L = 7$ with equalization center $\Delta = 0$ was chosen. The step-sizes were set to $\mu_B = 1$ and $\tilde{\mu} = 0.001$.

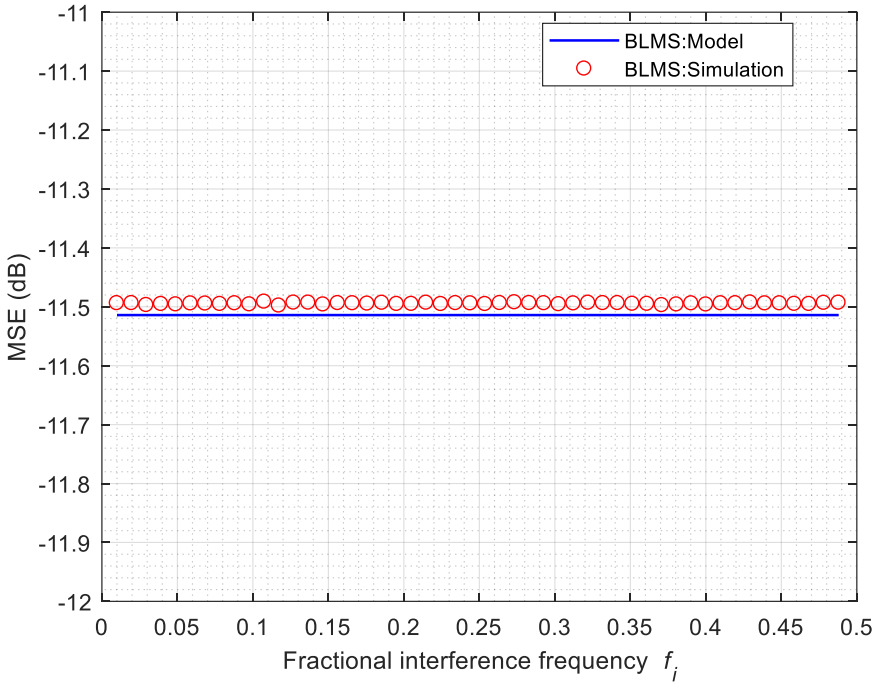

Figure 4-6: Predicted MSE (-) and observed MSE (o) for BNLMS as a function of fractional interference frequency f_i for μ_B = 1.

Figure 4-6 shows that the MSE performance of the BNLMS equalizer is independent of the interference frequency. Note that for the NLMS equalizer the frequency independence of the MSE performance was seen in Figure 2-5. The predicted MSE is consistent with the observed values.

4.6.2 BER performance of the BNLMS equalizer

A simulation environment identical to the one described in Section 3.4 is used to compute the observed BER values. Hence our desired signal cases are represented by:

i. QPSK symbols, which make the alphabet size $M = 4$.
ii. 16-QAM symbols, which make the alphabet size $M = 16$.

The observed value of BER is calculated using a Monte Carlo simulation technique by ensemble averaging of independent runs. Unless specified otherwise, the ensemble size is

100 runs for all of the subsequent simulations. A single run consists of 100,000 independent symbols generated randomly, which are then corrupted by AWGN and the narrowband interference.

In Figure 4-7 the BER performance of a BNLMS equalizer and a NLMS equalizer of length $L = 7$ and $\Delta = 0$ are compared as a function of the normalized step-size for a QPSK system. Note that the normalized step-size is denoted by μ_B and μ for BNLMS and NLMS respectively. For the BNLMS equalizer, $\tilde{\mu}$ was set to $0.001\mu_B$. ISR was set to 20 dB with a fractional frequency of $f_i = 0.368$ and SNR was set to 18 dB. The weights of the NLMS equalizer are initialized with the steady state NLMS weights in (2-21), whereas both sets of BNLMS weights $\mathbf{w}_{B,n}$ and $\mathbf{w}_n$ were initialized using the Wiener weights given in (2-14). The observed values are compared with the BER values predicted by using the corresponding GSM expressions (in (3-37) for NLMS, in (4-39) for BNLMS) and the AGSM (in (3-43) for NLMS, in (4-42) for BNLMS) for each equalizer.

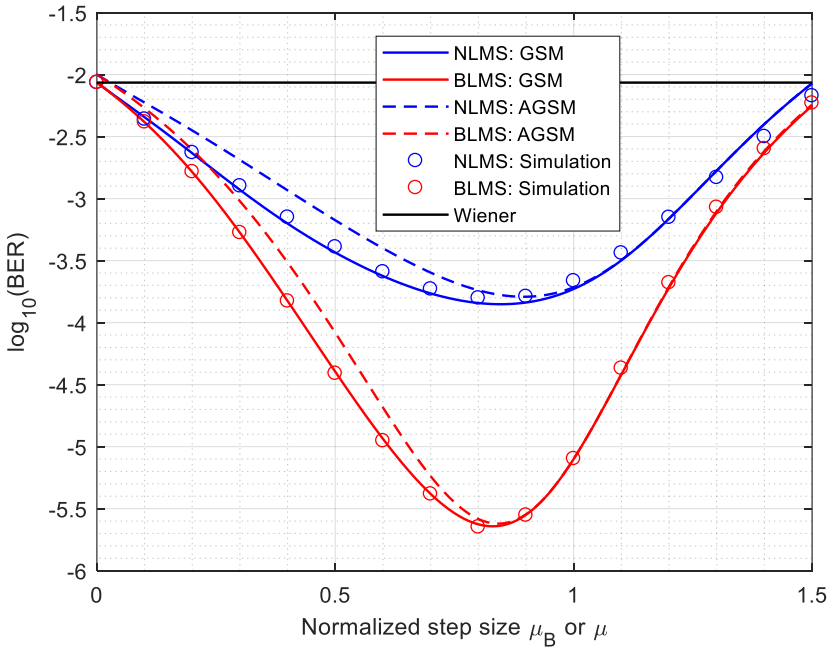

Figure 4-7: Predicted BER from GSM (-), AGSM (--), and observed BER (o), for NLMS and BNLMS as a function of step-size for a QPSK system.

Figure 4-7 shows that the BNLMS equalizer outperforms the NLMS equalizer in terms of BER performance. Note that the ~2 dB improvement in MSE performance of the BNLMS equalizer over the NLMS equalizer, as shown in Figure 4-2, results in an improvement of the BER performance by 2 orders of magnitude. The proposed GSM expression predicts the BER performance of the BNLMS equalizer accurately for the entire range of step-sizes. The AGSM approximation leads to marginally under-estimated BNLMS performance for $\mu_B < 0.7$. For $\mu_B > 0.7$, the BER predicted using the AGSM expression is consistent with the observed values. Thus, the AGSM expression can be used to give a conservative upper bound for the BER performance of the BNLMS equalizer.

In Figure 4-8 the observed BER performance of a BNLMS equalizer is shown as a function of SNR, for an equalizer of length $L = 7$ and $\Delta = 0$ with the step-sizes set to $\mu_B = 1$ and $\tilde{\mu} = 0.001$ for a QPSK system. ISR was set to 20 dB and the fractional interference frequency was $f_i = 0.368$. Both sets of BNLMS weights, $\mathbf{w}_{B,n}$ and $\mathbf{w}_n$, were initialized using the Wiener weights given in (2-14). Predicted BER performance of the BNLMS equalizer is computed using both the GSM model in (4-39) and the AGSM model in (4-42).

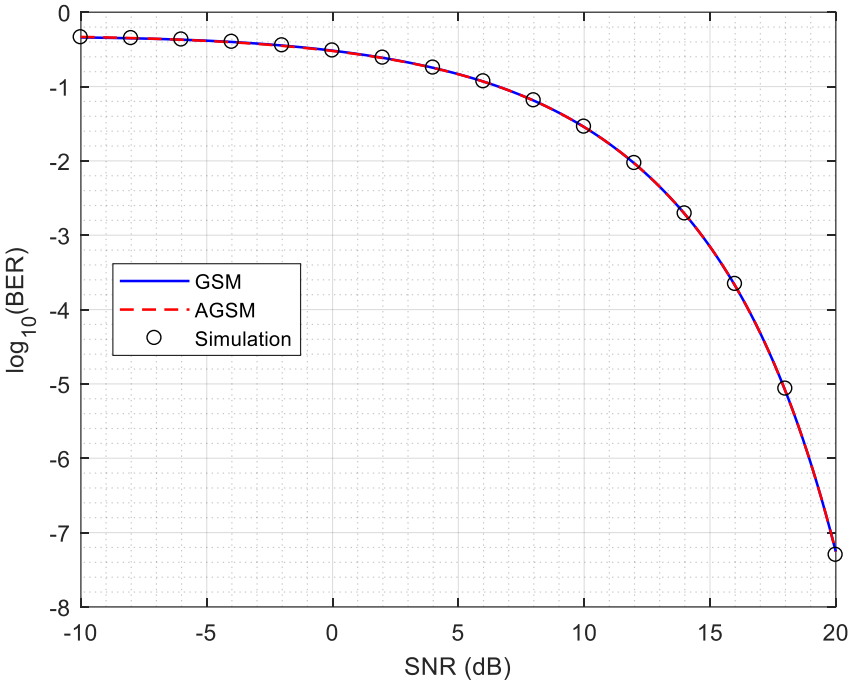

Figure 4-8: BER predicted from GSM (-), AGSM (--), and observed BER (o) for BNLMS with L = 7 and μ_B = 1 as a function of SNR for a QPSK system.

Figure 4-8 shows that the BER predicted by using either symbol-conditioned equalizer output PDF expression is consistent with the observed BER for the entire range of SNR values shown. Note that in order to get a stable measurement for BER at SNR = 20 dB the ensemble size was increased from 100 to 1000.

Figure 4-9 shows the comparison between the observed and predicted (using both the GSM model in (4-39) and the AGSM model in (4-42)) BER performance for the BNLMS equalizer as a function of ISR for a QPSK system. Similar to the setup used to generate Figure 4-7, an equalizer of length $L = 7$ and $\Delta = 0$ was used with the step-sizes set to $\mu_B = 1$ and $\tilde{\mu} = 0.001$. SNR was set to 18 dB with the fractional interference frequency $f_i = 0.368$.

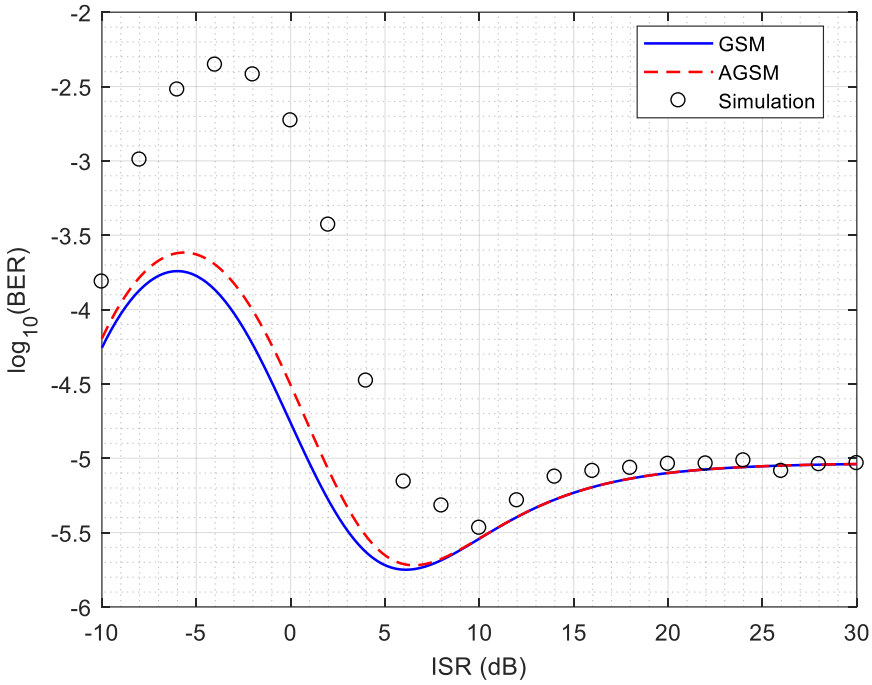

Figure 4-9: BER predicted from GSM (-), AGSM (--), and observed BER (o) for BNLMS with L = 7 and μ_B = 1 as a function of ISR for a QPSK system.

Figure 4-9 shows that using both the GSM and AGSM expressions lead to accurate predictions for the BER performance of the BNLMS equalizer for ISR > 10 dB. In other words, the modeled BER performance improves as the interference power increases. A similar phenomenon was observed in Figure 4-5 where the MSE predicted by the model for ISR > 10 dB were accurate. Note that the predicted MSE over-estimated equalizer performance by ~3 dB for ISR < 10 dB, whereas both BER models over-estimate the BER performance by almost 2 orders of magnitude for the same ISR range. A follow up analysis of why the model fails for low ISR is presented in Chapter 5.

Figure 4-10 shows a comparison between the predicted (using both the GSM model in (4-39) and the AGSM model in (4-42)) and observed BER for the BNLMS equalizer as a function of the fractional interference frequency f_i for a QPSK system. ISR and SNR were set to 20 dB and 18 dB respectively. The equalizer parameters were identical to the ones used to generate Figures 4-7 and 4-8, i.e. $L = 7$, $\Delta = 0$, $\mu_B = 1$, and $\tilde{\mu} = 0.001$.

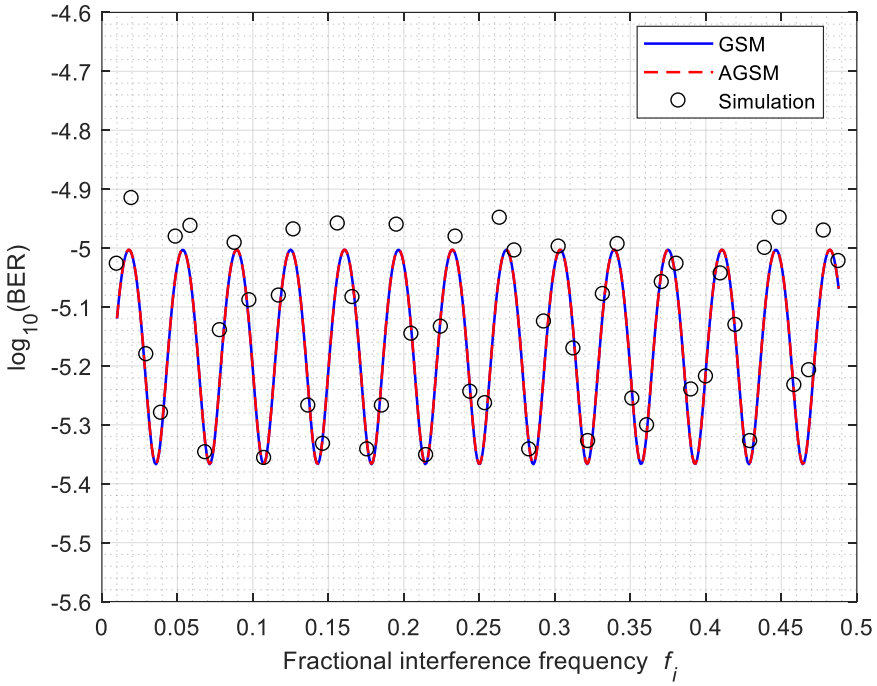

Figure 4-10: BER predicted from GSM (-), AGSM (--), and observed BER (o) for BNLMS with L = 7 and μ_B = 1 as a function of f_i for a QPSK system.

Figure 4-10 shows the frequency dependence of the BER performance of the BNLMS equalizer, which is unlike the case of MSE performance (Figure 4-5). The predictions made by both models are accurate (the maximum deviation between the predicted and the observed value is on the order of $10^{0.1}$, i.e. $1/10$ order of magnitude) over the entire range of f_i. Similar to the NLMS case, the BER performance of the BNLMS equalizer is frequency dependent.

In Figure 4-11 the BER predicted using AGSM (shown in (4-42)) is compared with the observed BER for a BNLMS equalizer for a 16-QAM system. An equalizer of length $L = 7$, $\Delta = 0$, and $\tilde{\mu} = 0.001\mu_B$ is chosen. Other simulation parameters include SNR = 20 dB, ISR = 20 dB and $f_i = 0.368$. Note that similar to the NLMS case, computing the

predicted BER using the GSM model is computationally cumbersome for the BNLMS case as well.

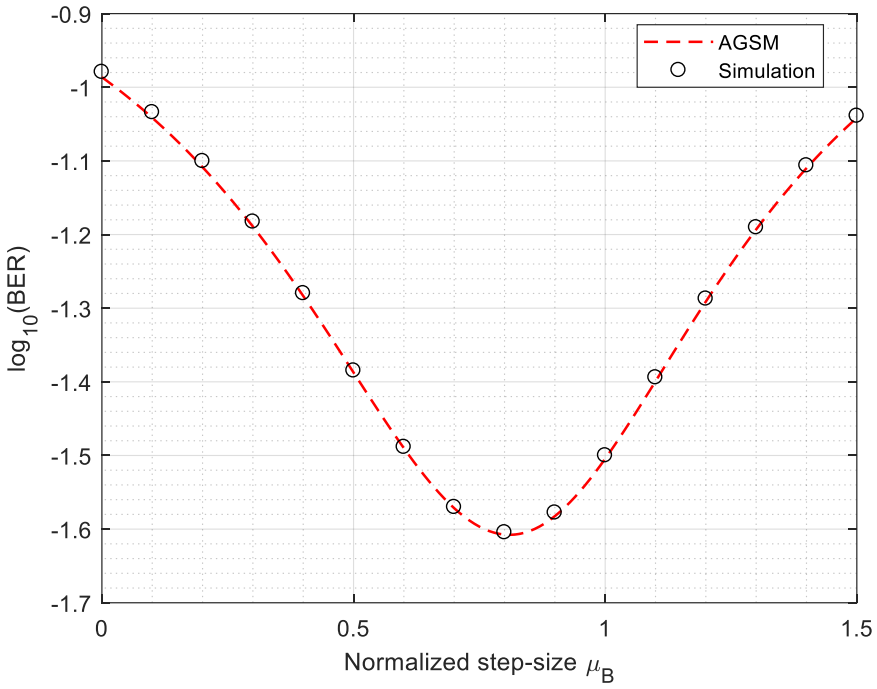

Figure 4-11: BER predicted from AGSM (--) and observed BER (o) for BNLMS as a function of step-size, for *L* = 7 for a 16-QAM system.

Similar to the NLMS case (Figure 3-12), observe that in Figure 4-11, the BER performance gain for a 16-QAM system with a BNLMS equalizer is less than an order of magnitude for $\mu_B \approx 0.8$ compared to $\mu_B = 0$. Observe that the AGSM predictions are consistent with the simulation results for the entire range of step-sizes shown.

In Figure 4-12 the BER performance – both predicted (using the AGSM model shown in (4-42)) and observed – of a BNLMS equalizer is shown for an equalizer of length $L = 21$, $\Delta = 0$, and $\tilde{\mu} = 0.001\mu_B$ as a function of normalized step-size. The other simulation parameters are SNR = 22 dB, ISR = 20 dB, and $f_i = 0.368$.

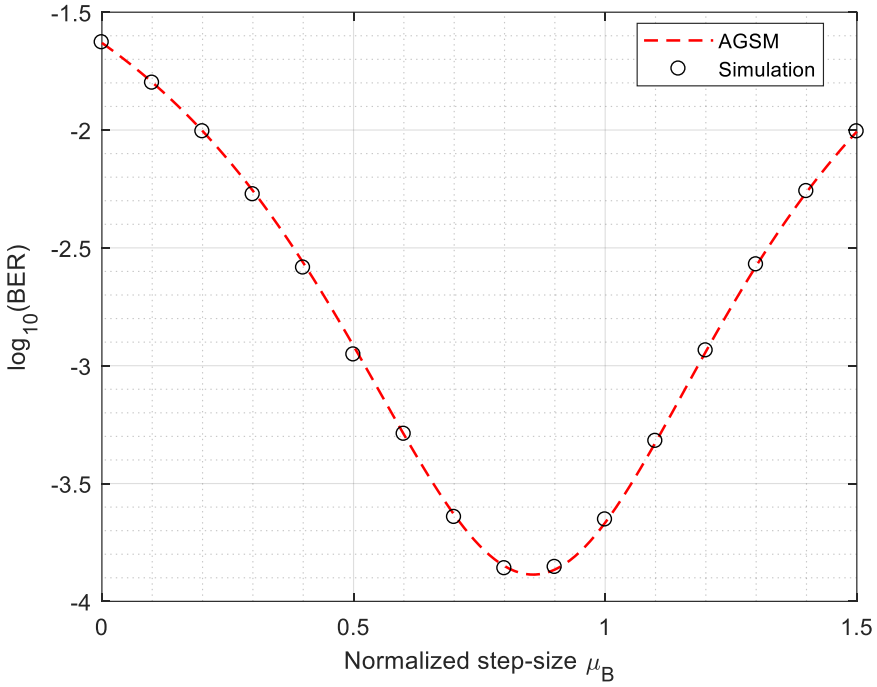

Figure 4-12: BER predicted from AGSM (--) and observed BER (o) for BNLMS as a function of step-size, for *L* = 21 for a 16-QAM system.

From Figure 4-12, observe that the AGSM predictions are consistent with the simulation results similar to in Figure 4-11. With the increase in equalizer length from $L=7$ to $L=21$ the non-Wiener characteristic of the BNLMS equalizer is more prominent – almost 2 orders of magnitude BER improvement when step-size is changed from $\mu_B=0$ to $\mu_B=0.8$. Note that the BER predictions using the AGSM model are more accurate for the BNLMS equalizer compared to for the NLMS case (Figure 3-13) for a 16-QAM system.

In Figure 4-13 the observed BER performance of a BNLMS equalizer is shown as a function of SNR, for an equalizer of length $L=21$ and $\Delta=0$ with the step-sizes set to $\mu_B=1$ and $\tilde{\mu}=0.001$ for a QPSK system. ISR was set to 20 dB and the fractional interference frequency was $f_i=0.368$. Predicted BER performance of the BNLMS equalizer is computed using AGSM model shown in (4-42).

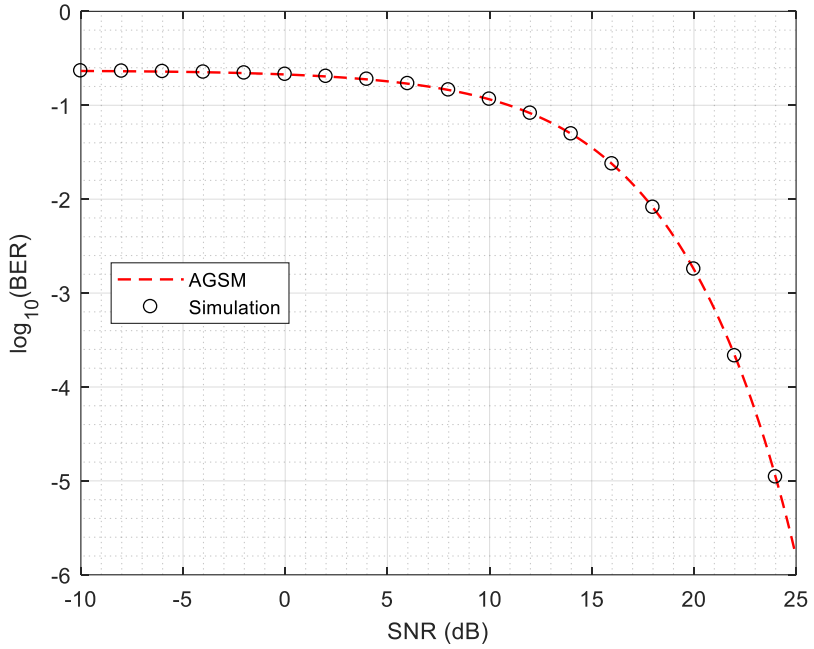

Figure 4-13: BER predicted from AGSM (--) and observed BER (o) for BNLMS as a function of SNR with μ_B = 1 and L = 21 for a 16-QAM system.

Similar to the NLMS case (Figure 3-14), the AGSM model leads to an accurate prediction for the BER performance of a 16-QAM system for the entire range of SNR, as shown in Figure 4-13.

Figure 4-14 shows the comparison between the observed and (AGSM based) predicted BER performance for the BNLMS equalizer as a function of ISR for a 16-QAM system. Similar to the setup used to generate Figure 4-13, an equalizer of length $L = 21$ and $\Delta = 0$ was used with the step-sizes set to $\mu_B = 1$ and $\tilde{\mu} = 0.001$. SNR was set to 22 dB with the fractional interference frequency $f_i = 0.368$.

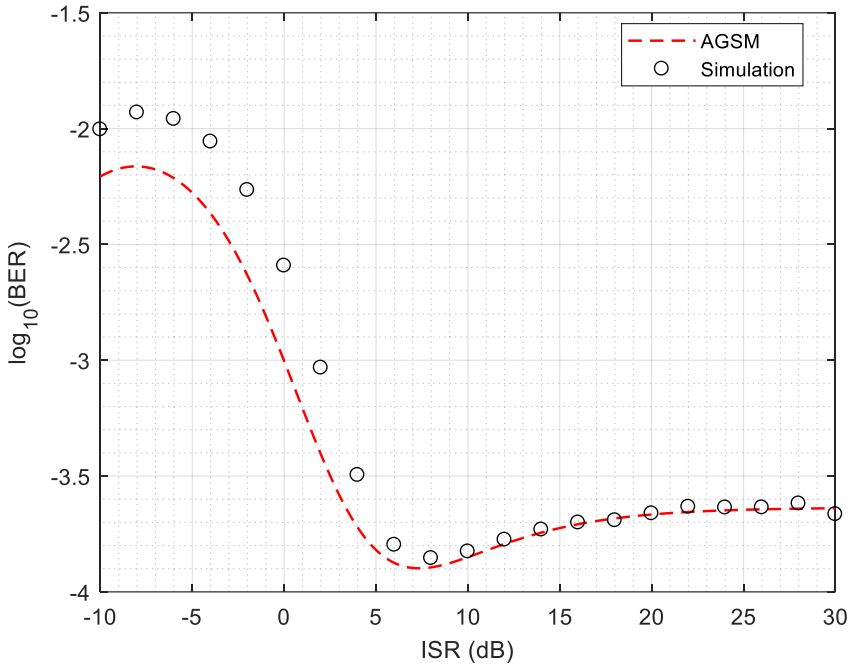

Figure 4-14: BER predicted by AGSM (--) and observed BER (o) as a function of ISR for BNLMS with μ_B = 1 and L = 21 for a 16-QAM system.

The BER predictions based on AGSM are accurate for ISR > 5 dB for a 16-QAM system with a BNLMS equalizer. This is in contrast with what was seen for the QPSK system (Figure 4-9) with a BNLMS equalizer.

Figure 4-15 shows a comparison between the predicted (using AGSM model shown in (4-42)) and observed BER for the BNLMS equalizer as a function of the fractional interference frequency f_i for a QPSK system. ISR and SNR were set to 20 dB and 22 dB respectively. The equalizer parameters were identical to the ones used to generate Figures 4-13 and 4-14, i.e. $L = 21, \Delta = 0$, $\mu_B = 1$, and $\tilde{\mu} = 0.001$.

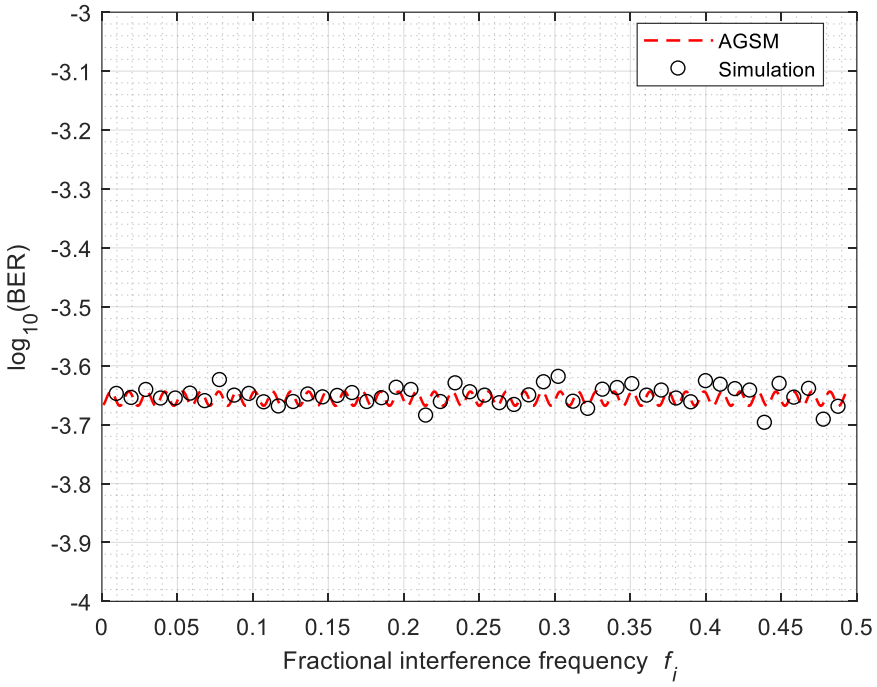

Figure 4-15: BER predicted from AGSM (--) and observed BER (o) as a function of f_i for BNLMS with $\mu_B = 1$ and $L = 21$ for a 16-QAM system.

In Figure 4-15, observe that the BER performance of a BNLMS equalizer for a 16-QAM system is practically independent of the interference frequency unlike in the QPSK case (Figure 4-10). The AGSM model leads to accurately predicting this lack of dependence on interference frequency for the entire range of interference frequency.

Figures 4-11 through 4-15 showed that the BNLMS equalizer exhibits the non-Wiener characteristic for higher order modulations, such as 16-QAM for example. The AGSM expression for the symbol-conditioned equalizer output PDF provides for an accurate and efficient way to predict the BER performance of the BNLMS equalizer when a higher order modulation is used.

4.7 Summary

In this chapter, an in-depth analysis of the Bi-scale NLMS equalizer in the presence of a strong narrowband interference is presented. An initial experiment motivated the utility

of the BLMS equalizer; this was followed by a detailed derivation leading to a closed form expression for its MSE behavior. An expression for the BER prediction along the lines of the one derived for the NLMS case was also presented. Predictions for both the MSE and the BER were validated by simulations and shown to be accurate for a wide range of system parameters.

CHAPTER 5 ENHANCED BER MODEL FOR NLMS EQUALIZATION

In this chapter, the BER behavior of the NLMS equalizer operating in a 'low' ISR environment is analyzed in detail because the predictions of the BER model derived in Chapter 3 – under the assumption of a high ISR environment – over-estimates system performance by almost 2 orders of magnitude for ISR < 15 dB. In Section 5.1, we revisit the originally derived GSM expression for the symbol-conditioned equalizer output PDF and analyze its different components for the case when ISR is low. Based on the observations presented in Section 5.1, a modified model is proposed in Section 5.2. In Section 5.3 the BER predicted using the new model is compared with simulation results.

5.1 Analysis of variance of $\tilde{y}_n$

In Section 3.2, the conditional PDF $f\left(\tilde{y}_n \mid d_{n-\Delta} = \phi_m\right)$ was expressed in (3-37) as a sum of M^L Gaussians. In this section, to determine from where the low ISR discrepancy arises, the aim is to compare the theoretical variance of the individual Gaussians with observed variance. Recall that each of the terms in the Gaussian mixture had equal variance, as given in (5-1):

$$V_T = \xi_v \sigma_v^2 + \xi_i \sigma_i^2 \tag{5-1}$$

where ξ_v and ξ_i are defined in (3-15) and (3-22) respectively.

Figure 5-1 shows the conditioned output $\left(y_n \mid d_{n-\Delta} = \phi_m\right)$ for an equalizer of length $L = 3$ and $\Delta = 0$. Similar to the setup used in Figure 3-3, our desired signal d_n is represented by QPSK symbols. Since we are interested in investigating the residual

interference component $\tilde{y}_{i,n}$ and its corresponding variance $\xi_i\sigma_i^2$, SNR was set to 80 dB so that $\xi_i\sigma_v^2$ is negligible. The fractional interference frequency was set to $f_i = 1/e$.

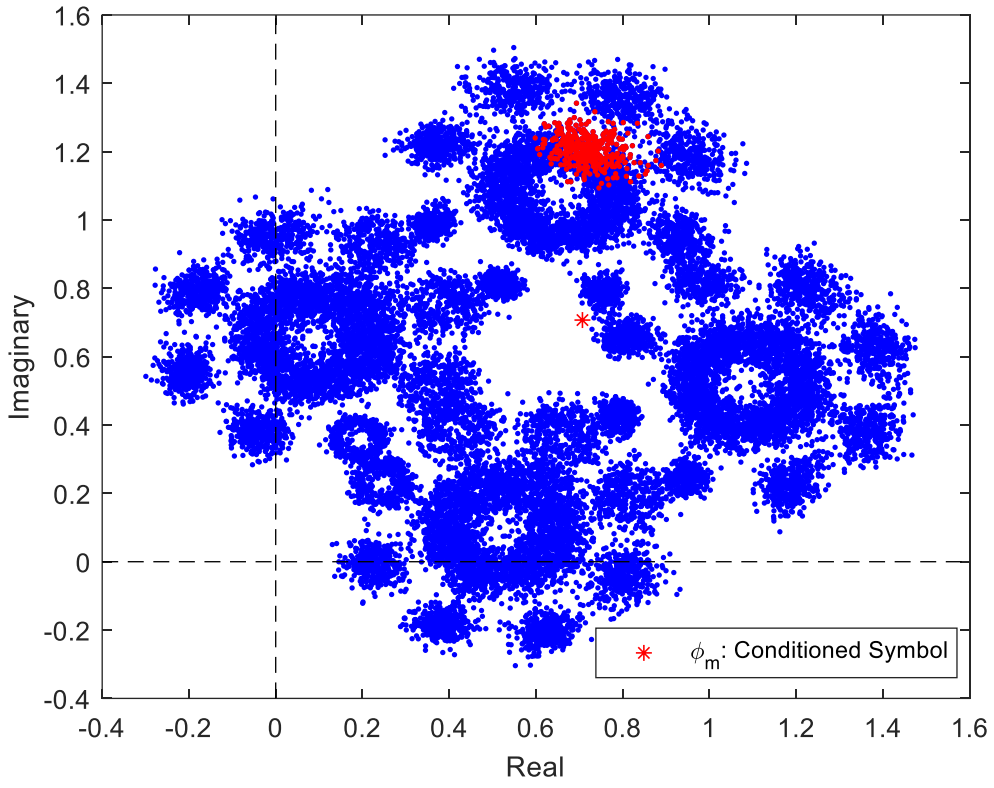

Figure 5-1: Output constellation y_n highlighting a single Gaussian component.

Figure 5-1 shows the output y_n conditioned on $\phi_m = e^{j\pi/4}$ denoted by blue dots. The red dots highlight a single Gaussian component, out of the possible $M^L\left(=4^3\right)$. Note that in order to estimate V_T experimentally, we have to first isolate the points of y_n which belong to a single Gaussian component. In order to achieve that y_n is conditioned on a particular sequence of input symbols. For example, the highlighted portion (red dots) in Figure 5-1 is conditioned on the following particular sequence of input symbols: $d_n = d_{n-1} = \ldots = d_{n-L} = \phi_m$.

Figure 5-2 shows the predicted variance V_T of the individual Gaussian and the experimentally measured variance, as a function of ISR for different step-sizes. The other simulation parameters were exactly the same as the ones used to generate Figure 5-1, i.e. $L = 3$, $\Delta = 0$, and $f_i = 1/e$.

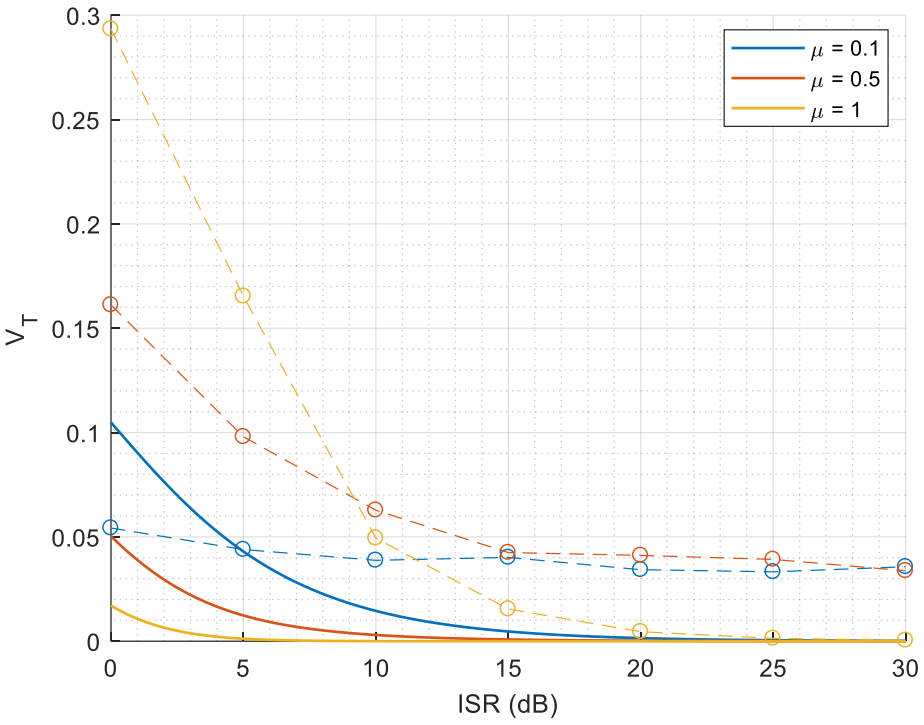

Figure 5-2: Predicted Variance (-) and observed variance (-o) as a function of ISR.

Figure 5-2 highlights the fact that the predicted variance V_T is substantially under-estimated, particularly for ISR < 10 dB. Since the variance was under-estimated, the BER predicted by the model was significantly less (2 orders of magnitude) than the observed BER (Figure 3-9). For Figure 5-2, since the noise variance σ_v^2 was almost negligible, we have $V_T \approx \xi_i \sigma_i^2$, which means that a model enhancement is required to explain the variance caused by the residual interference.

5.2 Enhanced GSM model for NLMS equalization

Based on the observations from Section 5.1, the interference component $\tilde{y}_{i,n}$ is analyzed. Re-writing (3-18),

$$\begin{aligned}\tilde{y}_{i,n} &= (1-\mu\beta)\bar{\mathbf{w}}^H\mathbf{i}_n \\ &= (1-\mu\beta)\sigma_i\bar{\mathbf{w}}^H\begin{bmatrix} e^{j(\omega_i n+\theta)} & e^{j(\omega_i(n-1)+\theta)} & \cdots & e^{j(\omega_i(n-L+1)+\theta)}\end{bmatrix}\end{aligned} \tag{5-2}$$

where $\beta = \dfrac{\sigma_i^2}{\sigma_i^2+\sigma_d^2+\sigma_v^2}$ and θ is the random phase following a uniform distribution over the range $[0, 2\pi)$. Simplifying (5-2):

$$\begin{aligned}\tilde{y}_{i,n} &= (1-\mu\beta)\sigma_i\bar{\mathbf{w}}^H e^{j(\omega_i n+\theta)}\begin{bmatrix}1 & e^{-j\omega_i} & \cdots & e^{-j\omega_i(L-1)}\end{bmatrix} \\ &= (1-\mu\beta)\sigma_i\bar{\mathbf{w}}^H\mathbf{e}e^{j(\omega_i n+\theta)}\end{aligned} \tag{5-3}$$

where $\mathbf{e} = \begin{bmatrix}1 & e^{-j\omega_i} & \cdots & e^{-j\omega_i(L-1)}\end{bmatrix}$. Note that (5-3) is a constant term multiplied by a complex exponential with a random phase. The above equation can therefore be re-written as:

$$\tilde{y}_{i,n} = \rho e^{j(\omega_i n+\theta)} \tag{5-4}$$

where

$$\rho = (1-\mu\beta)\sigma_i\bar{\mathbf{w}}^H\mathbf{e} \tag{5-5}$$

Note that the mean of (5-4) computed in (3-19) came out to be 0. However, the term never assumes the value 0. In fact, the magnitude of $\tilde{y}_{i,n}$ is always the constant ρ. To model the variability contributed by $\tilde{y}_{i,n}$, a heuristic ξ_H is introduced which is defined as:

$$\xi_H = 4\mu(1-\beta)\sigma_i\bar{\mathbf{w}}^H\mathbf{e} \tag{5-6}$$

The proposed heuristic has a form similar to (5-5), with the difference being that the coefficient of $\sigma_i \bar{\mathbf{w}}^H \mathbf{e}$ is $4\mu(1-\beta)$ instead of $(1-\mu\beta)$. The proposed modification was made based on the observations regarding Figure 5-2. In Figure 5-2, note that the variance of the interference component is low as ISR increases independent of the step-size μ. This makes sense since with the increase in interference power the equalizer is able to track the interference better and is able to mitigate it. Thus, $(1-\beta) \to 0$ as σ_i^2 increases.

The variance of the interference component is low in the low ISR region (< 10 dB) when the step-size is low but high when the step-size is high. So the term $\mu(1-\beta)$ changes the radius of the term according to the trend seen in Figure 5-2. Finally, the constant 4 in (5-6) represents the maximum variability (equal to twice the radius) along each of the real and imaginary axes. For the enhanced modified model, ξ_H can thus better account for the variance of $\tilde{y}_{i,n}$.

The enhanced GSM (EGSM) model for the conditional output PDF $f_E\left(\tilde{y}_n \mid d_{n-\Delta} = \phi_m\right)$ is still given by a sum of M^L Gaussians but with modified variance parameters:

$$f_E\left(\tilde{y}_n \middle| d_{n-\Delta} = \phi_m\right) = \frac{1}{M^L} \sum_{k_0=1}^{M} \sum_{\substack{k_1=1 \\ k_l \neq \Delta}}^{M} \cdots \sum_{k_L=1}^{M} CN\left(\kappa + \tilde{\phi}, \xi_v \sigma_v^2 + \xi_H\right) \tag{5-7}$$

Note that the only difference between the original expression in (3-37) and the EGSM expression in (5-7) is the replacement of $\xi_i \sigma_i^2$ by ξ_H. The performance resulting from the EGSM model is compared with simulation results as well as with using the previously derived original GSM expression (Section 3.2) and the AGSM expression (Section 3.3) for the NLMS equalizer operating in a narrowband interference contaminated environment.

5.3 Results

Since we want to compare results from using the proposed EGSM model and using the GSM and AGSM models, the simulation environment is identical to the one used in Section 3.4. This means that our desired signal consists of symbols from a QPSK constellation. The observed BER values are obtained by ensemble averaging of 100 independent trials, with each trial containing 100,000 symbols.

Figure 5-3 shows a comparison between the observed BER and the predicted BER as a function of ISR; the predictions result from using the EGSM expression in (5-7), the GSM expression in (3-37), and the AGSM expression in (3-43). An equalizer of length $L = 7$, with $\Delta = 0$, and $\mu = 1$ was chosen. SNR was set to 20 dB and the interference frequency was $f_i = 0.368$. Note that the simulation settings are identical to those used to generate Figure 3-9.

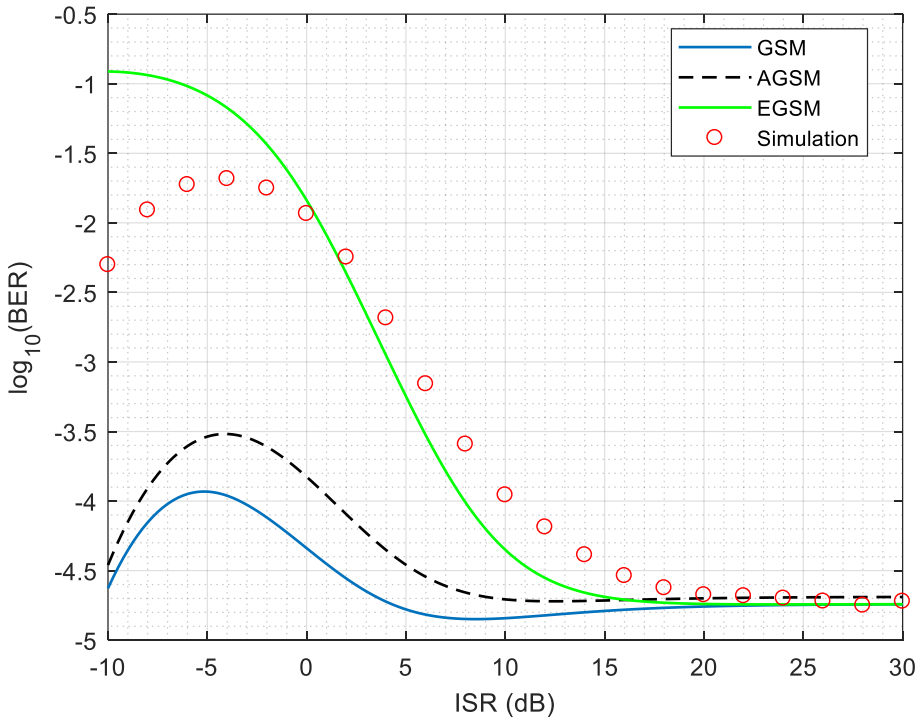

Figure 5-3: BER predicted using GSM, AGSM, EGSM and observed BER as a function of ISR for a NLMS equalizer of $L = 7$ and $\mu = 1$.

Observe that the proposed enhanced EGSM model yields a better BER estimate than either the GSM or AGSM model for ISR > 0 dB, while all BER predictions are quite accurate for ISR > 15 dB. EGSM slightly over-estimates (~ 1/5 orders of magnitude) the BER performance of the equalizer for ISR > 0 dB, compared to GSM which over-estimates the BER performance by 2 orders of magnitude. However, for negative ISR the predictions by EGSM deviate from the observed values by 1 order of magnitude. Note that for the negative ISR range the predictions by GSM and AGSM are off by 2 orders of magnitude. However, while EGSM under-estimates the performance of the equalizer by 1 order of magnitude both AGSM and GSM over-estimate the BER performance.

Figure 5-3 indicates that the proposed EGSM model is better at predicting the BER performance for positive ISR values than either the GSM or the AGSM model. However, for a fair comparison between the models additional experiments are required. Figure 5-4 compares the BER predicted from the EGSM, GSM, and AGSM models with observed values as a function of step-size. The other simulation parameters that were used are: $L = 7$, $\Delta = 0$, ISR = 20 dB, SNR = 20 dB, and $f_i = 0.368$.

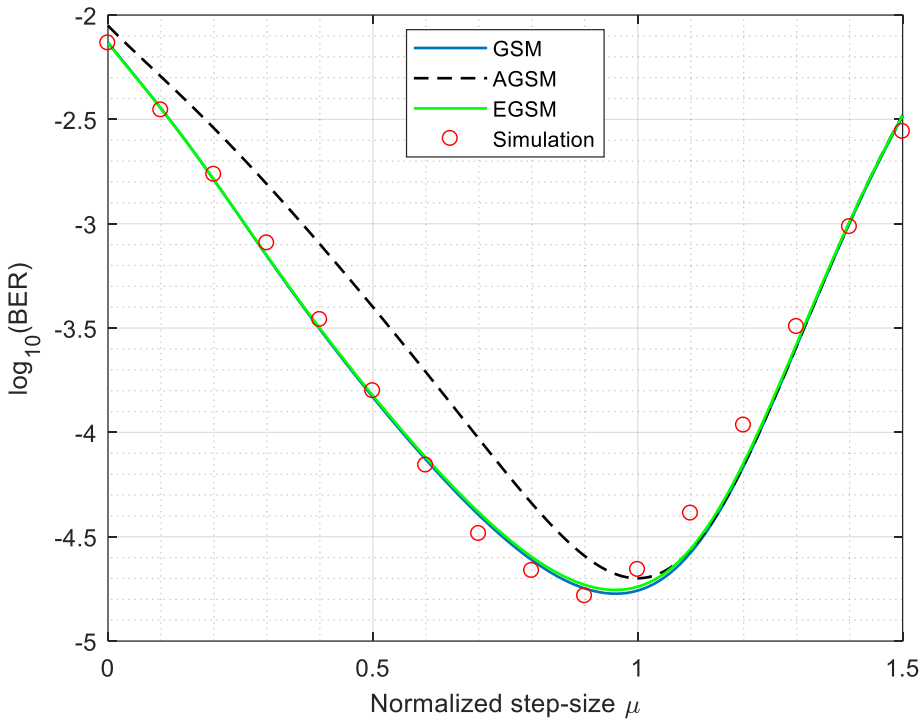

Figure 5-4: BER predicted by GSM, AGSM, EGSM, and observed BER as a function of step-size for a NLMS equalizer of *L* = 7.

The predictions made using the proposed EGSM model coincide with the GSM-based predictions, which earlier were shown to be consistent with the observed BER values for the entire range of the step-sizes studied. Figure 5-5 compares the BER predicted using the models with the observed BER as a function of SNR. The other simulation parameters that were used are: $L = 7$, $\Delta = 0$, $\mu = 1$, ISR = 20 dB, and $f_i = 0.368$. Similar to Figure 5-4, in Figure 5-5 the BER estimates using the EGSM model align with those made using the derived GSM expression.

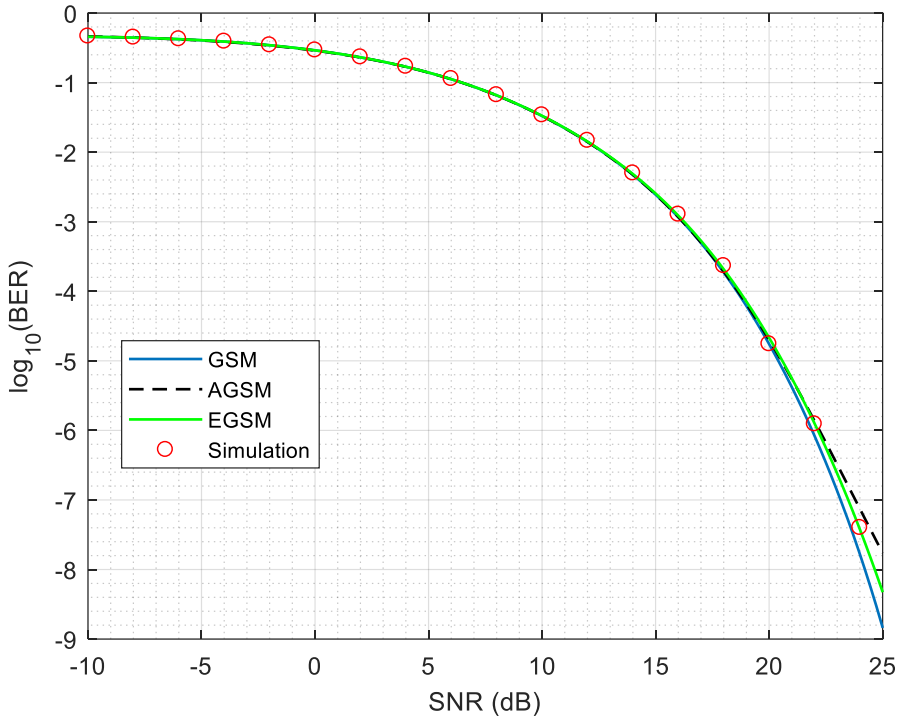

Figure 5-5: BER predicted using GSM, AGSM, EGSM and observed BER as a function of SNR for a NLMS equalizer of *L* = 7..

Finally, in Figure 5-6, the observed and predicted BER values are compared as a function of fractional interference frequency. Similar to Figure 5-5, the equalizer parameters were chosen to be $L = 7$, $\Delta = 0$, and $\mu = 1$. SNR and ISR were both set to 20 dB. Similar to what was observed in Figures 5-4 and 5-5, Figure 5-6 also shows that the predictions due to using both the EGSM and GSM models are accurate estimates of the BER performance of the NLMS equalizer in the narrowband interference dominated environment. Thus, the enhanced EGSM model extends the GSM model for ISR > 0 dB and remains equally accurate across a wide range of system parameters such as SNR, μ, and f_i, as seen in Figures 5-4 through 5-6. All these experiments illustrate the efficacy of the proposed heuristically enhanced model.

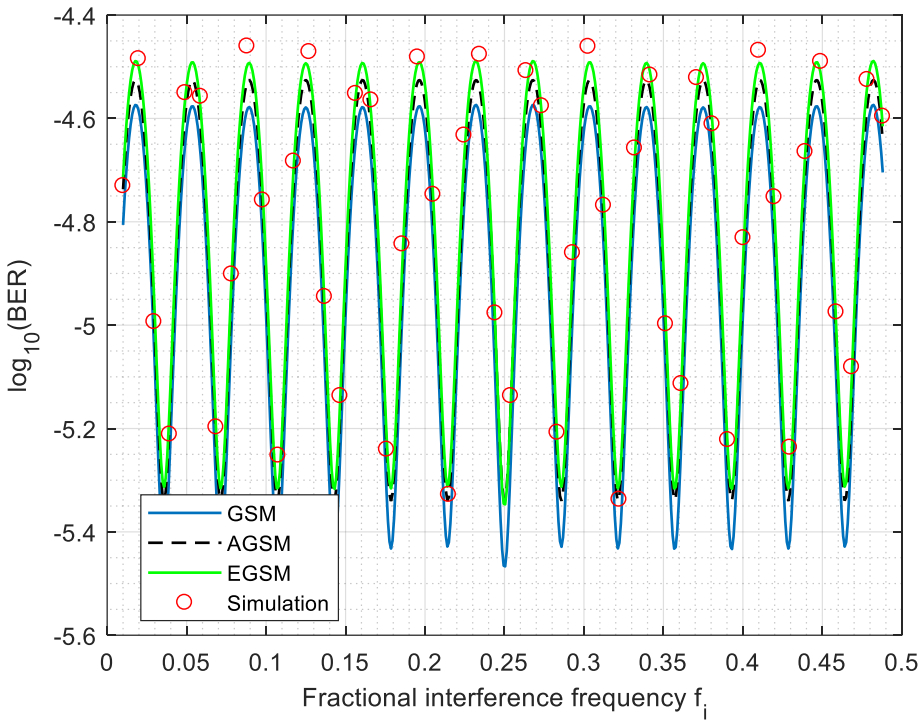

Figure 5-6: BER predicted using GSM, AGSM, and EGSM and observed BER as a function of f_i for a NLMS equalizer of L = 7.

Apart from Figure 5-4, in all the cases reflected in Figures 5-3 through 5-6 the step-size was kept at $\mu = 1$. Figure 5-7 compares the BER predicted using the EGSM model and the observed BER as a function of ISR for 5 different step-sizes. An equalizer was used of length $L = 7$, with $\Delta = 0$, along with SNR = 20 dB, and $f_i = 0.368$ for all the combinations of step-size and ISR.

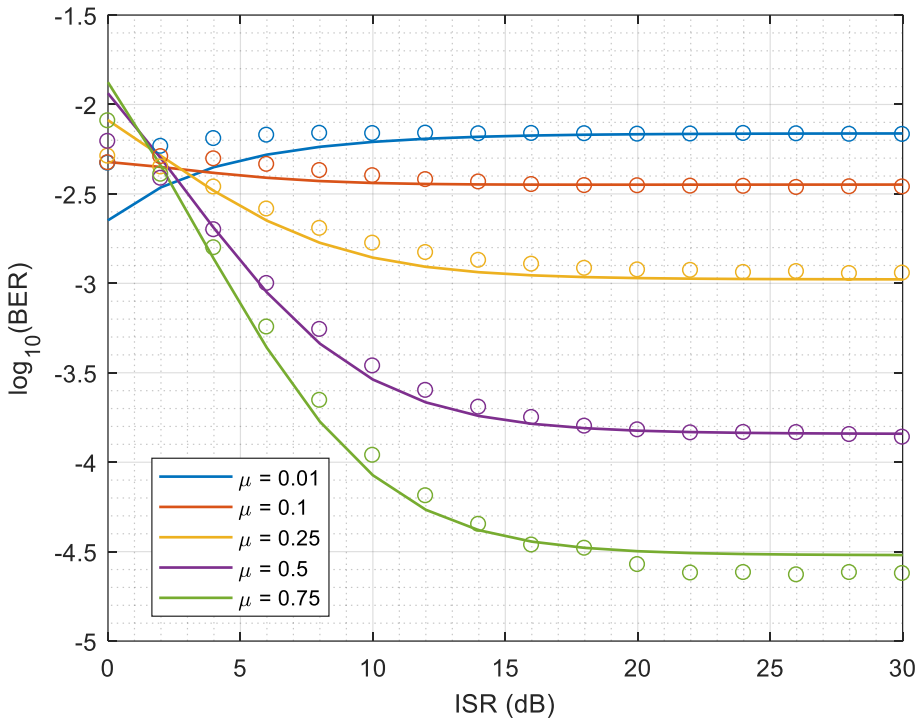

Figure 5-7: BER predicted by EGSM as a function of ISR for different step-sizes μ for a NLMS equalizer of L = 7.

Figure 5-7 highlights a couple of important points. Firstly, the EGSM model yields accurate BER predictions across the range of step-sizes for ISR > 0 dB. Secondly, the non-Wiener characteristic becomes prominent for ISR > 5 dB, at which point changing the step-size from $\mu = 0.01$ to $\mu = 0.75$ improves BER performance by almost 1 order of magnitude. So it is important to have a model that leads to accurately predicting the BER behavior for such ISR values. The originally derived GSM expression led, at 5 dB ISR, to over-estimating the BER performance by an order of magnitude (Figure 5-3) and thus did not produce a good bound on the BER performance of NLMS for the ISR range between 0 and 10 dB. The EGSM model on the other hand produces an accurate BER estimate for positive ISR and various step-sizes.

5.4 Summary

In this chapter, a heuristic enhancement of the GSM expression – used for predicting BER – is presented to address the inadequacy of the originally derived GSM and AGSM models towards predicting NLMS equalizer BER performance at low ISR. Simulation results verify that the BER estimates using the EGSM model are significantly more accurate than the ones provided by the GSM and AGSM models when the ISR is low to moderate ($0 < ISR < 15$ dB). For $ISR > 15$ dB the EGSM model induced predictions converge to the predictions produced with the GSM model. In fact, the phenomenon of EGSM model induced predictions converging to GSM induced predictions is observed for all the cases shown in this chapter barring the case when $ISR < 15$ dB, for which the EGSM model explicitly incorporates a heuristic in order to improve on predictions based on the GSM expression. Recall that the GSM expression was derived under the assumption of high ISR.

CHAPTER 6 TWO INTERFERER PROBLEM

The analysis and modeling presented in Chapters 3 through 5 was for a single narrowband (CW) interferer corrupting the signal of interest. In this chapter the two interferer problem is introduced in Section 6.1. Section 6.2 includes two case studies showing the non-Wiener behavior of (N)LMS equalizers in the presence of two narrowband interferers.

6.1 Two interferer system description

For the two interferer problem the system diagram is identical to the one shown in Figure 2-1 with the only difference being that, instead of a single interference component i_n, we have two interferers $i_{n,1}$ and $i_{n,2}$. Since both $i_{n,1}$ and $i_{n,2}$ are additive, the overall interference component is given by:

$$i_n = i_{n,1} + i_{n,2} \tag{6-1}$$

The individual interferences are modeled as in (2-6), i.e

$$i_{n,k} = \sigma_{i,k} e^{j\left(2\pi f_{i,k} n + \theta_k\right)} \qquad k = 1, 2 \tag{6-2}$$

where θ_k follows a uniform distribution over the range $[0, 2\pi)$. Note that the random phases θ_k are independent of one another, resulting in the independence of $i_{n,1}$ and $i_{n,2}$. The corresponding Wiener weights for the two interferer system can be calculated using the Wiener-Hopf equation in (2-13).

$$\mathbf{w}_w = \eta\left(\mathbf{p}_\Delta - \tilde{\mathbf{w}}_w\right) \tag{6-3}$$

where

$$\eta = \frac{\sigma_d^2}{\sigma_d^2 + \sigma_v^2} \tag{6-4}$$

$$\mathbf{p}_\Delta = \left[\underbrace{\underbrace{0 \quad \cdots \quad 0}_{\Delta} \quad 1 \quad 0 \quad \cdots \quad 0}_{L} \right]^T \tag{6-5}$$

$$\tilde{\mathbf{w}}_w = \frac{1}{\lambda_{\max}} \left(\sigma_{i,1}^2 \mathbf{e}_1 + \sigma_{i,2}^2 \mathbf{e}_2 \right) \tag{6-6}$$

and

$$\mathbf{e}_k \triangleq e^{j\omega_{i,k}\Delta} \left[1 \quad e^{-j\omega_{i,k}} \quad \ldots \quad e^{-j\omega_{i,k}(L-1)} \right]^T \qquad k = 1, 2 \tag{6-7}$$

$$\lambda_{\max} \triangleq L\left(\sigma_{i,1}^2 + \sigma_{i,2}^2 \right) + \sigma_v^2 + \sigma_d^2 \tag{6-8}$$

In the next section the MSE and BER performance of the Wiener equalizer designed according to (6-3) is compared with the NLMS equalizer performance for the two interferer case.

6.2 Case Studies

6.2.1 Total interference power constant

For this case, the overall interference power $\left(\sigma_{i,1}^2 + \sigma_{i,2}^2 \right)$ is kept constant. In Figures 6-1 through 6-3 the MSE and BER performance of the Wiener equalizer and the NLMS equalizer are investigated for three different combinations of total interference power distribution across two interferers. For comparison, the performance for the single interferer case, i.e. where one of the interferers has zero power, is also shown.

For Figures 6-1 through 6-3, the total interference power is kept constant, i.e. $\sigma_{i,1}^2+\sigma_{i,2}^2=100$. SNR was set to 20 dB (assuming $\sigma_d^2=1$). The fractional frequency of the first interferer is kept constant, at $f_{i,1}=0.368$. The equalizer parameters, $L=7$ and $\Delta=0$, are kept the same for the Wiener and NLMS equalizer. For NLMS the step-size $\mu=1$ was used; while this choice is not necessarily the optimal one, it is expected to illustrate non-Wiener effects when using NLMS. MSE and BER performance of the equalizers are shown as a function of the fractional interference frequency for the second interferer $f_{2,i}$. Note that for the Wiener case the optimal weights were calculated using (6-3).

In Figure 6-1 the MSE and BER behavior are compared for the Wiener equalizer as a function of $f_{i,2}$. The two interferers have equal power, i.e. $\sigma_{i,1}^2=\sigma_{i,2}^2=50$. Note that the MSE and BER for the one interferer case, with $\sigma_{i,1}^2=100$ and $\sigma_{i,2}^2=0$, is also shown (dotted lines).

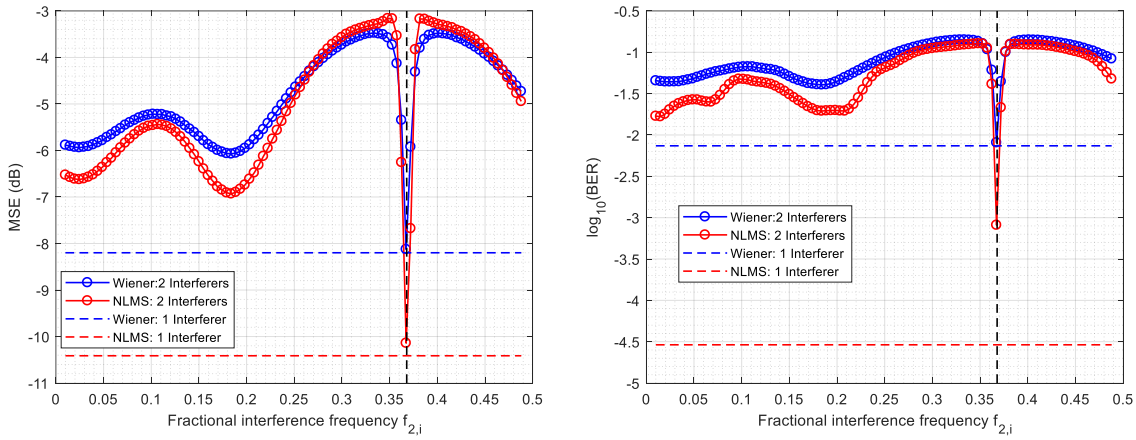

(a) MSE **(b) BER**

Figure 6-1: MSE and BER performance comparison of Wiener and NLMS for the two interferer case $\left(\sigma_{i,1}^2=\sigma_{i,2}^2=50\right)$.

From Figure 6-1, observe that when $f_{i,1} \approx f_{i,2}$ the two-interferer Wiener performance converges to the single-interferer Wiener performance. However, for the NLMS equalizer, although the MSE performance for the two interferer case converges to the single interferer case, the BER performance is poorer by more than an order of magnitude. Note that for $f_{i,1} \approx f_{i,2}$, i.e. approximately the single interferer case, two-interferer NLMS outperforms two-interferer Wiener by ~2 dB in terms of MSE and more than 1 order of magnitude in terms of BER. For the remainder of the frequency range the performance of the two equalizers is comparable, except when $f_{i,1} \approx 0.18$ where the NLMS equalizer outperforms the Wiener equalizer by ~1 dB in terms of MSE and ~0.25 orders of magnitude in terms of BER.

Figure 6-2 shows the MSE and BER behavior for $\sigma_{i,1}^2 = 90$ and $\sigma_{i,2}^2 = 10$, i.e. the interferer whose frequency is varied is 9 times weaker. Figure 6-3 shows the MSE and BER behavior for $\sigma_{i,1}^2 = 10$ and $\sigma_{i,2}^2 = 90$, i.e. the interferer whose frequency is varied is 9 times stronger. Note that in both Figures 6-2 and 6-3, the MSE and BER for the one interferer case, with $\sigma_{i,1}^2 = 100$ and $\sigma_{i,2}^2 = 0$, is also shown (dotted line).

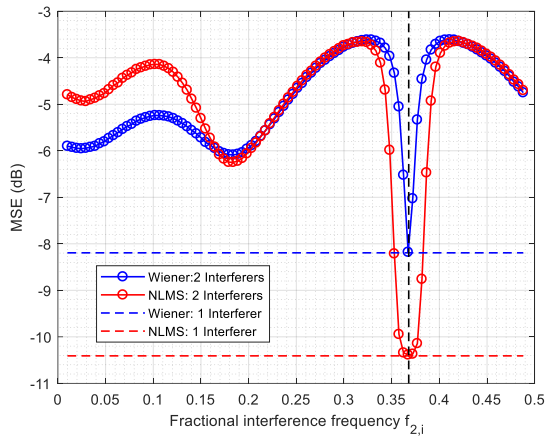

(a) MSE

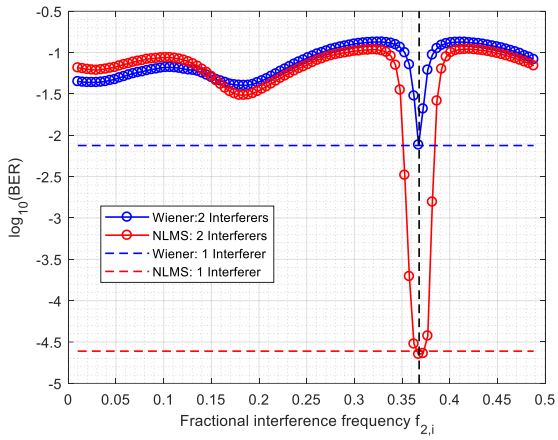

(b) BER

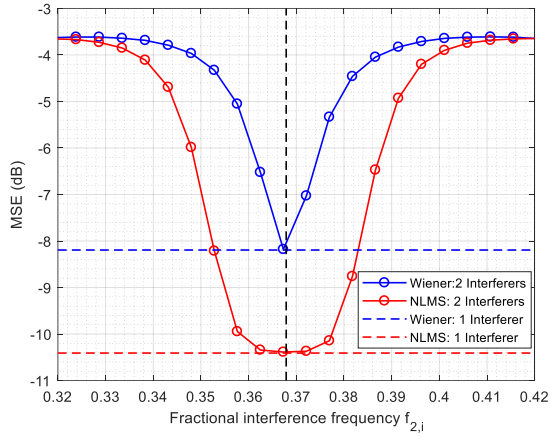

(c) MSE (zoomed)

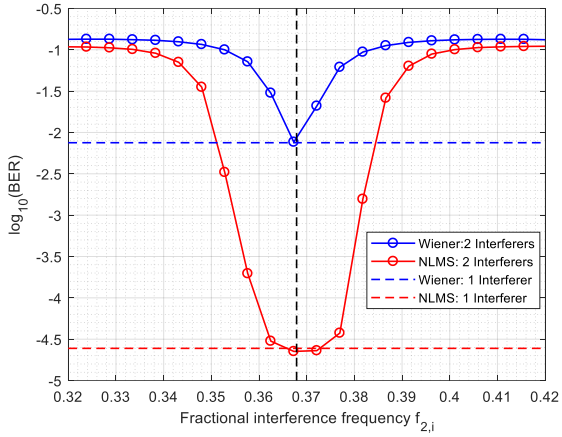

(d) BER (zoomed)

Figure 6-2: MSE and BER performance comparison of Wiener and NLMS for the two-interferer case $\left(\sigma_{i,1}^2 = 90, \sigma_{i,2}^2 = 10\right)$**.**

Similar to Figure 6-1, in Figure 6-2 the two-interferer Wiener equalizer performance converges to the single-interferer Wiener performance when $f_{i,1} \approx f_{i,2}$. Unlike in Figure 6-1, we observe in Figure 6-2 that the two-interferer NLMS performance (in terms of MSE as well as BER) converges to the single-interferer NLMS performance. However, the most important difference is the observed non-Wiener characteristic, i.e. the NLMS equalizer outperforms the Wiener equalizer in the vicinity of $f_{i,1}$ for both MSE (Figure 6-

2a) and BER (Figure 6-2b). Hence, the neighborhood of $f_{i,1}$ is zoomed in to and shown in Figures 6-2c and 6-2d.

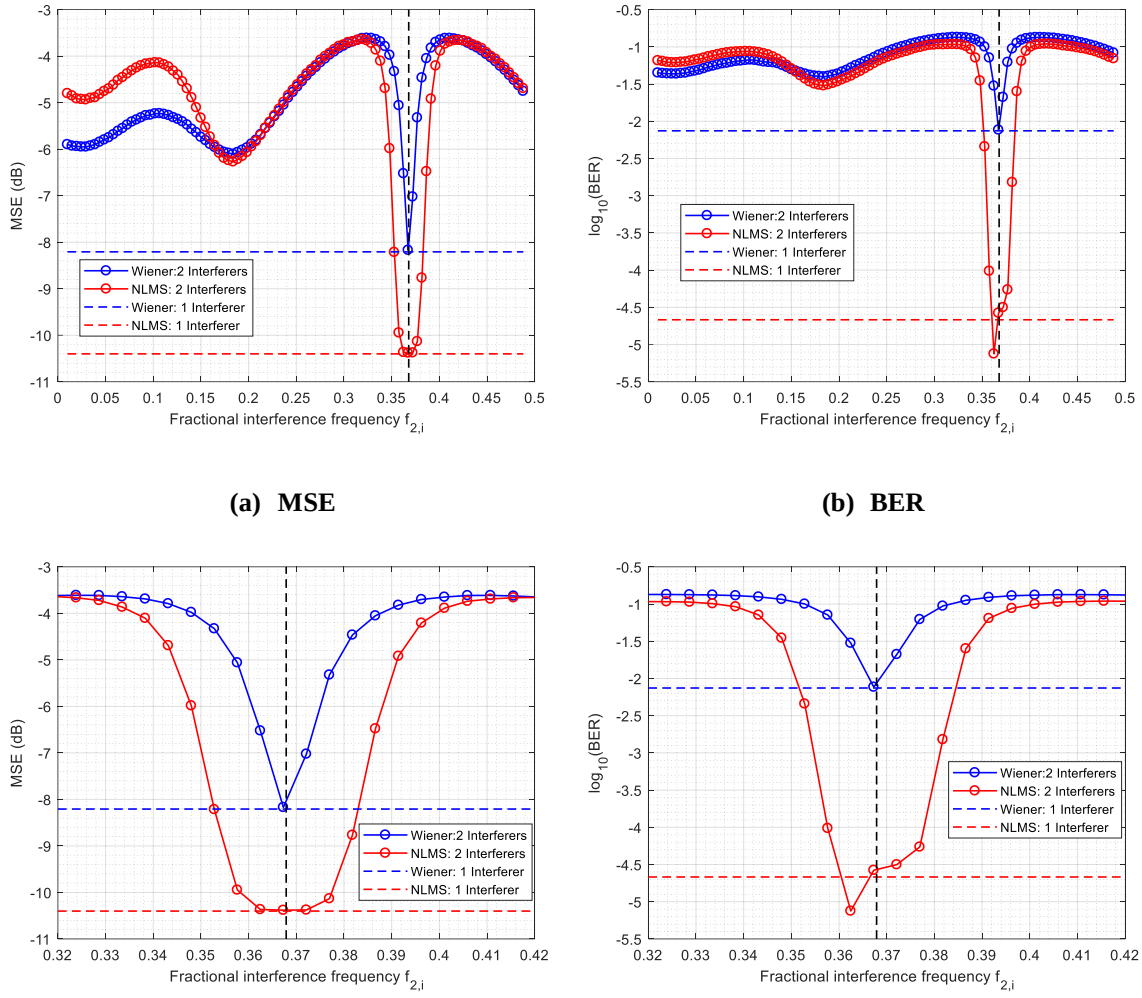

(a) MSE **(b) BER**

(c) MSE (zoomed) **(d) BER (zoomed)**

Figure 6-3: MSE and BER performance comparison of Wiener and NLMS for the two-interferer case $\left(\sigma_{1,i}^2 = 10, \sigma_{2,i}^2 = 90\right)$.

We see that the observations made for Figure 6-2 also hold for Figure 6-3, i.e. flipping the interferer power from the fixed interferer to the varied interferer makes no major observable difference. A small difference is that the single-interferer BER levels are slightly different in Figures 6-2b and 6-3b for $f_{i,1} \approx f_{i,2}$.

Observe in Figures 6-2c, 6-2d, 6-3c and 6-3d that the two-interferer NLMS equalizer begins to outperform the two-interferer Wiener equalizer when $0.34 < f_{i,2} < 0.4$, both in terms of MSE and BER. The largest performance difference in terms of MSE is observed when $f_{i,1} \approx f_{i,2}$, where the two-interferer NLMS equalizer outperforms the two-interferer Wiener equalizer by 2 dB.

In terms of the BER behavior, NLMS begins to outperform Wiener for $f_{i,2} \approx 0.34$ as seen in both Figure 6-2d and 6-3d. However, the peak BER performance is not exactly the same in the two figures. In Figure 6-2d, when $f_{i,1} \approx f_{i,2}$, the NLMS BER performance for the two-interferer case converges to the single-interferer NLMS equalizer BER performance. In Figure 6-3d, for $f_{i,1} \approx f_{i,2}$, the two interferer BER performance is marginally poorer than in the single-interferer NLMS case. However, for $f_{i,2} = 0.3625$ the BER performance for the two-interferer NLMS case is marginally better than for its single-interferer counterpart. Figures 6-2 and 6-3 thus indicate the presence of non-Wiener characteristics when the frequencies of the two interferers are close $\left(\left| f_{i,1} - f_{i,2} \right| < 0.06\right)$.

6.2.2 Interference injection

In this case study, the 'interference injection' problem is studied. We want to investigate if the single-interferer NLMS equalizer performance can be improved by intelligently adding a narrowband interference component. Performance is compared to the system corrupted by a single interferer.

For Figure 6-4 the performance of the Wiener and NLMS equalizers is compared for a system which is corrupted by a narrowband interference of power $\sigma_{i,1}^2 = 100$ at fractional frequency $f_{i,1} = 0.368$. SNR was set to 20 dB (assuming $\sigma_d^2 = 1$). An equalizer of length $L = 7$ with equalization center $\Delta = 0$ was chosen for both the Wiener and NLMS equalizers. For the NLMS equalizer a step-size of $\mu = 1$ is chosen. A narrowband

interferer of power $\sigma_{i,2}^2 = 10$, with a variable frequency $f_{i,2}$ is then added to – or injected at – the equalizer system input. The baseline performance (for both MSE and BER) of the respective systems refers to the case when no additional interference is injected.

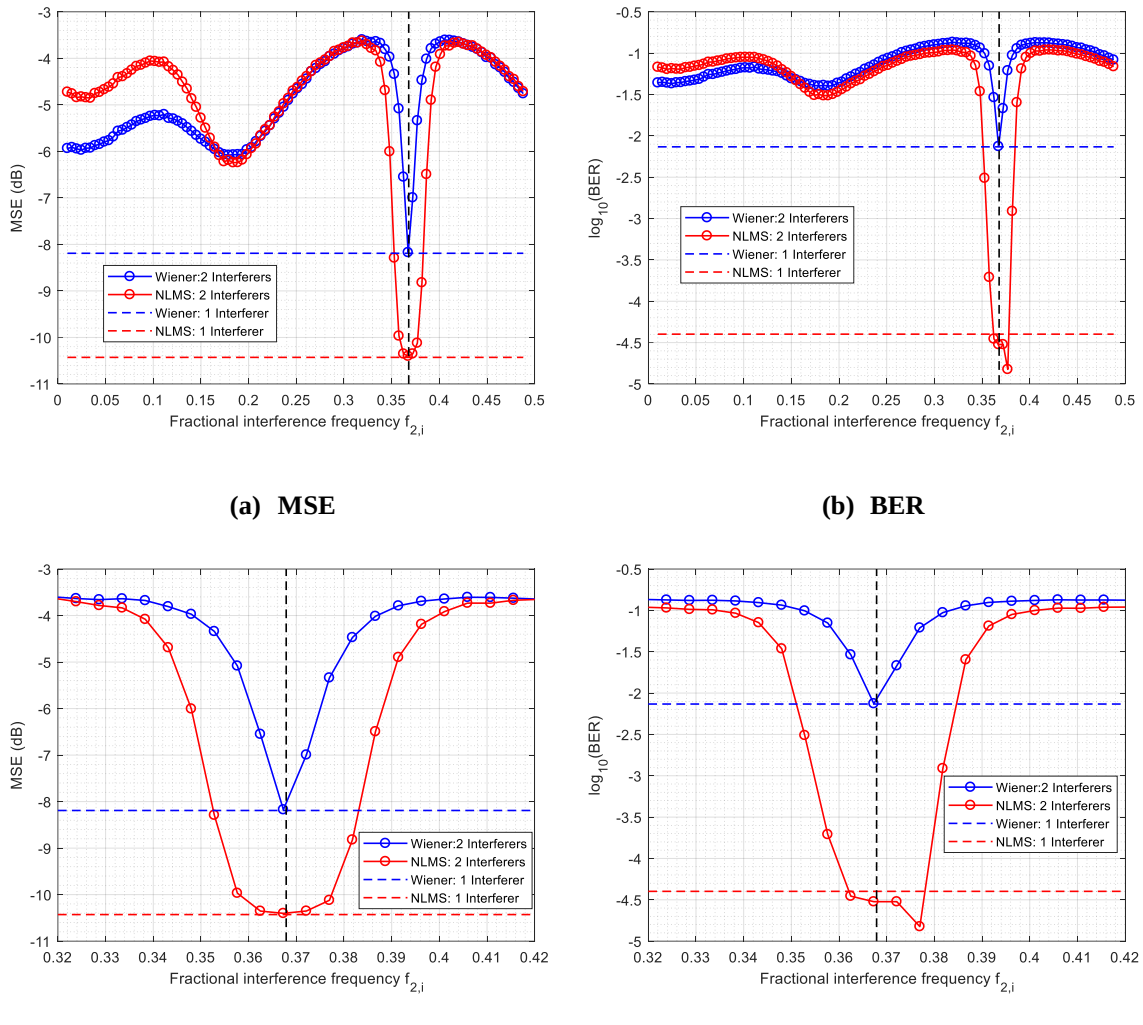

(a) MSE **(b) BER**

(c) MSE (zoomed) **(d) BER (zoomed)**

Figure 6-4: MSE and BER performance comparison of Wiener and NLMS for interference injection $\left(\sigma_{1,i}^2 = 100, \sigma_{2,i}^2 = 10\right)$.

Observe that injecting the interferer with 10 times less power than the already present interferer does not provide any improvement in terms of MSE (Figure 6-4a) for either of the equalizers. MSE performance approaches the single interferer case as the frequency of the injected interferer $f_{i,2}$ approaches $f_{i,1}$ (Figure 6-4c). The BER performance

exhibits similar characteristics, i.e. performance approaching the single-interferer case for both the Wiener and NLMS equalizers (Figure 6-4b), when $f_{i,2} \approx f_{i,1}$. For the NLMS case, the BER performance is marginally better when $0.36 < f_{i,2} < 0.38$, with the maximum improvement ($\sim 10^{0.4}$) seen for $f_{i,2} = 0.3769$ (Figure 6-4d).

Finally, in Figure 6-5 the performance of the Wiener and NLMS equalizers is compared for a system which is corrupted by a narrowband interference of power $\sigma_{i,1}^2 = 10$ (less than in the previous case) and fractional frequency $f_{i,1} = 0.368$. For this case again, a narrowband interferer of power $\sigma_{i,2}^2 = 10$ with a variable frequency $f_{i,2}$ is added to the system. The other simulation parameters are kept identical to the ones used to generate Figure 6-4, i.e. $L = 7$, $\Delta = 0$, $\mu = 1$, and SNR = 20 dB. Baseline performance (for both MSE and BER) of the respective systems refers to the case when no additional interference is injected.

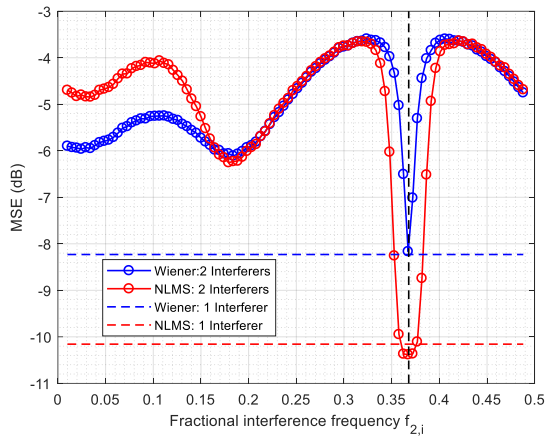

(a) MSE

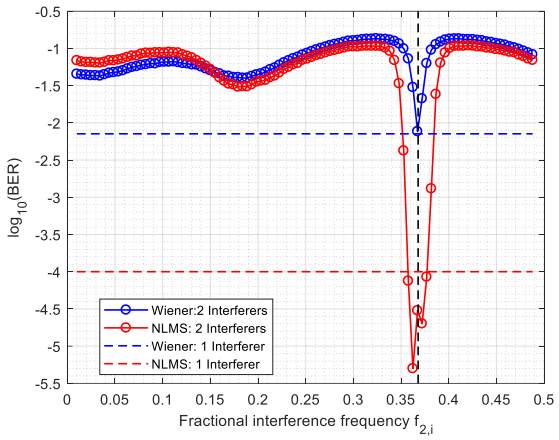

(b) BER

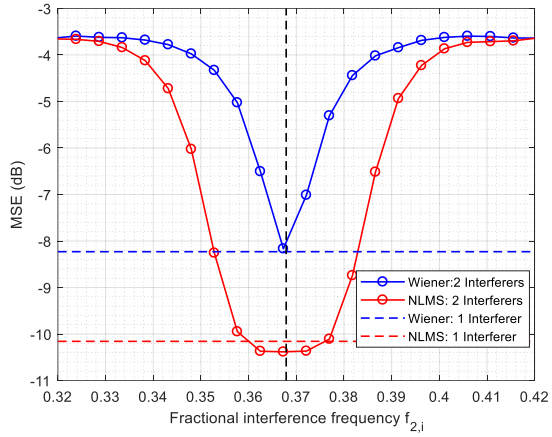

(c) MSE (zoomed)

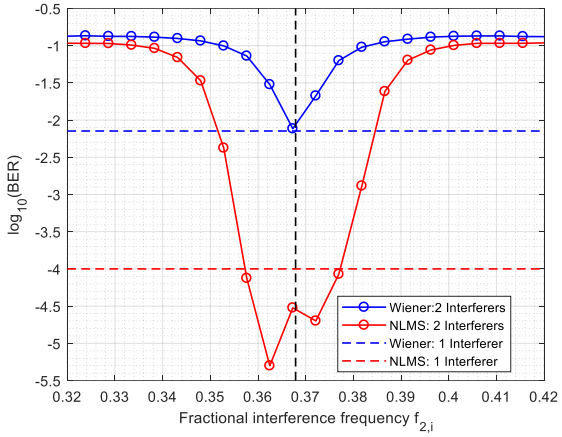

(d) BER (zoomed)

Figure 6-5: MSE and BER performance comparison of Wiener and NLMS for interference injection $\left(\sigma_{1,i}^2 = 10, \sigma_{2,i}^2 = 100\right)$.

In Figures 6-5a and 6-5c, observe that the Wiener MSE performance is slightly improved by the interferer injection. For the NLMS equalizer, when $f_{i,2} \approx f_{i,1}$, MSE performance is marginally (~0.2 dB) better than for the single interferer case. Figure 6-5b shows that injecting the interferer is beneficial for the NLMS equalizer as its BER performance is improved by more than an order of magnitude when $f_{i,2} \approx f_{i,1}$. In fact, the BER performance for the single interference case using NLMS equalization is better with injection than without injection when the injected interferer falls in $0.36 < f_{i,2} < 0.38$.

Investigating the possible reasons behind the performance improvement shown in Figure 6-5d and its dependence on equalization parameters (L, μ, and Δ) can be a possible direction for future research.

6.3 Summary

This chapter introduced the two-interferer problem. The first case studies presented here showed the presence of non-Wiener characteristics of the NLMS equalizer in the presence of two narrowband interferers. The second case study pointed towards the possibility of improving the NLMS equalizer performance by injecting a narrowband interference.

CHAPTER 7 CONCLUSION

7.1 Concluding remarks

This work presented a thorough analysis for the BER behavior of the (N)LMS equalizer in the presence of a narrowband interference. Observation showed the difference in MSE and BER behavior of the NLMS equalizer, particularly the dependence of the BER behavior on interference frequency; MSE performance shows no such dependence. Starting from the NLMS equalizer algorithm, a BER model was derived that can accurately predict this frequency varying behavior. Moreover, the analytically derived expression for the symbol-conditioned PDF of the equalizer output – which for digital modulations, such as QPSK and 16-QAM takes the form of a Gaussian sum mixture – facilitates accurate prediction of the BER behavior of the NLMS equalizer operating in a narrowband interference dominated environment. The BER predictions are accurate over a wide range of SNR, ISR, interference frequency, and over all step-sizes where NLMS stably operates. An approximate BER model is also derived and is computationally less demanding than the full model. The approximate BER model is extremely useful for predicting the BER performance for higher order modulations (e.g. 16-QAM) and/or larger equalizers when using the full model is not feasible computationally.

Bi-scale NLMS, a variant of the NLMS equalizer which provides significant performance improvement over NLMS, was also analyzed in detail. A BER model as well as a MSE model was derived for BLMS performance characterization. Simulation results verified that both models were able to predict BLMS equalizer performance accurately for different combinations of signal and system parameters, again for the narrowband interference dominated environment.

The derivation of the original BER model assumes that the equalizer is operating in the presence of a strong narrowband CW interference. Not too surprising, the model predictions are not accurate when interference power is not sufficiently strong (ISR < 15

dB). An enhanced BER model is introduced which augments the original BER model for the low ISR region. Simulation results show that the BER predictions based on the enhanced model are more accurate towards the lower ISR cases. Moreover, the enhanced model predictions coincide with the original model predictions when ISR is high. It is worth mentioning that non-Wiener characteristics are observed from ISR > 5 dB. Thus, the enhanced model is able to predict the BER performance of a NLMS equalizer for the entire range of ISR where the non-Wiener characteristic is present.

The two narrowband interferer problem was introduced. Initial results show the presence of non-Wiener behavior of the (adaptive) NLMS equalizer in the presence of two interferers. Additionally, an experimental result indicates that BER performance may be gained in the single interferer case by judicious injection of an additional narrowband interferer.

Overall this dissertation provided insight in the non-Wiener characteristics of LMS type equalizers from a bit error rate perspective – a topic with hitherto scant presence in the existing literature.

7.2 Future Work

To extend the work described in this dissertation there are (at least) three possible avenues for further exploration. Firstly, the two-interferer problem introduced in Chapter 6 indicates the presence of non-Wiener behavior of NLMS equalizers, as well as the possible improvement in BER performance by judicious interference injection. An in-depth analysis of the equalizer performance and weight behavior for the two-interferer case thus seems worth pursuing. In fact, a more general problem of a system with multiple narrowband interferers can be studied examining the possibility of adding narrowband signals intelligently to improve overall system performance in the face of multi-tone interference.

The second area that can be pursued further – in order to more rigorously develop a model that improves BER prediction for the low ISR region – is to model the steady state

dynamic behavior of the NLMS weights in terms of the input signal statistics, in particular for the large step-sizes at which the non-Wiener effects are most prominent. Most of the existing literature related to modeling the dynamic weight behavior assumes either Gaussian inputs or small step-sizes. However, linking the steady state dynamic weight behavior to the input signal statistics and/or system parameters – for NLMS equalizers operating at large step-sizes in the presence of non-Gaussian inputs – is yet to be done. Some preliminary work can be found in [55].

Finally, this work can be extended to analyze and model the non-Wiener characteristics of the (N)LMS equalizer for a multi-carrier communication system, such as LTE.

REFERENCES

[1] C. N. Smyth, "CONTINUOUS WAVE INTERFERENCE WITH TELEVISION RECEPTION," *Nature,* vol. 148, p. 539, 11/01/online 1941.

[2] R. Johannessen. (1997) Interference: Sources and symptoms. *GPS World*. 44-48.

[3] A. T. Balaei, A. G. Dempster, and L. L. Presti, "Characterization of the Effects of CW and Pulse CW Interference on the GPS Signal Quality," *IEEE Transactions on Aerospace and Electronic Systems,* vol. 45, no. 4, pp. 1418-1431, 2009.

[4] D. Borio, "GNSS Acquisition in the Presence of Continuous Wave Interference," *IEEE Transactions on Aerospace and Electronic Systems,* vol. 46, no. 1, pp. 47-60, 2010.

[5] F. Ye, H. Yu, and Y. Li, "Continuous Wave Interference Effects on Global Position System Signal Quality," *World Academy of Science, Engineering and Technology, International Journal of Computer, Electrical, Automation, Control and Information Engineering,* vol. 10, no. 12, pp. 1995-2000, 2016.

[6] F. Dovis, *GNSS Interference Threats and Countermeasures*. Artech House, 2015.

[7] M. V. Clark, "Adaptive frequency-domain equalization and diversity combining for broadband wireless communications," *IEEE Journal on Selected Areas in Communications,* vol. 16, no. 8, pp. 1385-1395, 1998.

[8] V. Bladel, "Time-domain equalization for multicarrier communication," in *Global Telecommunications Conference*, 1995, pp. 167-171: IEEE.

[9] J. W. Choi, R. J. Drost, A. C. Singer, and J. Preisig, "Iterative multi-channel equalization and decoding for high frequency underwater acoustic communications," in *5th IEEE Sensor Array and Multichannel Signal Processing Workshop*, 2008, pp. 127-130.

[10] M. F. Mosleh and A.-N. Aseel Hameed, "Combination of LMS and RLS adaptive equalizer for selective fading channel," *European Journal of Scientific Research*, vol. 43, no. 1, pp. 127-137, 2010.

[11] J. C. Lin, "Least-Squares Channel Estimation for Mobile OFDM Communication on Time-Varying Frequency-Selective Fading Channels," *IEEE Transactions on Vehicular Technology,* vol. 57, no. 6, pp. 3538-3550, 2008.

[12] R. W. Lucky, "Techniques for adaptive equalization of digital communication systems," *The Bell System Technical Journal,* vol. 45, no. 2, pp. 255-286, 1966.

[13] B. Widrow, P. E. Mantey, L. J. Griffiths, and B. B. Goode, "Adaptive antenna systems," *Proceedings of the IEEE,* vol. 55, no. 12, pp. 2143-2159, 1967.

[14] J. G. Proakis and J. Miller, "An adaptive receiver for digital signaling through channels with intersymbol interference," *IEEE Transactions on Information Theory,* vol. 15, no. 4, pp. 484-497, 1969.

[15] S. U. H. Qureshi, "Adaptive equalization," *Proceedings of the IEEE,* vol. 73, no. 9, pp. 1349-1387, 1985.

[16] L. B. Milstein, "Interference rejection techniques in spread spectrum communications," *Proceedings of the IEEE*, vol. 76, no. 6, pp. 657-671, 1988.
[17] J. D. Laster and J. Reed, "Interference rejection in digital wireless communications," *IEEE Signal Processing Magazine*, vol. 14, no. 3, pp. 37-62, 1997.
[18] H. V. Poor, "Active interference suppression in CDMA overlay systems," *IEEE Journal on Selected Areas in Communications*, vol. 19, no. 1, pp. 4-20, 2001.
[19] A. Batra, "Mitigation Techniques for Severe Narrowband Interference," Ph. D., UC San Diego, 2009.
[20] R. C. North, R. A. Axford, and J. R. Zeidler, "The performance of adaptive equalization for digital communication systems corrupted by interference," in *Asilomar Conference on Signals, Systems and Computers*, 1993, vol. 2, pp. 1548-1553
[21] S. Haykin, *Adaptive Filter Theory*, 5th ed. Prentice Hall, 2013.
[22] M. Reuter and B. Zeidler, "Non-Wiener effects in LMS-implemented adaptive equalizers," in *IEEE International Conference on Acoustics, Speech, and Signal Processing* 1997, vol. 3, pp. 2509-2512
[23] K. J. Quirk, J. R. Zeidler, and L. B. Milstein, "Bounding the performance of the LMS estimator for cases where performance exceeds that of the finite Wiener filter," in *IEEE International Conference on Acoustics, Speech and Signal Processing*, 1998, vol. 3, pp. 1417-1420.
[24] M. Reuter and J. R. Zeidler, "Nonlinear effects in LMS adaptive equalizers," *IEEE Transactions on Signal Processing*, vol. 47, no. 6, pp. 1570-1579, 1999.
[25] M. Reuter, K. Quirk, B. Zeidler, and L. Milstein, "Non-linear effects in LMS adaptive filters," in *Adaptive Systems for Signal Processing, Communications, and Control Symposium*, 2000, pp. 141-146.
[26] A. A. (Louis) Beex and J. R. Zeidler, "Data structure and non-linear effects in adaptive filters," in *International Conference on Digital Signal Processing*, 2002, vol. 2, pp. 659-662.
[27] A. A. (Louis) Beex and J. R. Zeidler, "Non-Wiener effects in recursive least squares adaptation," in *Seventh International Symposium on Signal Processing and Its Applications*, 2003, vol. 2, pp. 595-598
[28] A. A. (Louis) Beex and J. R. Zeidler, "Linking sequence behavior in ANC," in *IEEE International Conference on Acoustics, Speech, and Signal Processing*, 2004, vol. 2, pp. ii-833-6
[29] T. Ikuma, A. A. (Louis) Beex, and J. R. Zeidler, "Non-Wiener Weight Behavior of LMS Transversal Equalizers," in *IEEE International Conference on Acoustics, Speech and Signal Processing*, 2007, vol. 3, pp. III-1297-III-1300.
[30] H. J. Butterweck, "Iterative analysis of the steady-state weight fluctuations in LMS-type adaptive filters," *IEEE Transactions on Signal Processing*, vol. 47, no. 9, pp. 2558-2561, 1999.
[31] T. Ikuma, A. A. (Louis) Beex, and J. R. Zeidler, "Non-Wiener Mean Weight Behavior of LMS Transversal Equalizers With Sinusoidal Interference," *IEEE Transactions on Signal Processing*, vol. 56, no. 9, pp. 4521-4525, 2008.

[32] T. Ikuma and A. A. (Louis) Beex, "Improved Mean-Square Error Estimate for the LMS Transversal Equalizer With Narrowband Interference," *IEEE Transactions on Signal Processing*, vol. 56, no. 10, pp. 5273-5277, 2008.

[33] T. Ikuma, "Non-Wiener Effects in Narrowband Interference Mitigation Using Adaptive Transversal Equalizers," Ph. D. Dissertation, Virginia Tech, 2007.

[34] R. A. Iltis and L. B. Milstein, "An Approximate Statistical Analysis of the Widrow LMS Algorithm with Application to Narrow-Band Interference Rejection," *IEEE Transactions on Communications*, vol. 33, no. 2, pp. 121-130, 1985.

[35] M. E. Davis and L. B. Milstein, "Anti-jamming properties of a DS-CDMA equalization filter," in *IEEE Military Communications Conference*, 1993, vol. 3, pp. 1008-1012 vol.3.

[36] A. J. Coulson, "Bit error rate performance of OFDM in narrowband interference with excision filtering," *IEEE Transactions on Wireless Communications*, vol. 5, no. 9, pp. 2484-2492, 2006.

[37] T. Roy and A. A. (Louis) Beex, "BER modeling for interference canceling FIR Wiener equalizer," in *International Conference on Computing, Networking and Communications (ICNC)*, 2013, pp. 278-282.

[38] T. Roy, "BER Modeling for Interference Canceling Adaptive NLMS Equalizer," M.S. Thesis, Virginia Tech, 2014.

[39] N. J. Bershad and J. C. M. Bermudez, "Sinusoidal interference rejection analysis of an LMS adaptive feedforward controller with a noisy periodic reference," *IEEE Transactions on Signal Processing*, vol. 46, no. 5, pp. 1298-1313, 1998.

[40] J. C. M. Bermudez and N. J. Bershad, "A nonlinear analytical model for the quantized LMS algorithm-the arbitrary step size case," *IEEE Transactions on Signal Processing*, vol. 44, no. 5, pp. 1175-1183, 1996.

[41] J. Chen, J. C. M. Bermudez, and C. Richard, "Steady-State Performance of Non-Negative Least-Mean-Square Algorithm and Its Variants," *IEEE Signal Processing Letters*, vol. 21, no. 8, pp. 928-932, 2014.

[42] S. Koike, "Adaptive threshold nonlinear algorithm for adaptive filters with robustness against impulse noise," *IEEE Transactions on Signal Processing*, vol. 45, no. 9, pp. 2391-2395, 1997.

[43] S.-C. Chan and Y.-X. Zou, "A recursive least M-estimate algorithm for robust adaptive filtering in impulsive noise: fast algorithm and convergence performance analysis," *IEEE Transactions on Signal Processing*, vol. 52, no. 4, pp. 975-991, 2004.

[44] S. i. Koike, "Analysis of normalized least mean modulus algorithm for adaptive filters in impulsive noise environments," in *International Symposium on Intelligent Signal Processing and Communication Systems*, 2010, pp. 1-4.

[45] N. J. Bershad, J. C. M. Bermudez, and J. Y. Tourneret, "An Affine Combination of Two LMS Adaptive Filters-Transient Mean-Square Analysis," *IEEE Transactions on Signal Processing*, vol. 56, no. 5, pp. 1853-1864, 2008.

[46] M. Scarpiniti, D. Comminiello, G. Scarano, R. Parisi, and A. Uncini, "Steady-State Performance of Spline Adaptive Filters," *IEEE Transactions on Signal Processing*, vol. 64, no. 4, pp. 816-828, 2016.

[47] S. S. Kozat, A. T. Erdogan, A. C. Singer, and A. H. Sayed, "Steady-State MSE Performance Analysis of Mixture Approaches to Adaptive Filtering," *IEEE Transactions on Signal Processing*, vol. 58, no. 8, pp. 4050-4063, 2010.

[48] S. S. Kozat, A. T. Erdogan, A. C. Singer, and A. H. Sayed, "Transient Analysis of Adaptive Affine Combinations," *IEEE Transactions on Signal Processing*, vol. 59, no. 12, pp. 6227-6232, 2011.

[49] M. A. Donmez and S. S. Kozat, "Steady State and Transient MSE Analysis of Convexly Constrained Mixture Methods," *IEEE Transactions on Signal Processing*, vol. 60, no. 6, pp. 3314-3321, 2012.

[50] F. D. Neeser and J. L. Massey, "Proper complex random processes with applications to information theory," *IEEE Transactions on Information Theory*, vol. 39, no. 4, pp. 1293-1302, 1993.

[51] B. Widrow, J. M. McCool, M. G. Larimore, and C. R. Johnson, "Stationary and nonstationary learning characteristics of the LMS adaptive filter," *Proceedings of the IEEE*, vol. 64, no. 8, pp. 1151-1162, 1976.

[52] P. Clarkson and P. White, "Simplified analysis of the LMS adaptive filter using a transfer function approximation," *IEEE Transactions on Acoustics, Speech, and Signal Processing*, vol. 35, no. 7, pp. 987-993, 1987.

[53] A. Leon-Garcia, *Probability, Statistics and Random Processes For Electrical Engineering*, 3rd ed. Prentice Hall, 2008.

[54] A. A. (Louis) Beex and T. Ikuma, "Bi-scale LMS equalization for improved performance," in *2008 IEEE 9th Workshop on Signal Processing Advances in Wireless Communications*, 2008, pp. 511-515.

[55] A. A. (Louis) Beex and T. Ikuma, "Nonlinear Dynamic Effects of Adaptive Filters in Narrowband Interference-Dominated Environments," in *Applications of Nonlinear Dynamics*, V. In, P. Longhini, and A. Palacios, Eds.: Springer, 2009, pp. 163-174.